NANOSTRUCTURED POLYMER SYSTEMS: DESIGN AND CONTROL OF THE GLASS TRANSITION AND DYNAMICS

by

Hyun Joon Oh

A dissertation submitted in partial fulfillment
of the requirements for the degree of
Doctor of Philosophy
(Materials Science and Engineering)
in The University of Michigan
2010

Doctoral Committee:

Professor Peter F. Green, Chair
Professor Richard E. Robertson
Professor Michael J. Solomon
Associate Professor Jinsang Kim

To my wife, Ji-In,

my son, Justin Taewon

and my daughter, Olivia Eunseo

And

To my parents and my younger brother

ACKNOWLEDGEMENTS

It is my great pleasure to thank the many people who made the completion of this thesis possible. I could not have reached the end of the long journey without their support and encouragement.

First and foremost, I would like to express my sincere gratitude to my advisor, Professor Peter F. Green, for his support, guidance, encouragement and patience throughout my Ph.D. years, ever since I joined his group at the University of Texas, Austin. The transition from the University of Texas, Austin to the University of Michigan, Ann Arbor was quite tough and challenging in various respects – adapting to distinctively different weather and environmental conditions, setting up a new lab, retaking all non-transferable courses, and so on. However, Professor Green has been a tremendous resource providing great advice and support that helped me overcome many difficulties and finish my degree. I shall be eternally grateful to him.

I would also like to appreciate my committee members, Professor Richard Robertson, Professor Michael Solomon, and Professor Jinsang Kim, for their valuable comments and suggestions on my research. My special thanks go to Professor Kim not only for his professional guidance but also for his personal advice. I would like to thank Professor Friedrich Kremer at the University of Leipzig and Dr. Anatoli Serghei at the University of Massachusetts Amherst for kindly providing me an opportunity to learn

their unique Dielectric Spectroscopy techniques which have significantly boosted my research.

I must thank all former and current members of the Green Group. I am particularly indebted to Dr. Abraham Arceo and Dr. Luciana Meli who generously helped this novice adapt to the world of polymer physics. Dr. Emmanouil Glynos, Dr. Ernest McIntyre, Chelsea Chen, and Jenny Kim made my lab life intellectually stimulating and highly enjoyable. I also thank Hengxi Yang and GaRam Jun who definitely had a hard time assisting this tricky old-timer. You guys are free now. I would also like to thank all Korean friends at the University of Michigan, and my best friends in Korea for their constant friendship, valuable advice and warm encouragement.

Finally, I wish to express my heartfelt thanks to my parents, Hai-Ryong Oh and Young-Ja Kim, as well as my younger brother, Seung-Hwan Oh, for their unconditional love, sacrifice, support and prayer throughout my life. I would also like to thank my in-laws for their encouragement and unwavering belief in me. Most importantly, I deeply thank my adorable son and daughter, Justin Taewon Oh and Olivia Eunseo Oh, as well as my beloved wife, Ji-In Won, who has patiently supported and cheered me throughout this long process. This thesis would not have been possible without my family's love, dedication and encouragement.

TABLE OF CONTENTS

LIST OF FIGURES

LIST OF TABLES

LIST OF APPENDICES

ABSTRACT

Nanostructured polymer composites, containing "additives" of nanoscale dimensions, have attracted significant attention because they exhibit unusual physical properties that are different and often improved beyond those of conventional macroscopic composites, which contain additives of dimensions on the order of microns or tens of microns. The properties of these nanostructured polymer composites are sensitive to the (domain) size and spatial distribution of the additives.

Two scientifically important questions were examined in this thesis with regard to a special class of nanocomposites: (1) What controls the morphology of nanostructured polymer composites with nanoscale additives?, and (2) How are properties such as the glass transition temperatures, T_gs, and the dynamics of polymers influenced with the presence of these additives? A fundamental understanding of these issues provides insights into the structure-properties-processing relations that govern the industrial applications of these materials. We studies systems in which four types of nanoscale additives were incorporated within homopolymer hosts. The additives were: (1) metallic nanoparticles onto which polymer chains of varying lengths and varying densities were grafted; (2) caged molecules onto which short polymer chains were attached; (3) A-b-B diblock copolymer (BCP) micelles composed of a core of polymer of type A, extended from which are chains of type B and (4) a different kind of homopolymers which gives rise to local heterogeneities in blends.

Through control of the characteristics of the additives, the morphology of the nanostructured composites could be changed; in doing so some basic rules that dictated how the properties could be controlled were developed. There were four basic findings in these studies. First, the number of A/B BCP micelles and structural organization within a homopolymer host of type A were sensitive to film thickness constraints. Additionally, a property such as the T_g was also sensitive to the structure of this system. The implications were that nanocomposite composed of polymer A mixed with metallic nanoparticles onto which polymer chains type-A were grafted (i.e. brush layer) might exhibit unusual properties. We show that in such an athermal system, the T_g could be manipulated significantly by controlling the brush layer thickness and density. Additionally, we showed how the dynamic properties of this system could undergo commensurate changes. The thesis addresses some general guidelines to understand the properties of such systems containing brush layer of type A in a host of polymer B, where the results are often very different. Lastly, it is shown that nanostructures due to the micro-phase separation in A/B homopolymer blends strongly influence the system dynamics.

CHAPTER 1

INTRODUCTION

1.1 Motivation and Research Objectives

Nowadays polymeric materials play a very significant role in a diverse range of fields: plastic bags and bottles to technological applications such as organic light-emitting diodes [1,2] and biosensors [3]. This is due largely to low production cost, ease of fabrication, light weight, corrosion-resistance or flexibility. However, the rapidly increasingly diverse applications have increased demands on the service and reliability of polymers for use in different environments. Although polymers with various physical and chemical properties can be synthesized by modifying chemical composition of monomers, molecular weights, polymer architecture, crystallinity, tacticity and so on, these modified polymers alone cannot satisfy the total demand for improved properties. Polymer nanocomposites, composed of polymers into which fillers are added, show significant promise. They can offer specific advantages over conventional macroscopic composites containing fillers of dimensions on the order of microns or tens of microns.

Nanostructured polymer composites, whose structural constituents have dimensions on the nanoscale, exhibit unique properties that are significantly different from the polymer host and that current theoretical methods often cannot explain. These unusual properties are due to collective intermolecular interactions, and are very sensitive

to the nanostructural features of the polymer composites. The nanofillers have an effect on the structure of the materials on length-scales beyond that of the immediate point of contact. This interphase, as this region around the filler is identified, can extend a few nanometers. Therefore, the problem is more complicated than considering effects associated only with the large interfacial area of contact between the nanofillers and the polymer host. Accordingly, it is not surprising that mechanisms responsible for changes in the properties are still not well understood. When polymer composites are confined at the nanoscale to thin films, interactions of the fillers with external walls can have a significant influence on the structure and hence the properties.

It is well known that even in thin homopolymer films, many properties change largely due to the increasing influence of confinement effects, as well as of entropic or enthalpic interfacial interactions between polymer chains and adjacent media, substrate or environment. In freely standing films, for example, the glass transition temperature, T_g, decreases with decreasing film thickness [4]. For films supported by substrates, the T_g may increase or decrease depending on the nature of the interactions between the polymer and the substrate [5]. A number of theories [6-10] based on so-called free volume models, configurational entropy, dynamic percolation or more phenomenological models have been proposed by research groups around the world to understand and to explain this thickness dependent behavior of T_g in thin homopolymer films. Clearly, confinement effects and interfacial interactions generally lead to significant changes in properties of polymer composite thin films [11-13].

In binary polymer blend or diblock copolymer thin films, preferential interactions between the external hard walls and components of the system are responsible for surface

enrichment or complete wetting of one preferred component [14-17]. This is also expected to occur at the free surface between the composite film and the air (soft wall) since a component with lower surface tension segregates to the interface to reduce the surface energy [14-17]. Another important phenomenon is the phase behavior of particles in polymer nanocomposite thin films. When polymer-grafted nanoparticles are incorporated into polymer thin films, their distribution is determined by a consequence of four major enthalpic/entropic contributions: (1) translational entropy of nanoparticles, (2) enthalpic interactions between nanoparticles and host chains, (3) conformational entropy of host chains near the nanoparticles, and (4) entropic constraint due to the penetrability of host chains into grafted brush layers.

The most typical morphological change driven by the combination of these interactions is nanoparticle segregation towards the hard walls. This segregation actually causes a translational entropy loss by approximately $k_{\mathrm{B}}T$ per nanoparticle, where k_{B} and T are Boltzmann's constant and temperature, respectively [18]. Moreover, in systems with attractive enthalpic interfacial interactions between nanoparticles and host chains, each nanoparticle loses enthalpic contact energy of $\sim (R_{\mathrm{NP}}/b)^2 \times e$ due to the segregation [18, 19]. Here, R_{NP} and b denote the nanoparticle radius and the monomer size, respectively and e represents the components' monomeric interaction energy. Nanoparticle dispersion leads to a loss of enthalpic energy for the system with repulsive interactions, though. These unfavorable contributions to the nanoparticle segregation can be balanced by the conformational entropy loss of host chains near the particles, occurring while chains stretch around particles. In this case, each chain acquires the stretching energy penalty by the ratio of $\sim R_{\mathrm{NP}}{}^2 / Pb^2$, where P is the degree of

polymerization of the host chains, and so bigger particles can be more easily pushed out of host chains to reduce this entropic penalty [20]. The last contribution mentioned above may promote or inhibit the particle segregation depending on the entropic interfacial interactions. This host chain-brush layer interaction is determined by three parameters: P, N, the degree of polymerization of grafted brush chains, and σ, the grafting density of the brush layer [21]. When the brush layer is sparsely grafted with sufficiently long chains, $\sigma\sqrt{N} << (P/N)^{-2}$, there is quite enough space where host chains can interpenetrate. Hence they form complete wet brush layers. However, by increasing σ or P/N, host chains begin to be partially extruded since the interpenetration is not energetically favorable in the densely packed short brush layer. Finally, they dewet the brush layer (a dry brush condition) when $\sigma\sqrt{N} > (P/N)^{-2}$ [21]. The implication is that these interfacial conditions induce attractive or repulsive entropic interactions which may influence the morphology of the system.

Particle aggregation has been often observed in both thin film and bulk polymer composite systems. When the interactions between nanoparticles and host chains are enthalpically or entropically non-attractive, there exists the depletion of host chains around particles due to the reduction in chain configurations [22]. When nanoparticles are far away from each other, no significant morphology change occurs. However, as particles are getting close to sense each other, host chains between particles begin to escape from this space where they experience the restriction in configurational freedom [23]. This is the driving force for the depletion-induced attractive interaction between nanoparticles, resulting in their aggregation [24]. In addition, van der Waals forces or the enthalpic attraction contributes to the aggregation. Surprisingly, particles even with

repulsive interactions can aggregate due to the apparent attraction between them. This attraction is caused by much stronger repulsive forces between host chains and particles than the particle/particle repulsion [25]. Therefore, it is very important to understand a collective interaction in order to interpret the structure of polymer composites.

It has been reported in numerous studies that these morphological changes in nanostructured polymer composites significantly influence their properties. Arceo et al. showed that the T_gs of polymer nanocomposite thin films vary by as much as 65°C due to a change in entropically-driven spatial distribution of nanoparticles [26]. It has been also shown that the aggregation of nanoparticles suppresses such effects on T_g [27]. In addition, recent research on polymer blend or nanocomposite thin film electronic devices indicates that many properties are ruled by their nanostructure [28-30]. Therefore, the importance of the role of the nanostructure cannot be overemphasized.

It is the main goal of my research to gain an understanding of the connection between interactions, nanostructure formation, and properties of polymer-based composites with various additives. To this end, the research has been performed on four primary systems: (1) nanostructured composites composed of homopolymers of type A and A-B block copolymer micelles; (2) nanostructured composites composed of homopolymers of type A and metallic nanoparticles onto which polymer chains of type A are grafted; (3) nanostructured composites composed of polymers of type A into which nanoparticles of type B are incorporated; and (4) nanostructured composites composed of miscible A/B homopolymer blends. In each case, the goal is to understand structure-processing-property relations in these systems.

1.2 References

1. Baldo, M.A., M.E. Thompson, and S.R. Forrest, *High-efficiency fluorescent organic light-emitting devices using a phosphorescent sensitizer.* Nature, 2000. **403**(6771): p. 750-753.

2. Tang, C.W. and S.A. VanSlyke, *Organic electroluminescent diodes.* Applied Physics Letters, 1987. **51**(12): p. 913-15.

3. Heeger, P.S. and A.J. Heeger, *Making sense of polymer-based biosensors.* Proceedings of the National Academy of Sciences of the United States of America, 1999. **96**(22): p. 12219-12221.

4. Forrest, J.A., et al., *Effect of free surfaces on the glass transition temperature of thin polymer films.* Physical Review Letters, 1996. **77**(10): p. 2002-2005.

5. Grohens, Y., et al., *Glass transition of stereoregular poly(methyl methacrylate) at interfaces.* Langmuir, 1998. **14**(11): p. 2929-2932.

6. Keddie, J.L., R.A.L. Jones, and R.A. Cory, *Interface and surface effects on the glass-transition temperature in thin polymer films.* Faraday Discussions, 1994. **98**(Polymers at Surfaces and Interfaces): p. 219-30.

7. Keddie, J.L., R.A.L. Jones, and R.A. Cory, *Size-dependent depression of the glass transition temperature in polymer films.* Europhysics Letters, 1994. **27**(1): p. 59-64.

8. DeMaggio, G.B., et al., *Interface and surface effects on the glass transition in thin polystyrene films.* Physical Review Letters, 1997. **78**(8): p. 1524-1528.

9. Long, D. and F. Lequeux, *Heterogeneous dynamics at the glass transition in van der Waals liquids, in the bulk and in thin films.* European Physical Journal E: Soft Matter, 2001. **4**(3): p. 371-387.

10. Kim, J.H., J. Jang, and W.-C. Zin, *Thickness dependence of the glass transition temperature in thin polymer films.* Langmuir, 2001. **17**(9): p. 2703-2710.

11. Pham, J.Q. and P.F. Green, *The glass transition of thin film polymer/polymer blends: Interfacial interactions and confinement.* Journal of Chemical Physics, 2002. **116**(13): p. 5801-5806.

12. Pham, J.Q. and P.F. Green, *Effective T_g of confined polymer-polymer mixtures. influence of molecular size.* Macromolecules, 2003. **36**(5): p. 1665-1669.

13. Pham, J.Q., et al., *Glass transition of polymer/single-walled carbon nanotube composite films.* Journal of Polymer Science, Part B: Polymer Physics, 2003. **41**(24): p. 3339-3345.

14. Karim, A., et al., *Phase-separation-induced surface patterns in thin polymer blend films.* Macromolecules, 1998. **31**(3): p. 857-862.

15. Tanaka, K., et al., *Ultrathinning-induced surface phase-separation of polystyrene poly(vinyl methyl-ether) blend film.* Macromolecules, 1995. **28**(4): p. 934-938.

16. Coulon, G., et al., *Surface-induced orientation of symmetric, diblock copolymers - a secondary ion mass-spectrometry study.* Macromolecules, 1989. **22**(6): p. 2581-2589.

17. Russell, T.P., et al., *Characteristics of the surface-induced orientation for symmetric diblock PS/PMMA copolymers.* Macromolecules, 1989. **22**(12): p. 4600-4606.

18. Krishnan, R.S., et al., *Self-assembled multilayers of nanocomponents.* Nano Letters, 2007. **7**(2): p. 484-489.

19. Mackay, M.E., et al., *General strategies for nanoparticle dispersion.* Science, 2006. **311**(5768): p. 1740-1743.

20. Ginzburg, V.V., *Influence of nanoparticles on miscibility of polymer blends. A simple theory.* Macromolecules, 2005. **38**(6): p. 2362-2367.

21. Ferreira, P.G., A. Ajdari, and L. Leibler, *Scaling law for entropic effects at interfaces between grafted layers and polymer melts.* Macromolecules, 1998. **31**(12): p. 3994-4003.

22. Starr, F.W., T.B. Schroder, and S.C. Glotzer, *Molecular dynamics simulation of a polymer melt with a nanoscopic particle.* Macromolecules, 2002. **35**(11): p. 4481-4492.

23. Xu, J., et al., *Morphology and interactions of polymer brush-coated spheres in a polymer matrix.* Journal of Polymer Science, Part B: Polymer Physics, 2006. **44**(19): p. 2811-2820.

24. Hooper, J.B. and K.S. Schweizer, *Contact aggregation, bridging, and steric stabilization in dense polymer-particle mixtures.* Macromolecules, 2005. **38**(21): p. 8858-8869.

25. Feng, J. and E. Ruckenstein, *Attractive interactions in dispersions of identical charged colloidal particles: A monte carlo simulation.* Journal of Colloid and Interface Science, 2004. **272**(2): p. 430-437.

26. Arceo, A., L. Meli, and P.F. Green, *Glass transition of polymer-nanocrystal thin film mixtures: Role of entropically directed forces on nanocrystal distribution.* Nano Letters, 2008. **8**(8): p. 2271-2276.

27. Kropka, J.M., et al., *Origin of dynamical properties in PMMA-C_{60}*

nanocomposites. Macromolecules, 2007. **40**(15): p. 5424-5432.

28. Kuila, B.K., A. Garai, and A.K. Nandi, *Synthesis, optical, and electrical characterization of organically soluble silver nanoparticles and their poly(3-hexylthiophene) nanocomposites: Enhanced luminescence property in the nanocomposite thin films.* Chemistry of Materials, 2007. **19**(22): p. 5443-5452.

29. Qiu, L.Z., et al., *Organic thin-film transistors based on blends of poly(3-hexylthiophene) and polystyrene with a solubility-induced low percolation threshold.* Chemistry of Materials, 2009. **21**(19): p. 4380-4386.

30. Yim, K.H., et al., *Phase-separated thin film structures for efficient polymer blend light-emitting diodes.* Nano Letters, 2010. **10**(2): p. 385-392.

CHAPTER 2

BACKGROUND

2.1 Glass Transition Temperature (T_g)

The glass transition temperature is the temperature at which the polymer goes through the transition from a rubbery state into a glassy state as it is cooled. Aspects of the glass transition bear some resemblance to a second-order phase transition wherein extensive thermodynamic parameters such as enthalpy (H), entropy (S) and volume (V) undergo substantially continuous changes as the system goes through the transition. In a first order phase transition, such as melting, the change would be discontinuous. A schematic of the specific volume vs. temperature is illustrated as an example in Figure 2.1. Indeed, the glass transition is not a true thermodynamic phase transition largely because it is a time-dependent kinetic phenomenon; the motions of molecules are "frozen" on the time scale of the experiment for $T < T_g$.

The glass transition is not well defined because it occurs gradually over a wide temperature range called the glass transition region. Operationally, T_g is often identified as the mid-point of this range and generally, determined by the intersection of the extrapolated tangent lines from the glassy region at lower temperatures and the rubbery region at higher temperatures. T_g depends on the thermal history of the sample such as the rate of cooling or the age of the material. Because different experimental techniques

may yield different T_gs [1], all the experimental conditions and the method of T_g measurement should be specified.

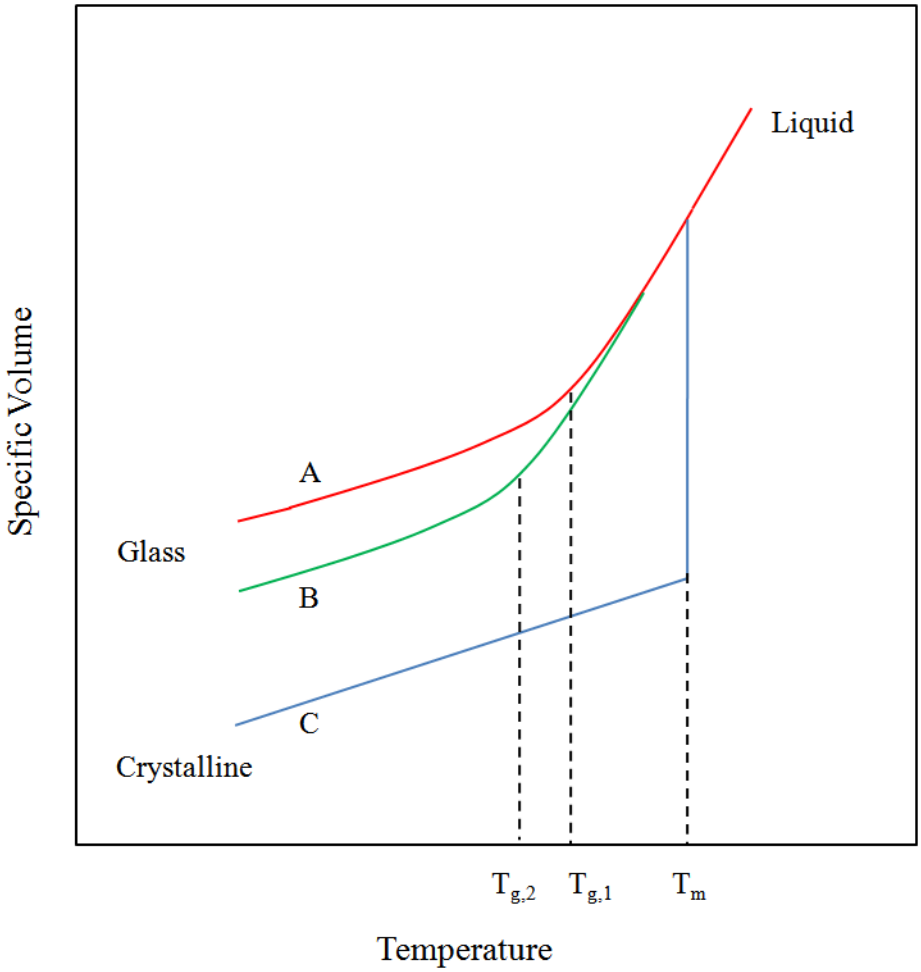

Figure 2.1 Schematic diagram of specific volume as a function of the temperature on cooling from liquid melts for amorphous (A and B) and crystalline (C) materials. Curve A which represents a measurement on faster cooling rate has a higher T_g ($T_{g,1}$), compared to curve B.

2.2 Experimental Techniques

Various experimental techniques have been used to evaluate properties of polymer composites. Spectroscopic ellipsomertry (SE) and differential scanning calorimetry (DSC) were used for thin film and bulk T_g measurements, respectively. In addition, both thin film and bulk T_gs were measured using dielectric spectroscopy (DS), providing chain dynamics information as well. Thin film depth profile, surface topography and morphology (two-dimensional projection) of samples were characterized by dynamic secondary ion mass spectrometry (DSIMS), scanning probe microscopy (SPM) and scanning transmission electron microscopy (STEM), respectively. Thermal gravimetric analysis (TGA) was performed for nanoparticle characterization.

As mentioned in the previous section, different experimental techniques may show inconsistent results depending on the experimental conditions and methods. Therefore, it is important to understand the principle of the experimental techniques. Accordingly, this section describes the basics of SE and DS, used for the measurements of T_g, the primary interest in this study. DSC is excluded from the discussion since it is a well established technique.

2.2.1 Spectroscopic Ellipsometry

SE is an optical technique that utilizes the polarization to determine the sample properties and has been extensively used to characterize the properties of thin films especially in the semiconductor industry because it is very sensitive to the change of the surface, non-destructive, reproducible and rapid. It is even possible to measure the sample properties in various experimental environments as long as the light penetrates

media.

The principles of ellipsometry can be found in literature [2-4] and will be briefly reviewed here based on that literature. When the linearly polarized light is incident to the surface, the reflected light becomes elliptically polarized. This reflected light experiences a phase shift and amplitude change of p- and s- components which are parallel and perpendicular to the plane of incident of the light (See Figure 2.2). Ellipsometry measures the change in polarization state of the reflected light in terms of Ψ and Δ. These ellipsometric parameters are related to the complex reflectance ratio ρ of Fresnel reflection coefficients, R_p and R_s, which can be expressed by the ratio of the reflected electric field vector over the incident electric field vector, i.e., E_{rp} / E_{ip} and E_{rs} / E_{is} for p- and s- components, respectively.

$$\rho = \frac{R_p (= E_{rp} / E_{ip})}{R_s (= E_{rs} / E_{is})} = \left| \frac{R_p}{R_s} \right| \exp i(\delta_p - \delta_s) = \tan \Psi \exp i\Delta \qquad (2.1)$$

, where $\delta_{p(s)}$ represents the phase shift of the p- (s-) component before and after the reflection. From this equation, we can know that tan Ψ denotes the amplitude ratio of the reflection coefficients of the p- and s- components and Δ are defined as the induced phase shift difference between those two components upon reflection:

$$\Psi = \tan^{-1} \left| \frac{R_p}{R_s} \right| \qquad (2.2)$$

$$\Delta = \delta_p - \delta_s \qquad (2.3)$$

Figure 2.2 shows the schematic diagram of reflection and refraction of the incident light at a single interface. Fresnel equations for reflection coefficients can be rewritten by considering the Maxwell equations with the boundary conditions at this

interface for electric and magnetic fields of the light as below:

$$R_s = \frac{N_0 \cos\Phi_0 - N_1 \cos\Phi_1}{N_0 \cos\Phi_0 + N_1 \cos\Phi_1} \tag{2.4}$$

$$R_p = \frac{N_1 \cos\Phi_0 - N_0 \cos\Phi_1}{N_1 \cos\Phi_0 + N_0 \cos\Phi_1} \tag{2.5}$$

Here, Φ_0 and Φ_1 are the angles of incidence and refraction, respectively, and N_0 and N_1 are the refractive indices of the media.

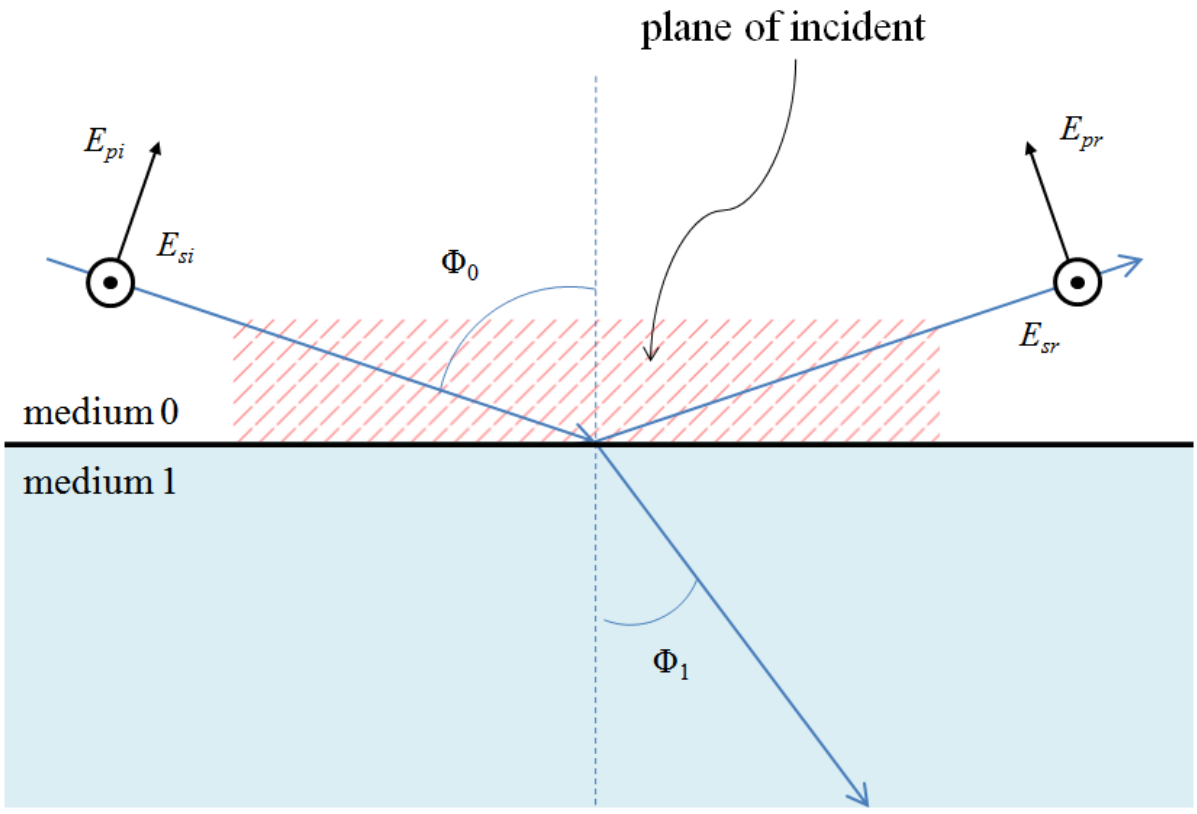

Figure 2.2 Schematic showing reflection and refraction of the incident light at a planar surface.

If the sample has multiple interfaces which are general for most applications, multiple reflections at all interfaces should be considered to determine reflection coefficients. For the three phase system which has a second medium with thickness d in the middle, the reflection coefficient $R_{p(s)}$ is derived as

$$R_{p(s)} = \frac{R_{01}^{p(s)} + R_{12}^{p(s)} \exp(-i2\beta)}{1 + R_{01}^{p(s)} R_{12}^{p(s)} \exp(-i2\beta)} \tag{2.6}$$

, where $R_{01}^{p(s)}$ and $R_{12}^{p(s)}$ are the Fresnel reflection coefficients at the interfaces between the incident medium 0 and the second medium 1 and between the second medium 1 and the last medium 2, respectively. β denotes the film phase thickness and can be expressed as

$$\beta = \frac{2\pi d}{\lambda} N_1 \cos\Phi_1 \tag{2.7}$$

, where λ is a wave length of the light and Φ_1 represents the propagation angle of the incident light. If all the variables except thickness d in Equation (2.6) and (2.7) are known, ellipsometric parameters can be theoretically calculated as a function of d.

$$\rho = \frac{R_p}{R_s} = \tan\Psi(d) \exp i\Delta(d) \tag{2.8}$$

Therefore, the thickness d can be extracted through the comparison of the calculated (Ψ, Δ) and the measured (Ψ, Δ) by ellipsometry.

When a substance is heated, in general, the vibration of its elements increases and elements gain kinetic energy, leading to an increase in expansion. As described in Chapter 2.1, the T_g of a bulk is defined as a temperature where the volume expansion goes through a pseudo-second order transition. However, since thin films are assumed to be constrained along the substrate surface, the thermal expansion parallel to the substrate can be neglected. Therefore, thin film T_g can be determined from the ellipsometry

experiment by measuring the 1-dimensional thickness change as a function of the temperature in a way analogous to the volume change as shown in Figure 2.3.

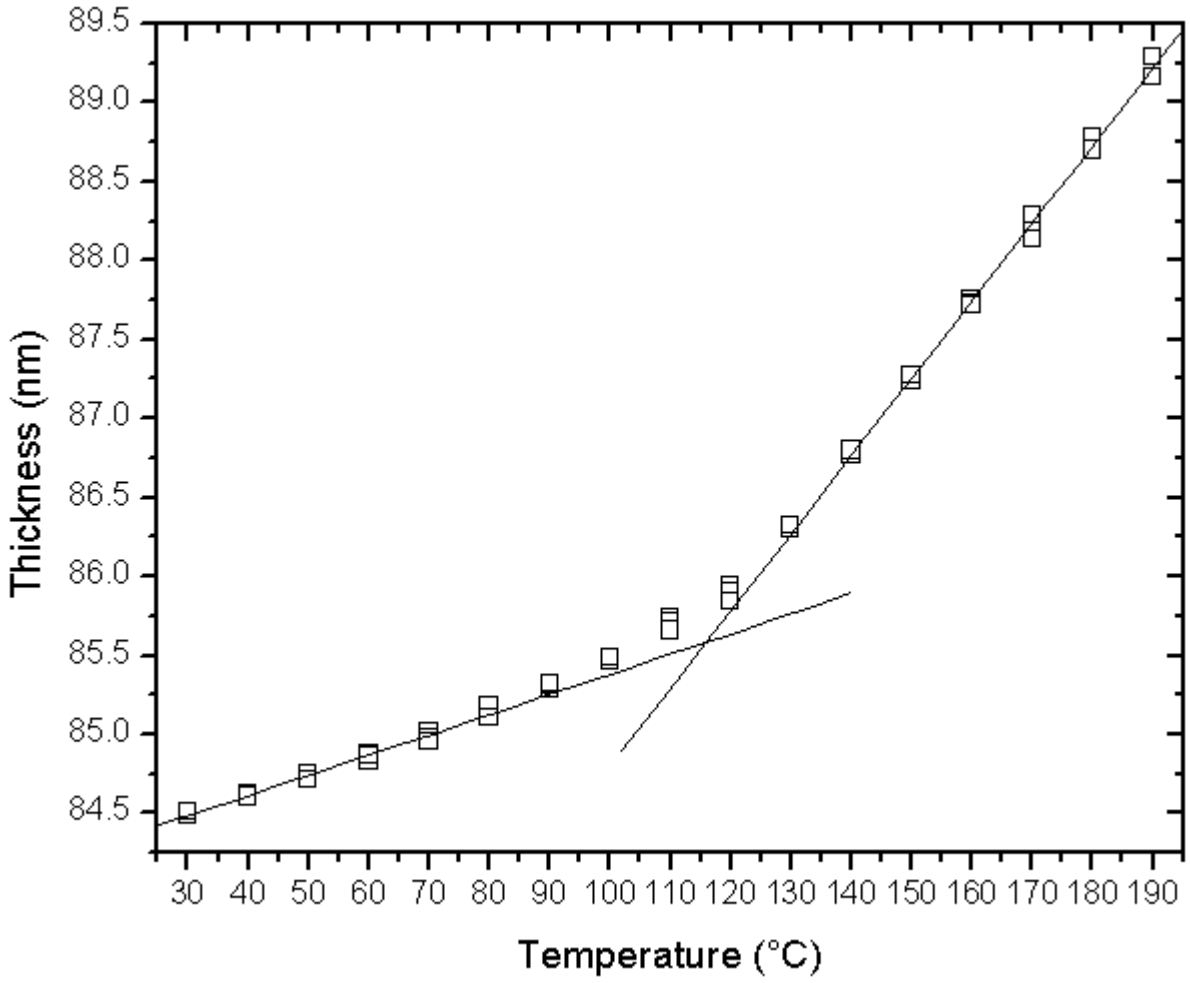

Figure 2.3 Ellipsometric heating scan at a rate of 10°C/min for 20 *wt*.% polystyrene-b-poly(methyl methacrylate) (PS-b-PMMA) diblock copolymers in PS with the thickness of 84.5 nm. The glass transition is identified by the intersection of two linear fits to the data in the rubbery and glassy regions.

2.2.2 Broadband Dielectric Spectroscopy

Broadband dielectric spectroscopy [5] is one of the most suitable and versatile techniques to access the molecular dynamics of polymeric systems over a wide range of time scales. By applying an alternating-current external electric field, DS can measure the complex dielectric permittivity, ε^* as a function of the frequency of the electric field.

The ε^* spectrum over a wide frequency range (10^{-6} Hz ~ 10^{12} Hz) is schematically illustrated in Figure 2.4. There are four different polarization mechanisms: electronic, atomic, orientational (dipolar) and interfacial (ionic) polarizations. First two polarizations which are shown up at higher frequencies than ~ 10^{12} Hz result from the dipole moments induced by the local electric field. It is due to the deformation of the negatively charged electron cloud around the atomic nucleus or the positive and negative atoms. The other two at low frequencies are caused by the permanent dipole moments. The orientational polarization occurs when randomly oriented dipolar molecules are aligned to the external electric field. The interfacial polarization specifically consists of the ionic conductivity and the interfacial and space charge relaxation. The former originates from the motion of ions under the electric field and the latter occurs when the space charges are trapped at the interfaces. The total polarization is determined as a sum of all these contributions. Although the maximum frequency range of broadband dielectric spectroscopy is very wide, we are interested in the range between 10^{-2} Hz and 10^{6} Hz where the crucial relaxations appear for the most of macromolecules.

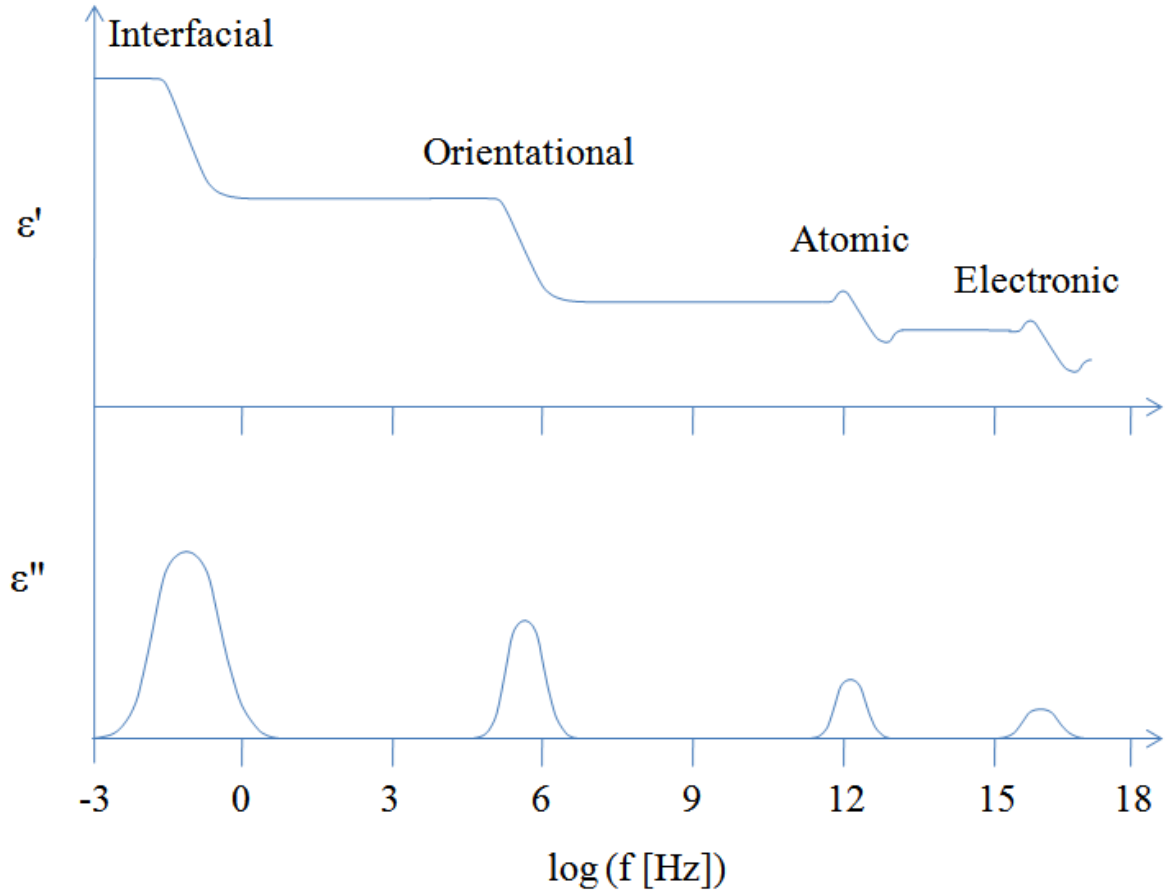

Figure 2.4 The frequency dependence of the real and imaginary part of the complex dielectric permittivity, ε^*.

The interaction of an external electric field with the dipole moments of the sample is often expressed by the complex dielectric permittivity:

$$\varepsilon^* = \varepsilon_0 \varepsilon_r^* = \varepsilon' - i\varepsilon'' \tag{2.9}$$

$$\tan\delta = \frac{\varepsilon''}{\varepsilon'} \tag{2.10}$$

, where ε' is the real part or the dielectric storage of electric field energy and ε'' is the imaginary part or the dielectric loss of electric field energy. Here, ε_0 denotes the vacuum

permittivity (≈8.8541878176 × 10^{-12} F/m) and tan δ is a loss factor. A single relaxation process of an ideal population of dipoles to the electric field can be explained by the Debye relaxation [6]:

$$\varepsilon^*(\omega) = \varepsilon_\infty + \frac{\varepsilon_s - \varepsilon_\infty}{1 + i\omega\tau} = \varepsilon_\infty + \frac{\Delta\varepsilon}{1 + i\omega\tau} \qquad (2.11)$$

, where ε_∞ denotes the dielectric permittivity at the high frequency limit, ε_s the static dielectric permittivity, $\Delta\varepsilon$ the dielectric relaxation strength, ω the angular frequency and τ the relaxation time. In practice, however, many systems show a more complex behavior such as an asymmetric broadening of the relaxation and several characteristic dielectric relaxation processes are often detected, e.g., the primary relaxation (α process) associated with the cooperative segmental motion of the polymer directly related to dynamic glass transition, or local relaxations involving simple bond rotation (β, γ, δ relaxation). These cases are generally described using empirical models listed in Table 2.1.

Table 2.1 Dielectric response function models for the frequency domain

Model	Dielectric Function	Parameters
Debye [6]	$\varepsilon^*(\omega) = \varepsilon_\infty + \frac{\Delta\varepsilon}{1 + i\omega\tau_D}$	
Cole-Cole [7]	$\varepsilon^*(\omega) = \varepsilon_\infty + \frac{\Delta\varepsilon}{1 + (i\omega\tau_{CC})^\alpha}$	$0 < \alpha \leq 1$
Cole-Davison [8]	$\varepsilon^*(\omega) = \varepsilon_\infty + \frac{\Delta\varepsilon}{(1 + i\omega\tau_{CD})^\beta}$	$0 < \beta \leq 1$
Havriliak-Negami [9]	$\varepsilon^*(\omega) = \varepsilon_\infty + \frac{\Delta\varepsilon}{(1 + (i\omega\tau_{HN})^\alpha)^\beta}$	$0 < \alpha \leq 1$ $0 < \alpha\beta \leq 1$

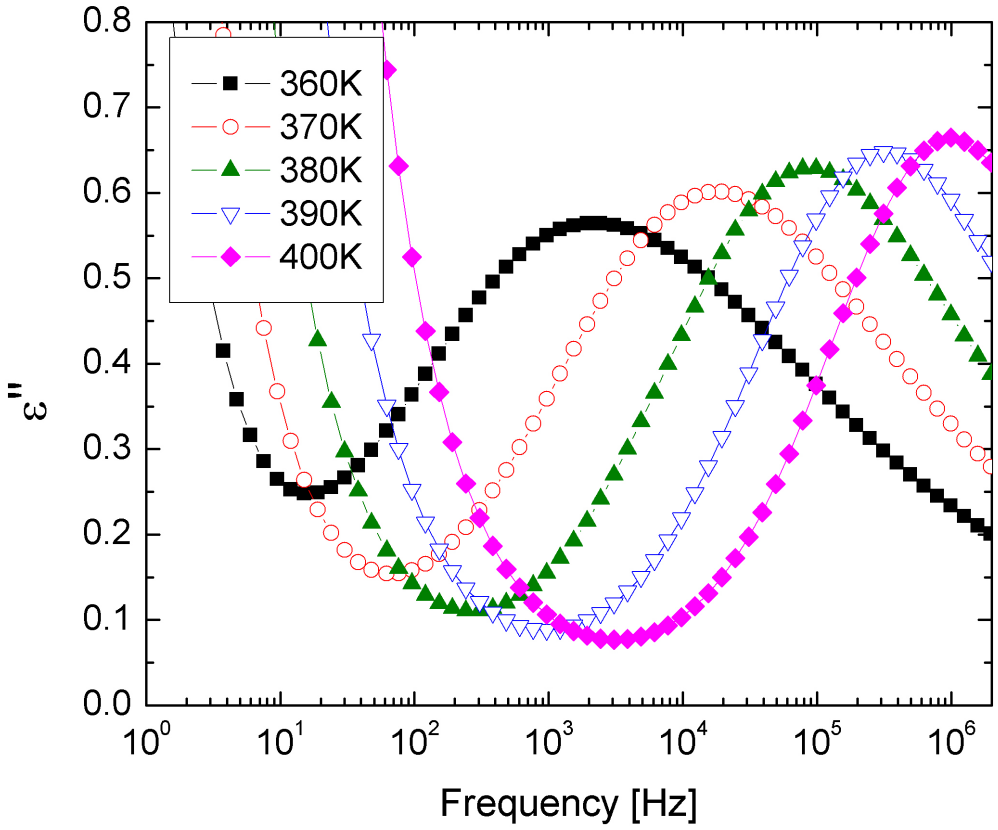

Figure 2.5 Loss spectra of a 113 nm pure i-PMMA film measured at different temperatures.

Figure 2.5 shows the frequency dependence of the dielectric loss for α relaxation of pure isotactic poly(methyl methacrylate) (i-PMMA) at a series of different temperatures. α relaxation process shifts to higher frequency with increasing temperature due to the increasing mobility of polymeric chains. A relaxation time, τ, is obtained from the maximum in ε'' at each given temperature using the empirical relaxation functions listed in Table 2.1 after subtracting the contribution of dc conductivity. The temperature dependence of the α relaxation time can be well described by the Vogel-Fulcher-

Tammann (VFT) equation:

$$\tau(T) = \tau_0 \exp\left(\frac{B}{T - T_V}\right) \tag{2.12}$$

, where τ_0 is the relaxation time at infinite temperature, B is a constant being related to the activation energy of the relaxation process, and T_v is the Vogel temperature at which the segments would be frozen if they were at equilibrium. The activation plot showing the relationship between the relaxation rate and the inverse temperature is illustrated in Figure 2.6.

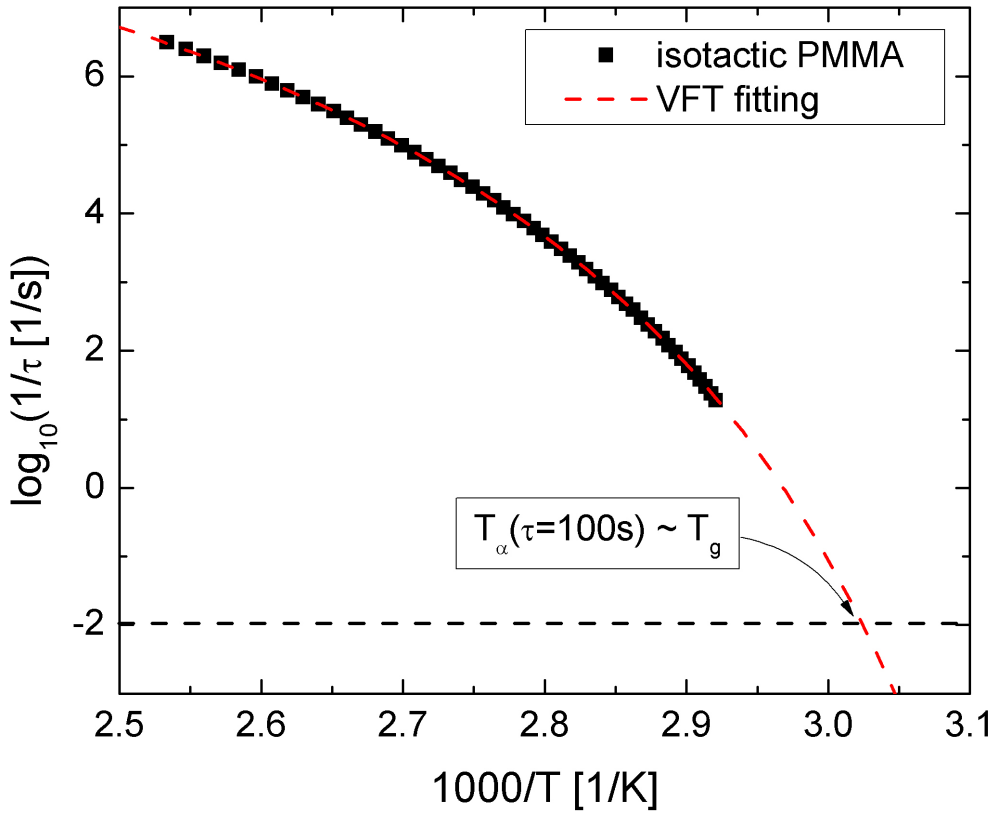

Figure 2.6 Activation plot (relaxation rates versus inverse temperature) for pure isotactic PMMA. T_g is defined as a temperature at which an extrapolated relaxation time is equal to 100 s.

There are two main methods for defining the T_g from dielectric data. First, it is possible to estimate the T_g by fitting the activation plot with the VFT equation since T_α (the peak temperature of α relaxation at a given frequency) at which the average relaxation time reaches 100 s is comparable to T_gs measured by other techniques [10].

Besides the dielectric relaxation, DS simultaneously provides dilatometric information which can be used for the T_g determination. This method, the so-called capacitive scanning dilatometry (CSD), is based on the fact that the temperature dependence of the capacitance C′ is sensitive to the linear thermal expansion. Figure 2.7 shows the normalized capacitance of pure PS as a function of temperature. It is obvious that there is a change in slope representing a change in the linear thermal expansion coefficient. T_g is defined as the temperature at which a change in slope occurs, i.e. the break of two extrapolated tangent lines from the glassy region at lower temperature and the rubbery region at higher temperature. There is a clear deviation from the linear dependence of capacitance at rubbery region, which arises from the appearance of α relaxation and becomes more pronounced at lower frequencies. Therefore, it is important to exclude those deviated data when the extrapolated lines are drawn. Further experimental and theoretical details can be found elsewhere [11, 12].

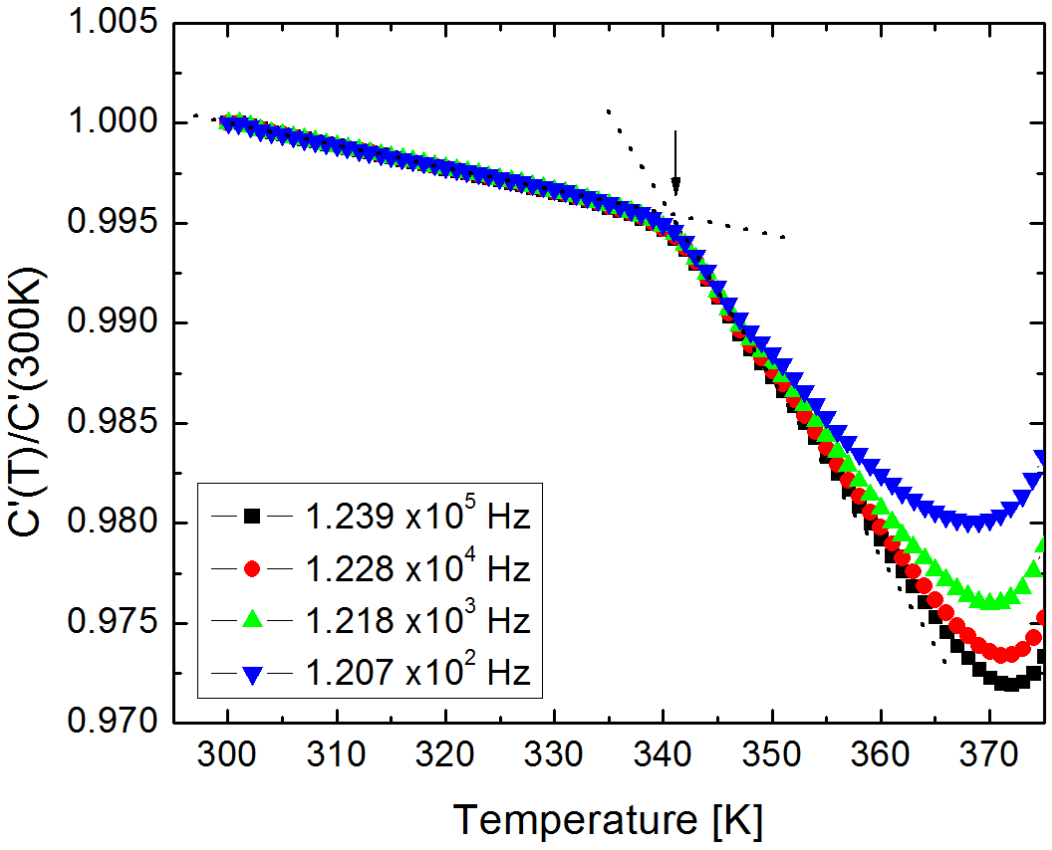

Figure 2.7 Temperature dependence of normalized capacitance C′ for pure PS at various frequencies. Extrapolated tangent lines are drawn using data, not affected by α relaxation. T_g is then determined as an intersection point between these two tangent lines and designated by an arrow.

2.3 References

1. Serghei, A., et al., *Discrepancies in the characterization of the glass transition in thin films of hyperbranched polyesters.* Journal of Polymer Science, Part B: Polymer Physics, 2006. **44**(20): p. 3006-3010.

2. Azzam, R.M.A. and N.M. Bashara, *Ellipsometry and polarized light*. Pbk. ed. 1987, Amsterdam ; New York: North-Holland ; sole distributors for the USA and Canada, Elsevier Science Publishing Co., Inc. xvii, 539 p.

3. Tompkins, H.G., E.A. Irene, and Knovel (Firm), *Handbook of ellipsometry*. 2005, William Andrew Pub. ; Springer: Norwich, NY; Heidelberg, Germany. p. xvi, 870 p.

4. Tompkins, H.G. and W.A. McGahan, *Spectroscopic ellipsometry and reflectometry : A user's guide*. 1999, New York: Wiley. xiv, 228 p.

5. Kremer, F. and A. Schönhals, *Broadband dielectric spectroscopy*. 2003, Berlin ; New York: Springer. xxi, 729 p.

6. Debye, P.J.W., *Polar molecules*. 1929, [New York]: Dover Publications. 172 p.

7. Cole, K.S. and R.H. Cole, *Dispersion and absorption in dielectrics. I. Alternating-current characteristics.* Journal of Chemical Physics, 1941. **9**: p. 341-51.

8. Davidson, D.W. and R.H. Cole, *Dielectric relaxation in glycerol.* Journal of Chemical Physics, 1950. **18**: p. 1417.

9. Havriliak, S. and S. Negami, *Complex plane analysis of a-dispersions in some polymer systems.* Journal of Polymer Science, Polymer Symposia, 1966. **No. 14**: p. 99-103.

10. Roland, C.M. and R. Casalini, *Temperature dependence of local segmental motion in polystyrene and its variation with molecular weight.* Journal of Chemical Physics, 2003. **119**(3): p. 1838-1842.

11. Fukao, K. and Y. Miyamoto, *Glass transition temperature and dynamics of alpha-process in thin polymer films.* Europhysics Letters, 1999. **46**(5): p. 649-654.

12. Bauer, C., et al., *Capacitive scanning dilatometry and frequency-dependent thermal expansion of polymer films.* Physical Review E: Statistical Physics, Plasmas, Fluids, and Related Interdisciplinary Topics, 2000. **61**(2): p. 1755-1764.

CHAPTER 3

ROLE OF DIBLOCK COPOLYMERS TOWARD CONTROLLING THE GLASS TRANSITION OF THIN POLYMER FILMS

The physical properties of thin polymer films are often thickness, h, dependent, influenced by confinement and by interfacial interactions between the chains and the external interfaces. We show that the magnitude and film thickness dependence of the average glass transition temperature, T_g, of the polystyrene-silicon oxide ($PS/SiO_x/Si$) system is influenced appreciably with the addition of polystyrene-b-poly(methyl methacrylate) (PS-b-PMMA) diblock copolymers. The T_g can be "tailored" to increase, or decrease, with decreasing h or to remain independent of h. T_g-shifts of as much of 35°C are obtained for films of $h \approx 20$ nm. Additionally, we report that the critical micelle concentration, ϕ_{cmc}, of the copolymer in thin films is considerably larger than for the bulk; specifically micelles form only beyond a critical film thickness, determined by the size of the chains and by the number of chains in the system. The h-dependence of T_g is not influenced by the ϕ_{cmc}, nor by the number of micelles in this system.

3.1 Introduction

Thin polymer films are of considerable interest technologically in a diverse range of areas, from coatings and organic electronic devices to large-area screens, for reasons that include: tunability of the chemical and physical properties, low production cost, ease of fabrication, and high flexibility. Organic light emitting diodes (OLED) [1, 2], organic photovoltaic cells (OPVC) [3-5], flexible displays [6], biosensors [7] represent specific examples of technologies in which thin polymer films are deployed. Use of thin polymer films in many applications necessarily involves the formation of interfaces with other materials. Consequently, a manifold of phenomena that influence processing and performance of these materials need to be understood: wetting [8], instabilities [9], viscoelasticity [10, 11], diffusion [12-14] and glass transition temperatures (T_g) [15-38]. The size-dependent properties, moreover, are often difficult to predict because they manifest the influence of confinement and of interfacial interactions between the material (chemical) constituents and the external interfaces. In this chapter we are interested in the glass transition temperature, as it is of fundamental importance with regard to processing of polymers.

Considerable research, using a variety of experimental probes, dielectric spectroscopy [15-18], X-ray and neutron reflectivities [19-23], positron lifetime spectroscopy [24], fluorescence spectroscopy [25], shear-modulated scanning force microscopy [26], Brillouin light scattering [27-29] and spectroscopic ellipsometry [30-37], reveal that the average T_g of films thinner than $h \approx$ 40-60 nm may increase, or decrease, with decreasing h. For instance, the T_gs of polystyrene (PS) on silicon substrates, with native oxide layer, and poly (methyl methacrylate) (PMMA) on the gold-

coated silicon substrate decrease with decreasing thickness [28, 30, 31, 33], while poly (2-vinyl pyridine) (P2VP), tetramethyl bisphenol-A polycarbonate (TMPC) and PMMA supported on silicon substrates, with native oxide layers, show an increase in T_gs with decreasing thickness [21, 25, 30, 32, 34, 35]. A summary of the overall observations is that T_g decreases with decreasing film thickness, h, ($\Delta T_g < 0$), if the film is freely standing or if the film resides on a substrate wherein the chain segments interact weakly (e.g.: non-wetting) with the substrate; otherwise if the interactions between the chain segments and the substrate are particularly strong, the glass transition increases with decreasing h ($\Delta T_g > 0$).

A number of theories have been proposed to explain the thickness dependent behavior of T_g. One class of models can be classified as "interface based" models; the phenomenological models of Keddie et al. [30, 31], DeMaggio et al. [24] and Kim et al. [37] are such examples. In order to reconcile the decrease of T_g with decreasing h, Keddie et al. proposed the existence of "liquid-like" layer, composed of comparatively high mobility chain segments, possessing a high configurational entropy, at the free surface. DeMaggio et al. explained the T_g vs. h behavior of the thin polymer film using the three-layer model: a "bulk-like" interior layer, a liquid-like layer near the free surface, and "dead" layer near the substrate possessing lower mobility and higher T_g due to the interaction between chain segments and the substrate. Kim and coworkers also proposed a multi layer model. The work of Ellison and Torkelson [39] indicates that the T_g changes locally with distance from an interface, which lends some credence to the layered "interface-based" models. Theories based on the energy landscape (configurational entropy) models, and more restrictive models that compare local density

profiles in thin films to the bulk to predict changes in T_g, yield results consistent with the experimentally determined thickness dependencies of T_g.

The foregoing models however are limited in that they do not provide a mechanism for the thickness dependence of T_g. The dynamic percolation model by Long and Lequeux [40] embodies a mechanism for the onset of T_g in thin films. In this model, thermal density fluctuations are responsible for the existence of spatially located domains characterized by "fast" and "slow" dynamics. Small differences in density are associated with significant differences in dynamics; this is due to the non-linear dependence of dynamics on density in structurally disordered materials. Particles enter and leave the domains in order to preserve ergodicity; hence the "fast" and "slow" domains are transient. The onset of percolation of the slow domains denotes the glass transition. The T_gs of thin films and bulk of the same material differ because the percolation thresholds in 2 and 3 dimensions are different. If the interactions between the chain segments and an interface are sufficiently strong, hence reducing appreciably the configurational freedom of the chains, then the fraction of "slow" domains in the system increases, leading to an enhancement of the local T_g. The effect of interfaces on the T_g of the system is apparent: (1) the T_g decreases with film thickness for freely standing films because the fraction of "fast" domains increase due to the enhanced configurational freedom of the chains at the free surfaces; (2) the T_g generally increases with decreasing h, for films in contact with hard "walls" at both interfaces due to the increase in the number of "slow" domains. In systems where only one interface is supported, the thickness dependence of T_g would be dictated by the fraction of "slow domains," which is largely determined by the nature of the interactions between the chains and the substrate.

There have been a number of experiments devoted to understanding the influence of a second component on the T_g of a homopolymer system. These have included experiments on homopolymer/homopolymer blends [34, 35]; here the effect of the second miscible component is to change the thickness dependence on T_g. In addition the notion of a "self-concentration," responsible for local concentration fluctuations, is invoked to understand the behavior of this system [41]. The second class of systems is the nanoparticle/ homopolymer blends [36], where the nanoparticle has the effect of changing the thickness dependencies of T_g. The nanoparticles in principle increase the number of interfaces in the system, and due to the particle polymer interactions, increases the fraction of "slow" domains in the system and hence the T_g. It is evident from these systems that the second component has the effect of changing the thickness dependence of T_g, but for fundamentally different reasons.

In this chapter we show that control of the interfacial interactions, through the use of block copolymers, provides a means by which the average T_g of the film can be "tailored". Due to their amphiphilic properties, diblock copolymers exhibit a natural tendency to segregate to the interfaces between melts and non-polymeric interfaces [42-46], and to immiscible homopolymer interfaces [47-50] leading to an increase of adhesion [51] and a decrease of interfacial tension [52-55]. We also show that the critical micelle concentration, ϕ_{cmc}, in thin films is significantly larger than in the bulk. In fact there exists a critical film thickness beyond which micelles form; this critical film thickness is largely determined by the size of the diblocks, for systems in which one block strongly adsorbs to an interface, and the number of chains required to create a brush layer at the interfaces.

3.2 Experimental Section

Solutions of different weight fractions of PS-b-PMMA in PS were prepared by dissolving PS homopolymer, with nominal average molecular weight of 590,000 g/mol (Pressure Chemical Co., M_w/M_n = 1.06), and asymmetric PS-b-PMMA copolymer, with number average molecular weight of 67,100 g/mol (Polymer Source Inc., M_w/M_n = 1.09), in toluene (Fisher Scientific Inc.). M_n of the PS component and M_n of the PMMA component of the copolymer are 46,100 g/mol and 21,000 g/mol, respectively. Before spin-coating onto silicon wafers, the solutions were mixed by an orbital shaker (MS 3 digital, IKA®) for a day at 1000 rpm.

Films between ~16 nm and ~170 nm were spin-coated onto <100> oriented silicon substrates having a ~2 nm native oxide layer (Wafer World Inc.) by adjusting the concentration of the solutions and the spinning rate. The samples were then annealed under vacuum at 120 °C for 16 hrs to remove the solvent (this allowed sufficient time for the samples to reach an equilibrium state) and then quenched to room temperature. At this point the samples were uniform in thickness, with smooth surfaces (no dewetting). The T_gs were measured in a custom-made heating stage by using a Variable Angle Spectroscopic Ellipsometer (J.A. Woollam Co., Inc.). The ellipsometric parameters, Ψ and Δ, which are related to the change in the polarization, were measured at 10 °C intervals as the temperature was increased at a rate of 1 °C/min. In some experiments, the temperature was increased as much as 190 °C in order to get an accurate determination of T_g. Three different measurements were performed in the wavelength range of 400 nm ~ 750 nm at each temperature. For the analysis of the thickness, the data were fitted to the Cauchy/SiO_x/Si model over the entire measured spectral range using the

WVASE32 ellipsometry analysis software (J.A. Woollam Co., Inc.). Experimental details are described elsewhere [30-36]. Typical data representing the temperature dependence of the thickness are shown in Figure 3.1. The plots show two distinctive regions: the glassy region at lower temperature and the rubbery region at higher temperature. T_g was determined by the break of the extrapolated tangent lines from these two regions of a 1st measurement. T_gs for all samples were collected in this way. We note that every sample including the pure PS-b-PMMA film exhibited a single break, i.e., one average T_g. A 2nd measurement was carried out subsequently after cooling to room temperature and equilibrating for ~ 10 min. Since no reduction in thickness during each measurement, even after a second temperature cycle, were observed, it is safe to say that there were no effects of oxidative degradation during our experimental time scale.

The bulk T_gs of pure PS and pure PS-b-PMMA were determined using a PerkinElmer DSC7 differential scanning calorimetr (DSC). T_g was determined by the onset of a step transition at the second heating in a heating/cooling/heating (10°C/-50°C/10°C per min) procedure. T_gs measured using DSC for PS homopolymer, PS blocks of PS-b-PMMA and PMMA blocks of PS-b-PMMA are 101.8°C, 101.8°C and 127.5°C, respectively.

Scanning Transmission Electron Microscopy (STEM) was used to examine the morphologies of the thin film samples. Films were spin-coated on glass slides and floated directly on the surface of deionized water. They were then placed on the silicon nitride membrane window grids (SPI supplies). After vacuum-annealing at 120 °C for 16 hrs, samples were exposed to vapor from aqueous RuO_4 solution for 5 minutes. This provides a contrast between the PS and PMMA because RuO_4 preferentially stains PS

segments by attacking its aromatic ring. Z-contrast images of the samples were generated in the STEM mode under an accelerating voltage of 200 kV by the JEOL 2010F Analytical Electron Microscope equipped with a high angle annular dark field (HAADF) detector. The contrast in HAADF imaging depends on the sample thickness and especially on the atomic number (Z). Therefore, PS domains having RuO_4 elements were presented much brighter than PMMA domains in the STEM images.

Dynamic Secondary Ion Mass Spectroscopy (DSIMS) measurements were performed on a series of films. Films possessing thicknesses of ~250 nm were cast on the silicon and silicon nitride substrates. After annealing the samples under the same conditions to the previous experiments, ~ 30 nm blended films of 40:60 deuterated PS (Polymer Source Inc., M_w= 85,000 g/mol, M_w/M_n = 2.0) to PS (Pressure Chemical Co., M_w= 288,800 g/mol, M_w/M_n = 1.06) were added as a sacrificial layer on the top of the samples by a floating method. The DSIMS experiments were performed on a Physical Electronics 6650 Quadrupole instrument at the University of California, Santa Barbara, by Dr. Tom Mates. A 6 keV, 100 nA Cs^+ primary ion beam was rastered over a 350 μm x 450 μm area and negative secondary ions of hydrogen, deuterium, carbon, oxygen and silicon were monitored from the center 20 % of the crater area. The sputtering time was converted into the depth scale based on the thickness measured by the spectroscopic ellipsometer and the amount of time spent between interfaces.

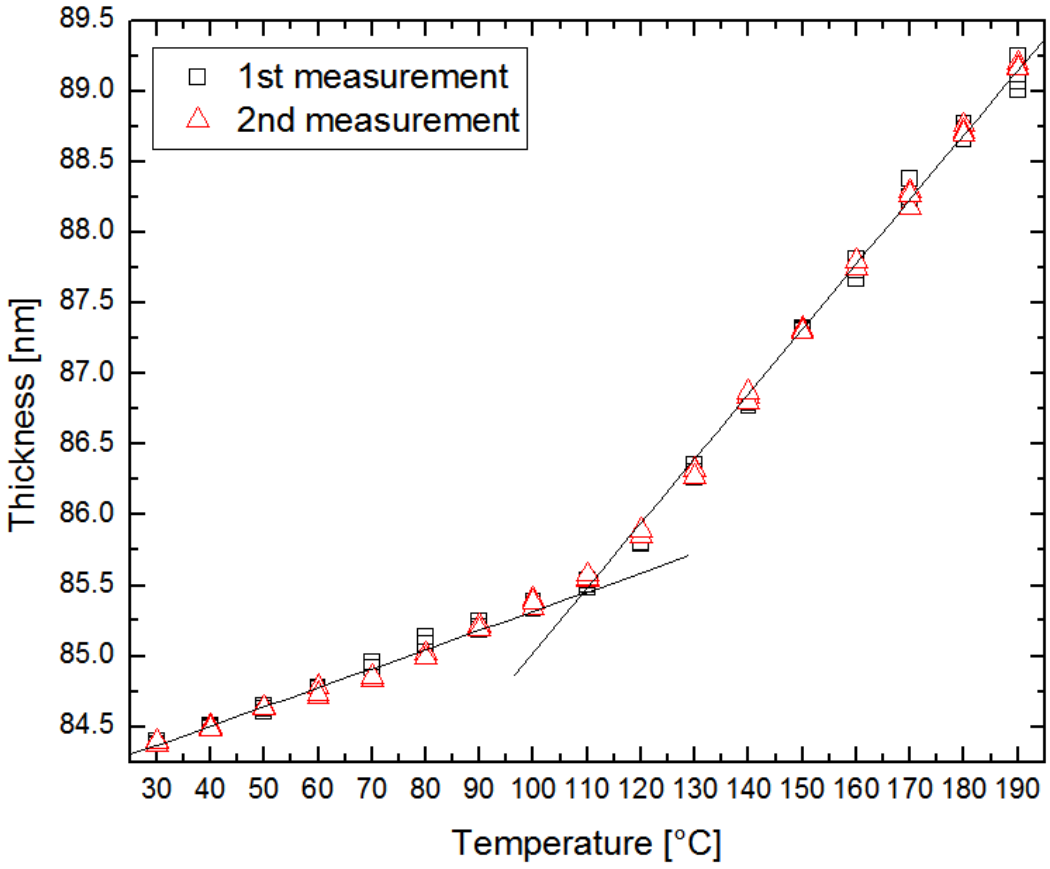

Figure 3.1 The typical dependence of thickness upon the surrounding temperature, shown via ellipsometry measurement. Data for pure PS with the thickness of 84.4 nm were plotted here. T_g was identified by the intersection of two extrapolated lines of 1st measurement (unfilled squares). A 2nd measurement (unfilled triangles) was subsequently performed to examine the repeatability and the oxidative degradation effects.

3.3 Results and Discussion

The film thickness dependences of the glass transition temperatures for various mixtures of PS with PS-b-PMMA, by weight (0 %, 3 %, 10 %, 20 % and 100 %) are plotted in Figure 3.2. As shown in this figure, the T_gs of the pure PS samples thinner than ~ 50 nm decrease with decreasing thickness; otherwise they remain independent of thickness for thicker films. These data are consistent with the published data on this system [30, 31]. With the addition of only 3 *wt*.% ($\omega = 0.03$) of the PS-b-PMMA diblock to PS, the T_gs increase by ~ 10 °C ($T_g \approx 116$ °C), throughout thicknesses of up to ~ 250 nm. For thicker films the T_g approaches that of bulk PS, as expected; 3 *wt*.% PS-b-PMMA is insufficient to change the average T_g of a bulk film. The glass transition temperatures of films containing 10 *wt*.% copolymer are independent of film thickness. When the samples contain 20 *wt*.% copolymer, the opposite trend occurs; T_g increases with decreasing h, for $h < 50$ nm. Note that for thinnest samples, e.g.: $h \approx 20$ nm, the overall increase of T_g is approximately 35 degrees; this is of significance as the PMMA component of the copolymer accounts for only ~ 6 *wt*.% of the sample.

An assessment of the effectiveness of the copolymer toward changing the average glass transition temperatures of the films may be made by considering the T_g vs. ω dependence of a film of thickness $h \approx 120$ nm. The data in Figure 3.3 reveals that the T_g of the mixture increases by over 10 degrees, to the value of the PS-b-PMMA copolymer, with only 3 *wt*.% PS-b-PMMA. It is well known that PS-b-PMMA diblock copolymers in PS hosts segregate to the silicon substrate [42, 46]. The PMMA blocks possess a strong affinity for the native silicon oxide, through hydrogen bonding (O-H ··· O). The copolymers subsequently form a brush layer. Oslanec et al. [46] reported that the driving

force for PS-b-PMMA adsorption is high enough to saturate the substrate with PS-b-PMMA chains if $P > 2N_{PS}$ where P and N_{PS} are the degrees of polymerization of the PS homopolymer and the PS block of the PS-b-PMMA, respectively. Since P (= 5673) >> $2N_{PS}$ (= 886), there exists a sufficiently strong driving force in our system. According to Green and Russell [42], the number of copolymer chains per unit area at the interface increases rapidly with concentration of the copolymers up to certain critical concentration and becomes independent above that concentration. They concluded that this is due to the saturation at the substrate by the brush layer. Therefore, we can infer from the foregoing that the rapid increase of T_g with weight fraction of the diblock copolymer is associated with the interfacial segregation of the diblock copolymer.

The increase in T_g due to the interfacial segregation of the copolymers can be understood from the following. The mobility and configurational freedom, of the copolymer chains near the substrate decreases due to this strong interaction, which in the language of dynamic heterogeneity, leads to an increase in the fraction of "slow" domains in that region, and hence the system. Once copolymers saturate the substrate, or their substrate coverage reaches a certain threshold, the T_gs become independent of the concentration (Figure 3.3). This plateau in T_g occurs before the brush layer is completely formed; this becomes evident later when we discuss the morphology of the samples.

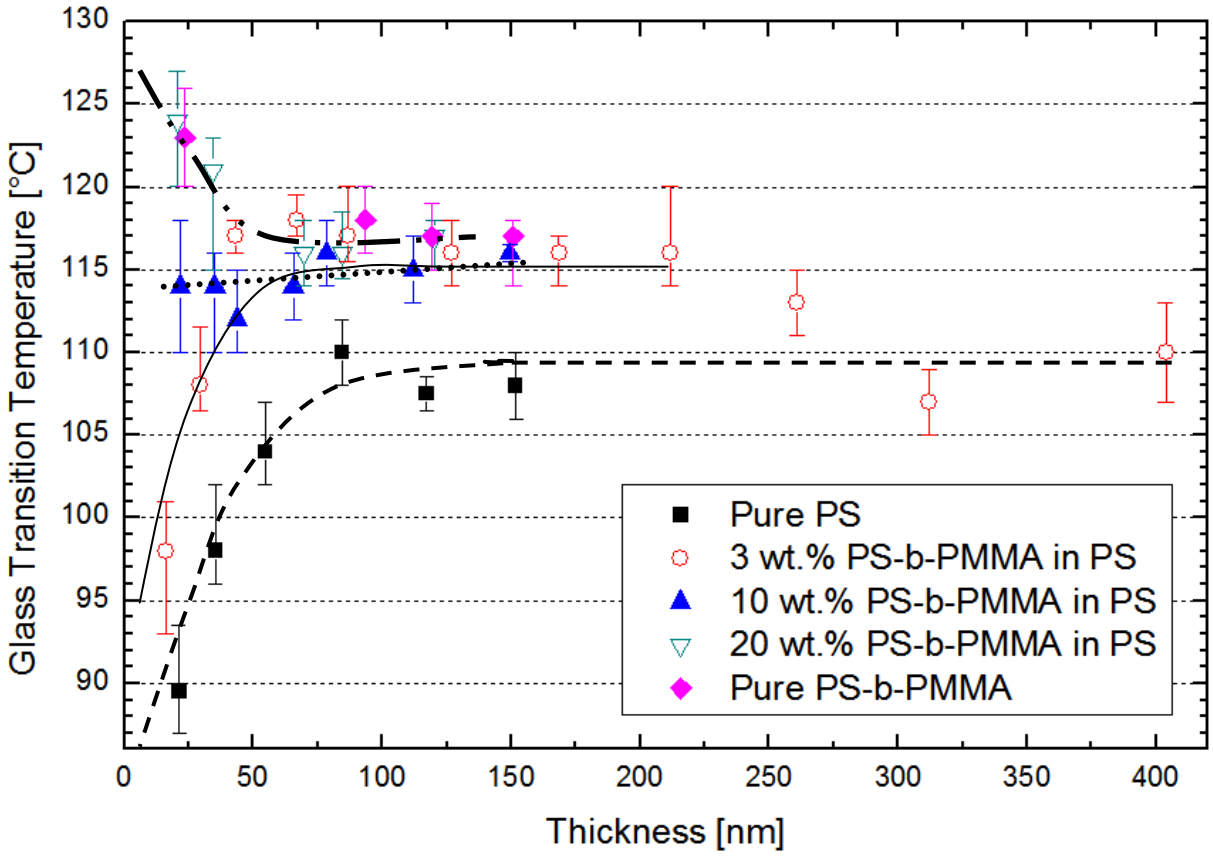

Figure 3.2 The film thickness dependence of the glass transition temperature for pure PS-b-PMMA (filled rhombi), pure PS (filled squares) and three different mixtures of PS-b-PMMA and PS. The lines are guides to the eye.

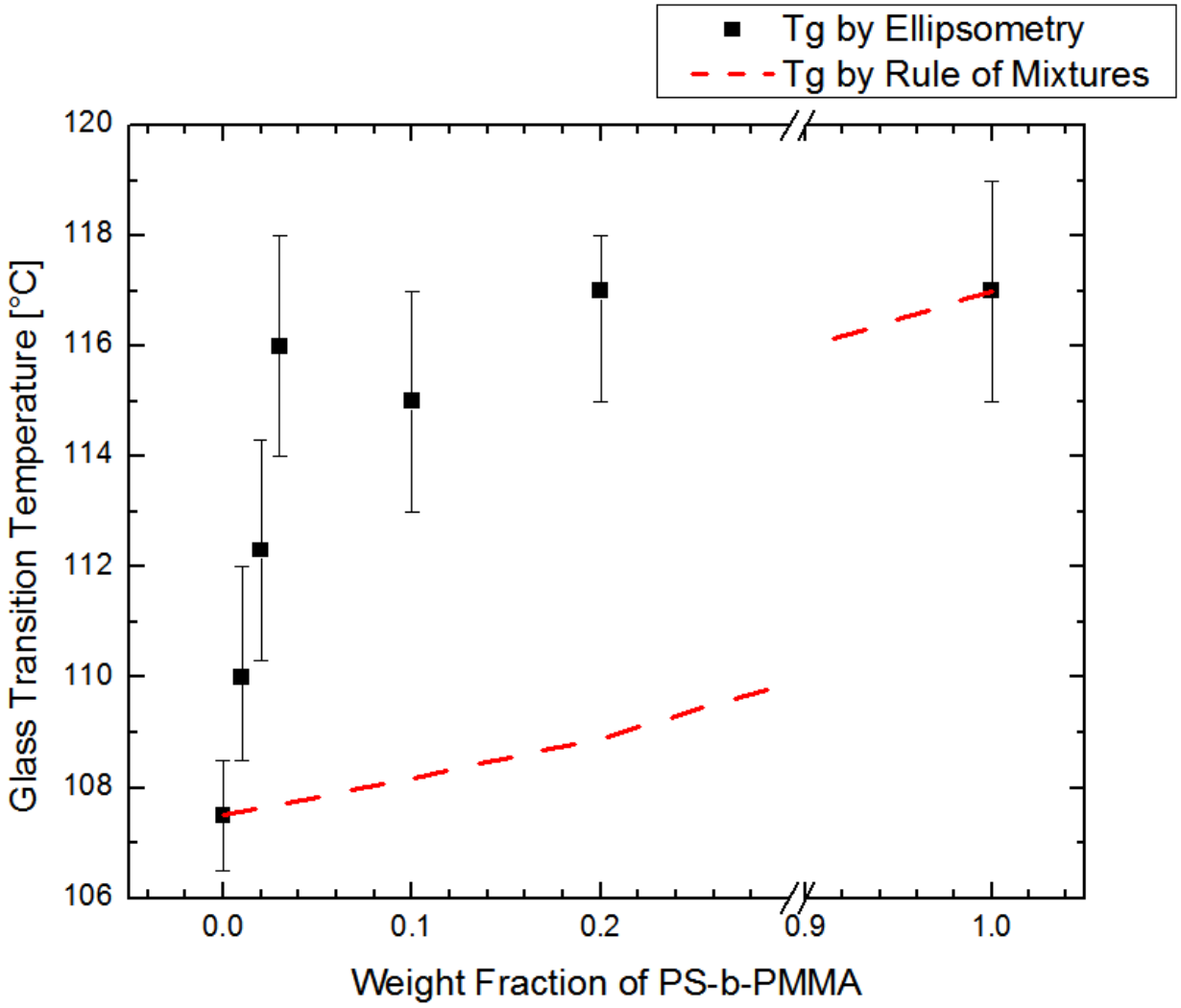

Figure 3.3 The glass transition temperature vs. weight fraction of PS-b-PMMA diblock copolymer in the PS-b-PMMA/PS blend at constant thickness, ~ 120 nm. The broken line (- - -) represents the calculated T_gs by the rule of mixtures based on the volumetric ratio of PMMA blocks to the total mixtures.

It is appropriate to consider the morphology of the samples in order to get a better appreciation of the structure-property behavior of this system. Due to the incompatibility between the PS and the PMMA components, the copolymers are anticipated to form micelles in the bulk at very low concentrations, far less than 1 %, as the critical micelle concentration (cmc), $\phi_{cmc} \sim \exp(\chi N)$. However, we see no evidence of micelle formation in samples thinner than 100nm, even with copolymer concentrations of 20 *wt*.%.

Before we explain the basic reasons for the absence of micelles in these thin ($h <$ ~ 100 nm) films, we begin by considering the morphology of thick samples ($h \approx 250$ nm) in which micelles are observed. Theoretical estimates of the micelle sizes are made and compared with the estimates. Silicon nitride (SiN) membranes (grown by low pressure chemical vapor deposition (LPCVD)) were used for the substrates in the STEM studies to learn about micelle formation because the polymer film does not have to be removed from the SiN substrate for the STEM observations. This is not an issue as the degree of segregation of copolymers in the SiN and SiO_x/Si substrates is virtually identical as shown in SIMS profile in Figure 3.4. The narrow peak at the outer, free, surface is due to micelles, with the PMMA core and PS corona chains. In Figure 3.4, the oxygen peak of the brush layer is nearly hidden due to the strong signal from the native oxide of the substrate at $d \approx 250$ nm, though a kink is evident at $d \approx 240$ nm. The peak at $d \approx 220$ nm represents a layer of micelles; its full width at half maximum exceeds the length of PMMA chains. Below, the micellar dimensions are estimated from a calculation of the micelle size, which would confirm that it does not represent the brush layer.

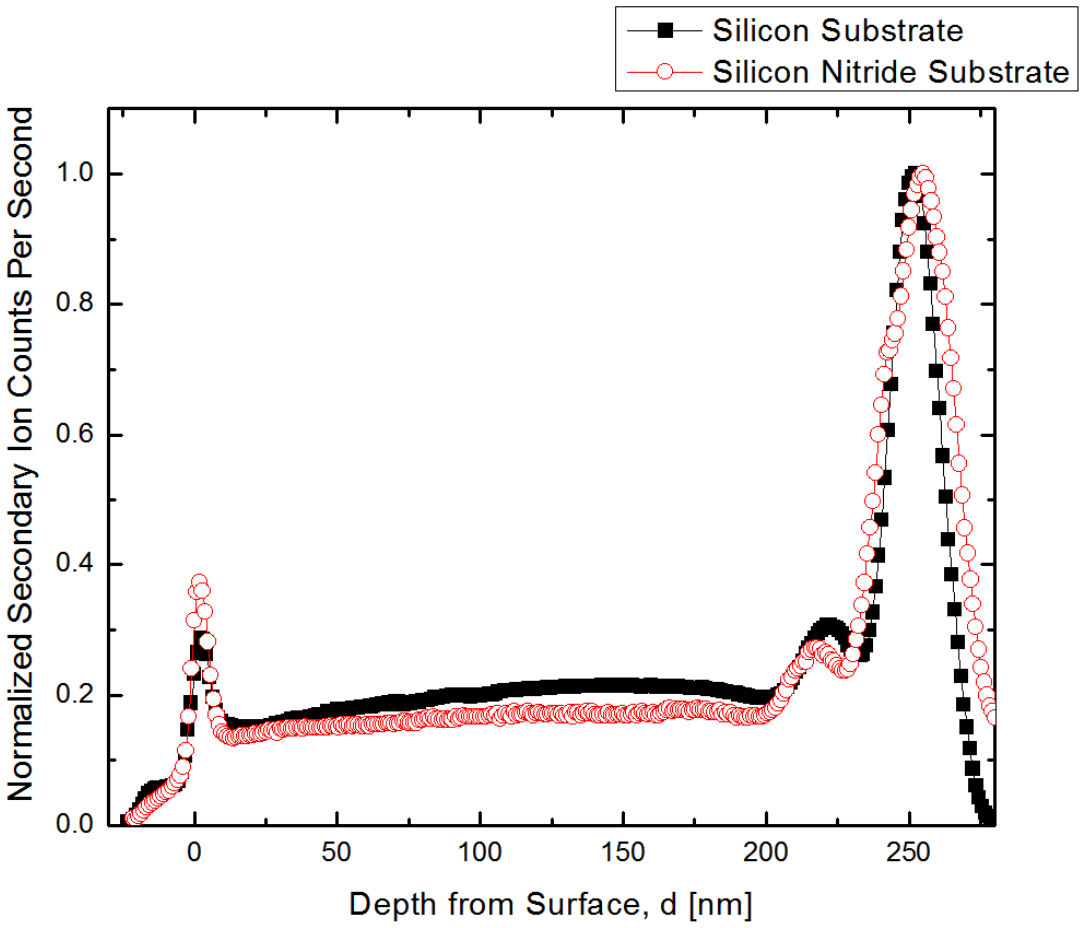

Figure 3.4 Normalized depth profiles of ^{16}O in 20 *wt*.% PS-b-PMMA samples, supported by a silicon substrate (filled squares) and by a silicon nitride substrate (unfilled circles). ~ 30 nm sacrificial layers are placed on top of the samples which have ~ 250 nm in thickness. Here, $d \approx 0$ nm and 250 nm denote the interfaces of sacrificial layer/ sample surface and sample/ substrate, respectively.

Figures 3.5a ~ 3.5c show the STEM images of RuO_4-stained films of thickness h ≈ 250 nm. In the images, the PMMA blocks of the copolymer appear darker than the PS because RuO_4 selectively oxidizes the PS component. The STEM image of the 20 *wt*.% PS-b-PMMA thick film, before annealing, is shown in Figure 3.5a; the sample appears homogeneous. However, the images for the annealed samples (Figures 3.5b and 3.5c) possess dark spots, revealing the cores of micelles. This means that micelles in Figures 3.5b and 3.5c formed during annealing. The average radius of a micelle core (R_{core}), measured via STEM images is approximately 15 nm yet the shortest distance between the centers of two adjacent, densely packed micelles is about 44 nm. Therefore, the radius of the micelle ($R_{micelle}$) may be about 22 nm, based on the supposition that these two neighboring micelles are in contact each other without deformation. We now briefly note that the bright spots in Figure 3b are over-stained domains, which are sometimes observed in the STEM images of the PS homopolymer samples. The grey background includes both the PS homopolymer matrix and the PS-b-PMMA brush layer near the substrate.

The size of the micelles can be now estimated theoretically and compared with our observations. We begin by noting that the equilibrium structure of a micelle is determined by the minimization of the total free energy which can be approximated as a sum of three dominant contributions [47, 54, 56, 57],

$$F = F_{core} + F_{corona} + F_{interface} \tag{3.1}$$

where the first two terms represent the conformational free energies (or the stretching free energies) of the core and corona blocks and the last term is the free energy of the interface separating the core and the corona. Since the molecular weight of the PS block

in PS-b-PMMA for our system, 46,100 g/mol, is much smaller than the molecular weight of the homopolymer PS, 590,000 g/mol, we can assume that the micelle possesses a dry corona layer; in other words, the corona layer, which consists of the PS blocks of PS-b-PMMA, has none or very little PS homopolymer. With the assumption that the interfacial region between the corona and the core is narrow compared to the corona and the core widths, and with the above assumption, Shull et al. [48] derived equations describing the radius of the spherical micelle. These equations may be re-written as

$$R_{\text{micelle}}^3 = \frac{3}{4\pi} \cdot \frac{\sqrt{\chi} N_{\text{cp}} N_{\text{core}} a^3}{0.337 - 0.194 g^{1/3}} \tag{3.2}$$

$$R_{\text{core}}^3 = \frac{3}{4\pi} \cdot \frac{\sqrt{\chi} N_{\text{core}}^2 a^3}{0.337 - 0.194 g^{1/3}} \tag{3.3}$$

, where R_{micelle} and R_{core} are the radii of a micelle and a core, N_{cp} and N_{core} are the degrees of polymerization of the overall copolymer and its core segments and g is the ratio of N_{core} to N_{cp}, i.e., $N_{\text{core}}/N_{\text{cp}}$. a and χ denote the statistical segment length and the Flory-Huggins interaction parameter between the core segments and the corona segments, respectively. Using Equation (3.2) and (3.3) and the set of parameters; N_{cp} = 651, N_{core} = 208, g = 0.3195, χ = 0.0379[58], a = 6.9Å [59] (Here, χ and a were calculated by assuming that they are independent of the symmetry of the diblock copolymer), $R_{\text{micelle}} \approx$ 21.6 nm and $R_{\text{core}} \approx$ 14.8 nm are obtained for the radii of the micelle and its core, respectively. These values are comparable to the values estimated by the STEM measurements.

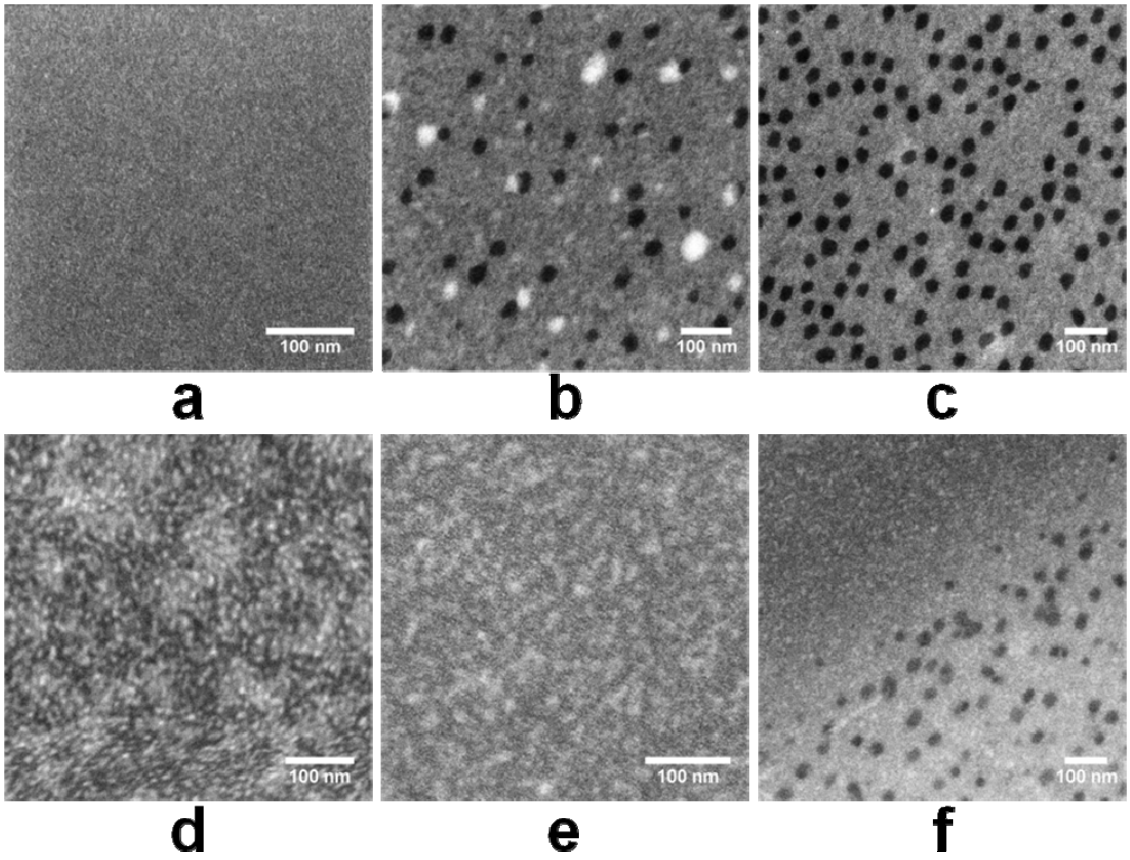

Figure 3.5 STEM images of RuO_4-stained samples on the silicon nitride window grids: **a**, *h* (thickness) ≈ 250 nm, 20 *wt*.% PS-b-PMMA as-cast sample; **b**, *h* ≈ 250 nm, 3 *wt*.% PS-b-PMMA sample; **c**, *h* ≈ 250 nm, 20 *wt*.% PS-b-PMMA sample; **d**, *h* ≈ 19 nm, 3 *wt*.% PS-b-PMMA sample; **e**, *h* ≈ 19 nm, 20 *wt*.% PS-b-PMMA sample; **f**. *h* ≈ 19 nm, 20 *wt*.% PS-b-PMMA sample with thickness gradient. Samples **b** ~ **f** were vacuum-annealed at 120 °C for 16 hrs.

We now discuss the reason the cmc in thin films is considerably higher than the bulk. No micelles were observed in 3 *wt*.% and 20 *wt*.% PS-b-PMMA thin film ($h \approx 20$ nm) samples (see Figures 3.5d and 3.5e). In fact, no micelles are formed in films with thicknesses $h < 100$ nm. This can be rationalized by the fact that PS-b-PMMA chains in the thin films are initially forced to form the brush layer at the substrate before forming micelles, due to the stronger driving force for interfacial segregation; the PMMA component of the copolymer resides at the oxide layer. The "brush" layer would be approximately 22 nm, based on the average diameter of the micelle. Therefore, a sample of $h \approx 100$ nm thick containing a 22 nm brush layer would need to contain roughly 22 % (22 nm/100 nm) of copolymer chains to create a saturated brush layer. Since the thinner samples we examined had 20 % or smaller weight fractions of chains, the brush layer remained unsaturated; hence no micelle formation. These observations can be confirmed by considering Figure 3.5f which shows the image of the 20 *wt*.% PS-b-PMMA sample with thickness gradient. The dark grey area in the upper left corner of the image where the film thickness is ~ 19 nm contains no micelles, as expected. However, in the lower right of the image where the thickness of the film increases ($h > 100$ nm), micelles exist. Before ending this section, it must be emphasized that when the films are sufficiently thick, the influence of the interface should diminish considerably and the behavior should approach that of the bulk, wherein ϕ_{cmc} should decrease considerably, as would the T_g. In the case of the 3 *wt*.% PS-b-PMMA, the T_g approaches the bulk T_g for $h > \sim 250$ nm (cf. Figure 3.2). With regard to the effect on micelle formation, we see evidence of micelles in the 250 nm samples containing 3 *wt*.% PS-b-PMMA, where 3 *wt*.% PS-b-PMMA is not sufficient to form a complete, saturated, brush layer. The behavior of films of this

thickness, and beyond, is clearly bulk-like behavior. We further anticipate that as the interaction parameter, χ, increases in magnitude this will enhance micelle formation in the interior of the system and will compete with the interfacial segregation. It should be clear that in sufficiently thin films, ϕ_{cmc} is orders of magnitude larger than the bulk.

A mechanism for understanding the T_g dependence on h, based on the dynamic heterogeneity model, might be as follows. Recall that for freely standing films, the chains in the vicinity of the free surfaces possess a higher degree of configurational freedom and this has the effect of increasing the fraction of "fast" domains in the sample. This effect largely accounts for the fact that T_g always decreases with decreasing h in freely standing films; the difference in the percolation threshold in 3D and quasi 2D notwithstanding. When one interface is constrained, the fraction of "slow" domains increases. Under these conditions it is the relative competition between the "fast" domains, associated with the free surface, and the "slow" domains, associated with the substrate interactions, that determine whether T_g increases or decreases with decreasing h. If the interactions between the chains and the substrate are weak, i.e.: non-wetting, as is the case for PS and SiO_x/Si, then the dynamics associated with the "fast" domains dominate and T_g decreases with decreasing h. However, in cases such as PMMA or TMPC on SiO_x/Si, where the chain/substrates are strong, the effective number of "slow" domain induced in the system is sufficiently large and T_g increases with decreasing h. In our system, the copolymers segregate to the interface due to the PMMA/SiO_x/Si interactions; the end result is an enhancement of the average T_g of the sample.

3.4 Conclusion

Film thickness dependencies of the average glass transition temperatures of thin polymer films are well documented. Typically, below a threshold film thickness, T_g may increase or decrease with decreasing h, depending on the polymer-substrate system (T_g decreases with decreasing h for freely standing systems). In the PS/SiO_x/Si system, T_g decreases with decreasing h, for $h < 50$ nm. We showed that with the addition of small quantities of an A-b-B diblock copolymer, the thickness dependence of T_g could be "tailored". Changes in T_g of as much as 35 degrees could be accomplished with the addition of the copolymer. The increase is associated with the increasing segregation of the diblock copolymers to the substrate to lower the free energy. The strong attraction of the PMMA for the oxide layer limits the configurational freedom, and the mobility, of the chains in the vicinity of the interface. Based on the dynamic heterogeneity model, this has the effect of increasing the fraction of "slow" domains in the system and hence the increase of T_g. There is a length scale over which the influence of the interfaces on T_g becomes unimportant, and this becomes clear from the following. The influence of the interfacial activity of the copolymers on the average T_g of the 3 *wt*.% PS-b-PMMA samples extends to samples with thickness on the order of 250 nm. Beyond this thickness, the T_g of the system becomes equivalent to the T_g of a bulk system, where the small concentration of copolymers (3 *wt*.%) is not sufficient to change the T_g of the system.

We also showed that the critical micelle concentration in thin films ($h < 100$ nm) is orders of magnitude larger than the bulk. At equilibrium, diblock copolymers segregate to the substrate due to the preferential attraction of the PMMA component. The formation of the brush layer ensures the chemical potential of copolymer chains is the

same throughout the system at equilibrium. The time scale for reaching equilibrium will depend on the film thickness and on χN. Further, there is the aforementioned length scale (film thickness effect) beyond which the system becomes bulk-like and so micelles are formed even at lower concentration sufficiently far from the substrate. In our system, the influence of the interface on the cmc of the system diminishes for films much thicker than 100 nm. In general, the critical micelle concentration of thin film homopolymer/copolymer systems is larger than the bulk due to the segregation of copolymers to an interface. A further study involving other systems is underway to develop some scaling rules.

3.5 References

1. Tang, C.W. and S.A. VanSlyke, *Organic electroluminescent diodes.* Applied Physics Letters, 1987. **51**(12): p. 913-15.

2. Baldo, M.A., M.E. Thompson, and S.R. Forrest, *High-efficiency fluorescent organic light-emitting devices using a phosphorescent sensitizer.* Nature, 2000. **403**(6771): p. 750-753.

3. Tang, C.W., *Two-layer organic photovoltaic cell.* Applied Physics Letters, 1986. **48**(2): p. 183-5.

4. Yu, G., et al., *Polymer photovoltaic cells: Enhanced efficiencies via a network of internal donor-acceptor heterojunctions.* Science (Washington, D. C.), 1995. **270**(5243): p. 1789-91.

5. Peumans, P., S. Uchida, and S.R. Forrest, *Efficient bulk heterojunction photovoltaic cells using small-molecular-weight organic thin films.* Nature, 2003. **425**(6954): p. 158-162.

6. Sheraw, C.D., et al., *Organic thin-film transistor-driven polymer-dispersed liquid crystal displays on flexible polymeric substrates.* Applied Physics Letters, 2002. **80**(6): p. 1088-1090.

7. Heeger, P.S. and A.J. Heeger, *Making sense of polymer-based biosensors.* Proceedings of the National Academy of Sciences of the United States of America, 1999. **96**(22): p. 12219-12221.

8. de Gennes, P.G., *Wetting: Statics and dynamics.* Reviews of Modern Physics, 1985. **57**(3): p. 827.

9. Besancon, B.M. and P.F. Green, *Moving fronts in entangled polymeric films.* Physical Review E (Statistical, Nonlinear, and Soft Matter Physics), 2004. **70**(5): p. 051808-8.

10. Alsten, J.V. and S. Granick, *Shear rheology in a confined geometry: Polysiloxane melts.* Macromolecules, 1990. **23**(22): p. 4856-62.

11. Hu, H.W. and S. Granick, *Viscoelastic dynamics of confined polymer melts.* Science (Washington, DC, United States), 1992. **258**(5086): p. 1339-42.

12. Frank, B., et al., *Polymer mobility in thin films.* Macromolecules, 1996. **29**(20): p. 6531-6534.

13. Zheng, X., et al., *Reptation dynamics of a polymer melt near an attractive solid interface.* Physical Review Letters, 1995. **74**(3): p. 407-10.

14. Zheng, X., et al., *Long-range effects on polymer diffusion induced by a bounding interface.* Physical Review Letters, 1997. **79**(2): p. 241-244.

15. Fukao, K. and Y. Miyamoto, *Glass transition temperature and dynamics of alpha-process in thin polymer films.* Europhysics Letters, 1999. **46**(5): p. 649-654.

16. Fukao, K. and Y. Miyamoto, *Glass transitions and dynamics in thin polymer films: Dielectric relaxation of thin films of polystyrene.* Physical Review E, 2000. **61**(2): p. 1743-1754.

17. Serghei, A., et al., *Molecular dynamics of hyperbranched polyesters in the confinement of thin films.* Eur Phys J E Soft Matter FIELD Full Journal Title:The European physical journal. E, Soft matter, 2005. **17**(2): p. 199-202.

18. Serghei, A., et al., *Discrepancies in the characterization of the glass transition in thin films of hyperbranched polyesters.* Journal of Polymer Science, Part B: Polymer Physics, 2006. **44**(20): p. 3006-3010.

19. Orts, W.J., et al., *Observation of temperature dependent thicknesses in ultrathin polystyrene films on silicon.* Physical Review Letters, 1993. **71**(6): p. 867-70.

20. Wallace, W.E., J.H. van Zanten, and W.L. Wu, *Influence of an impenetrable interface on a polymer glass-transition temperature.* Physical Review E: Statistical Physics, Plasmas, Fluids, and Related Interdisciplinary Topics, 1995. **52**(4-A): p. R3329-R3332.

21. van Zanten, J.H., W.E. Wallace, and W.-l. Wu, *Effect of strongly favorable substrate interactions on the thermal properties of ultrathin polymer films.* Physical Review E: Statistical Physics, Plasmas, Fluids, and Related

Interdisciplinary Topics, 1996. **53**(3): p. R2053-R2056.

22. Tsui, O.K.C., T.P. Russell, and C.J. Hawker, *Effect of interfacial interactions on the glass transition of polymer thin films.* Macromolecules, 2001. **34**(16): p. 5535-5539.

23. Kanaya, T., et al., *Annealing effects on thickness of polystyrene thin films as studied by neutron reflectivity.* Polymer, 2003. **44**(14): p. 3769-3773.

24. DeMaggio, G.B., et al., *Interface and surface effects on the glass transition in thin polystyrene films.* Physical Review Letters, 1997. **78**(8): p. 1524-1528.

25. Roth, C.B., et al., *Eliminating the enhanced mobility at the free surface of polystyrene: Fluorescence studies of the glass transition temperature in thin bilayer films of immiscible polymers.* Macromolecules, 2007. **40**(7): p. 2568-2574.

26. Sills, S., et al., *Interfacial glass transition profiles in ultrathin, spin cast polymer films.* J Chem Phys FIELD Full Journal Title:The Journal of chemical physics, 2004. **120**(11): p. 5334-8.

27. Forrest, J.A., et al., *Effect of free surfaces on the glass transition temperature of thin polymer films.* Physical Review Letters, 1996. **77**(10): p. 2002-2005.

28. Forrest, J.A., K. Dalnoki-Veress, and J.R. Dutcher, *Interface and chain confinement effects on the glass transition temperature of thin polymer films.* Physical Review E: Statistical Physics, Plasmas, Fluids, and Related Interdisciplinary Topics, 1997. **56**(5-B): p. 5705-5716.

29. Dalnoki-Veress, K., et al., *Molecular weight dependence of reductions in the glass transition temperature of thin, freely standing polymer films.* Physical Review E: Statistical, Nonlinear, and Soft Matter Physics, 2001. **63**(3-1): p. 031801/1-031801/10.

30. Keddie, J.L., R.A.L. Jones, and R.A. Cory, *Interface and surface effects on the glass-transition temperature in thin polymer films.* Faraday Discussions, 1994. **98**(Polymers at Surfaces and Interfaces): p. 219-30.

31. Keddie, J.L., R.A.L. Jones, and R.A. Cory, *Size-dependent depression of the glass transition temperature in polymer films.* Europhysics Letters, 1994. **27**(1): p. 59-64.

32. Grohens, Y., et al., *Glass transition of stereoregular poly(methyl methacrylate) at interfaces.* Langmuir, 1998. **14**(11): p. 2929-2932.

33. Kawana, S. and R.A.L. Jones, *Character of the glass transition in thin supported polymer films.* Physical Review E: Statistical, Nonlinear, and Soft Matter Physics, 2001. **63**(2-1): p. 021501/1-021501/6.

34. Pham, J.Q. and P.F. Green, *The glass transition of thin film polymer/polymer blends: Interfacial interactions and confinement.* Journal of Chemical Physics, 2002. **116**(13): p. 5801-5806.

35. Pham, J.Q. and P.F. Green, *Effective T_g of confined polymer-polymer mixtures. influence of molecular size.* Macromolecules, 2003. **36**(5): p. 1665-1669.

36. Pham, J.Q., et al., *Glass transition of polymer/single-walled carbon nanotube composite films.* Journal of Polymer Science, Part B: Polymer Physics, 2003. **41**(24): p. 3339-3345.

37. Kim, J.H., J. Jang, and W.-C. Zin, *Thickness dependence of the glass transition temperature in thin polymer films.* Langmuir, 2001. **17**(9): p. 2703-2710.

38. Torres, J.A., P.F. Nealey, and J.J. de Pablo, *Molecular simulation of ultrathin polymeric films near the glass transition.* Physical Review Letters, 2000. **85**(15): p. 3221-3224.

39. Ellison, C.J. and J.M. Torkelson, *The distribution of glass-transition temperatures in nanoscopically confined glass formers.* Nature Materials, 2003. **2**(10): p. 695-700.

40. Long, D. and F. Lequeux, *Heterogeneous dynamics at the glass transition in van der Waals liquids, in the bulk and in thin films.* European Physical Journal E: Soft Matter, 2001. **4**(3): p. 371-387.

41. Besancon, B.M., C.L. Soles, and P.F. Green, *Glass transition of miscible binary polymer-polymer thin films.* Physical Review Letters, 2006. **97**(5): p. 057801/1-057801/4.

42. Green, P.F. and T.P. Russell, *Adsorption of copolymer chains from a melt onto a flat surface.* Macromolecules, 1992. **25**(2): p. 783-7.

43. Budkowski, A., J. Klein, and L.J. Fetters, *Brush formation by symmetric and by highly asymmetric diblock copolymers at homopolymer interfaces.* Macromolecules, 1995. **28**(25): p. 8571-8.

44. Oslanec, R. and H.R. Brown, *Random copolymer adsorption at the polymer melt/substrate interface: Effect of substrate type.* Macromolecules, 2001. **34**(26): p. 9074-9079.

45. Oslanec, R., R.J. Composto, and P. Vlcek, *Black copolymer adsorption at the polymer melt/substrate interface: The effect of matrix competition.* Macromolecules, 2000. **33**(6): p. 2200-2205.

46. Oslanec, R., et al., *Crossover of a block copolymer brush in a polymer melt from a stretched to collapsed conformation.* Physical Review E: Statistical Physics, Plasmas, Fluids, and Related Interdisciplinary Topics, 1997. **56**(3-A): p. R2383-

R2386.

47. Shull, K.R., et al., *Segregation of block copolymers to interfaces between immiscible homopolymers.* Macromolecules, 1990. **23**(22): p. 4780-7.

48. Shull, K.R., et al., *Segregation of block copolymer micelles to surfaces and interfaces.* Macromolecules, 1991. **24**(10): p. 2748-51.

49. Green, P.F. and T.P. Russell, *Segregation of low molecular weight symmetric diblock copolymers at the interface of high molecular weight homopolymers.* Macromolecules, 1991. **24**(10): p. 2931-5.

50. Dai, K.H., E.J. Kramer, and K.R. Shull, *Interfacial segregation in two-phase polymer blends with diblock copolymer additives: The effect of homopolymer molecular weight.* Macromolecules, 1992. **25**(1): p. 220-5.

51. Brown, H.R., *Effect of a diblock copolymer on the adhesion between incompatible polymers.* Macromolecules, 1989. **22**(6): p. 2859-60.

52. Noolandi, J. and K.M. Hong, *Interfacial properties of immiscible homopolymer blends in the presence of block copolymers.* Macromolecules, 1982. **15**(2): p. 482-92.

53. Leibler, L., *Theory of phase equilibria in mixtures of copolymers and homopolymers. 2. Interfaces near the consolute point.* Macromolecules, 1982. **15**(5): p. 1283-90.

54. Leibler, L., *Block copolymers at interfaces.* Physica A: Statistical Mechanics and Its Applications, 1991. **172**(1-2): p. 258-68.

55. Anastasiadis, S.H., I. Gancarz, and J.T. Koberstein, *Compatibilizing effect of block copolymers added to the polymer/polymer interface.* Macromolecules, 1989. **22**(3): p. 1449-53.

56. Birshtein, T.M. and E.B. Zhulina, *Scaling theory of supermolecular structures in block copolymer-solvent systems. 1. Model of micellar structures.* Polymer, 1989. **30**(1): p. 170-7.

57. Shusharina, N.P., P. Linse, and A.R. Khokhlov, *Micelles of diblock copolymers with charged and neutral blocks: Scaling and mean-field lattice approaches.* Macromolecules, 2000. **33**(10): p. 3892-3901.

58. Russell, T.P., R.P. Hjelm, Jr., and P.A. Seeger, *Temperature dependence of the interaction parameter of polystyrene and poly(methyl methacrylate).* Macromolecules, 1990. **23**(3): p. 890-3.

59. McCoy, J.D., et al., *The interfacial thickness of symmetric diblock copolymers: Theory and experiment.* Journal of Chemical Physics, 1998. **108**(7): p. 3023-3027.

CHAPTER 4

POLYMER CHAIN DYNAMICS AND GLASS TRANSITION IN ATHERMAL POLYMER/NANOPARTICLE MIXTURES

Polymer nanocomposites (PNCs), prepared by incorporating nanoparticles within a polymer host, generally exhibit properties that differ significantly from the host, even with small amounts of nanoparticles. A significant challenge is how to tailor the properties of these materials for applications (structural and biomedical to optoelectronic), because PNCs derive their properties from a collective and complex range of entropic and enthalpic interactions. Here, we show that PNCs, prepared from athermal mixtures of polymer chain-grafted gold nanoparticles and unentangled polymer chains, may exhibit increases or decreases in their relaxation dynamics, and viscosity, by over an order of magnitude through control of nanoparticle concentration, nanoparticle size, grafting density and grafting chain degree of polymerization. In addition, we show how the glass transition may also be tailored by up to 10 degrees with the addition of less than 1.0 *wt.*% nanoparticles to the polymer host.

4.1 Introduction

The chain relaxation dynamics and glass transition of polymer nanocomposites (PNCs) are profoundly influenced by the relative strength of the chain-particle interactions and the morphology, particularly the particle dispersion and the interparticle spacing, l_D [1-10]. Sufficiently strong particle-chain enthalpic interactions lead to permanent attachment of chain segments to the nanoparticles. Under these conditions, PNCs have been shown to exhibit two glass transition temperatures, T_gs: one associated with polymer chains far from the nanoparticles, and a second, larger T_g, associated with chains in the vicinity of the particles [1]. Molecular Dynamics (MD) simulations show that the relaxations of chain segments in the immediate vicinity of the particles are necessarily slow compared to those far from the particles [2]. In the absence of permanent attachment of the chains, the system may exhibit a single, yet larger average T_g, accompanied an increase of the longest relaxation time, τ, and hence the viscosity, η, of the system ($\tau \propto \eta$) [3, 4]. In the case of polystyrene (PS)/PS-nanoparticle PNCs, where the interactions are entropic, η has been shown to exhibit a modest decrease under relatively restrictive conditions [5, 6]. Specifically, the η of highly entangled PS hosts decreased by a factor of two for $l_D \leq 2R_g$, where R_g is the radius of gyration of the host chains. In PS/silica (SiO_2) PNC materials, where the PS-SiO_2 interactions are non-wetting, the T_g is documented to decrease appreciably when l_D is smaller than a threshold value [7].

Here, we show that the relaxation dynamics, and the glass transition, of unentangled PS host chains undergo unusually large enhancements, or reductions, in magnitude with the addition of small concentrations of gold nanoparticles onto which PS

chains are grafted. These changes in T_g and τ were induced through careful control of the nanoparticle weight fraction, ϕ, size, D, and grafting chain degree of polymerization, N. This behavior may not be fully reconciled in terms of the conventional free volume framework, nor with chain confinement effects associated with l_D; alternate mechanisms are proposed.

4.2 Experimental Section

A modified version of a standard two-phase arrested precipitation method [11, 12] was used to synthesize gold nanoparticles functionalized with two different thiol-terminated PS (Polymer Source Inc.; M_n = 1,000 g/mol, M_w/M_n = 1.4 and M_n = 50,000 g/mol, M_w/M_n = 1.06). The gold nanoparticles are identified as $AuPS_{10}$, onto which PS chains of N = 10 were grafted and $AuPS_{481}$, onto which PS chains of N = 481 were grafted. A cleaning procedure to remove unbound ligands by precipitating nanoparticles from toluene solutions using methanol was performed ten times. The characterization of resulting PS-capped gold nanoparticles, performed using scanning transmission electron microscope (STEM) and thermogravimetric analysis (TGA), reveals an average Au core diameter of ~ 5 nm and the brush grafting densities of σ = 0.635 for $AuPS_{10}$ and σ = 0.760 for $AuPS_{481}$.

With regard to preparation of nanocomposites, a series of low molecular weight PS (Pressure Chemical Co.; M_w = 5,200 g/mol, M_w/M_n = 1.06) and gold nanoparticle blends with different contents were dissolved in toluene and mixed thoroughly at 1000 rpm with an orbital shaker (MS 3 digital, IKA®). The solutions were dried in air for ~ 2 days and under high vacuum for a day. These samples were subsequently annealed at

75 °C for 2 days to remove residual solvent. We note that moderate annealing temperature was used in order to avoid nanoparticle coarsening which might occur at elevated temperatures, particularly when the interparticle spacing is close. The nanocomposite films with a thickness of ~ 0.3 mm were compression-molded between two brass electrodes at 75 °C for dielectric and dilatometric measurements.

Samples were annealed once more in a nitrogen atmosphere at 75 °C for 18 hours to remove the possibility of water absorption during the sample transfer as well as to eliminate internal stresses. After in-situ annealing, dielectric relaxation measurements were performed using dielectric spectroscopy (DS; Novocontrol Technologies GmbH) in the frequency range from 0.1 Hz to 1 MHz at the temperatures between 310 K and 370 K for PNCs with $AuPS_{10}$ and between 320 K and 390 K for PNCs with $AuPS_{481}$. In addition to the dielectric spectroscopy measurements, simultaneous capacitive dilatometric measurements were performed to determine the T_gs of nanocomposites. This measurement, capacitive scanning dilatometry (CSD), is based on the fact that the temperature dependence of the capacitance C′ is sensitive to the linear thermal expansion of the sample. Experimental and theoretical details can be found elsewhere [13, 14].

Differential scanning calorimetry (DSC) measurements of ~ 10 mg PNCs were performed in a nitrogen atmosphere using a DSC7 (Perkin-Elmer). Each sample was first heated from 20 °C to 160 °C at a rate of 10 °C/min to erase previous thermomechanical history and then quenched to 20 °C at 100 °C/min. A second heating scan from 20 °C to 160 °C was immediately performed at 10 °C/min and T_g was determined as the temperature corresponding to half the complete change in heat capacity. DSC studies were also performed on mixtures of the PS homopolymer (P = 50) and lower molecular

weight PS homopolymer (Pressure Chemical Co.; M_w = 1,241 g/mol, M_w/M_n = 1.07).

Scanning transmission electron microscopy (STEM) was used to examine the dispersion of nanoparticles in the PS matrix before and after the dielectric spectroscopy experiments. Fresh compressed nanocomposite samples were first molded in the epoxy resin and then cross-sectioned using a Reichert-Jung ultracut microtome. Sectioned films were placed on a TEM copper grid and their images were generated in the STEM mode under an accelerating voltage of 200 kV by the JEOL 2010F Analytical Electron Microscope equipped with a high angle annular dark field (HAADF) detector. One of the key findings from STEM observation is that the morphology of our samples did not change during our analysis.

4.3 Results and Discussion

DS, DSC and CSD were used to examine the chain dynamics and T_g of athermal mixtures of unentangled PS, of the degree of polymerization P = 50, with ~ 5 nm gold nanoparticles onto which thiol-terminated PS ligands (of varying degrees of polymerization) were grafted (i.e., $AuPS_{10}$ and $AuPS_{481}$).

PNC materials containing $AuPS_{10}$ nanoparticles exhibited substantially lower T_gs than pure PS, as shown in Figure 4.1, where $\Delta T_g(\phi) = T_g(\phi) - T_g^{PS}$ is plotted as a function of Au weight percent, ϕ. $|\Delta T_g(\phi)|$ increased by an unprecedented 10 degrees for $\phi <$ ~ 1.0 *wt*.%; it decreased, though not substantially, for larger ϕ. Two factors may, at first glance, appear to be responsible for the reduction of T_g: (1) free low molecular weight chains distributed throughout the sample, which have the effect of increasing the free volume, and (2) chain confinements associated with the length scale l_D [5-7, 15].

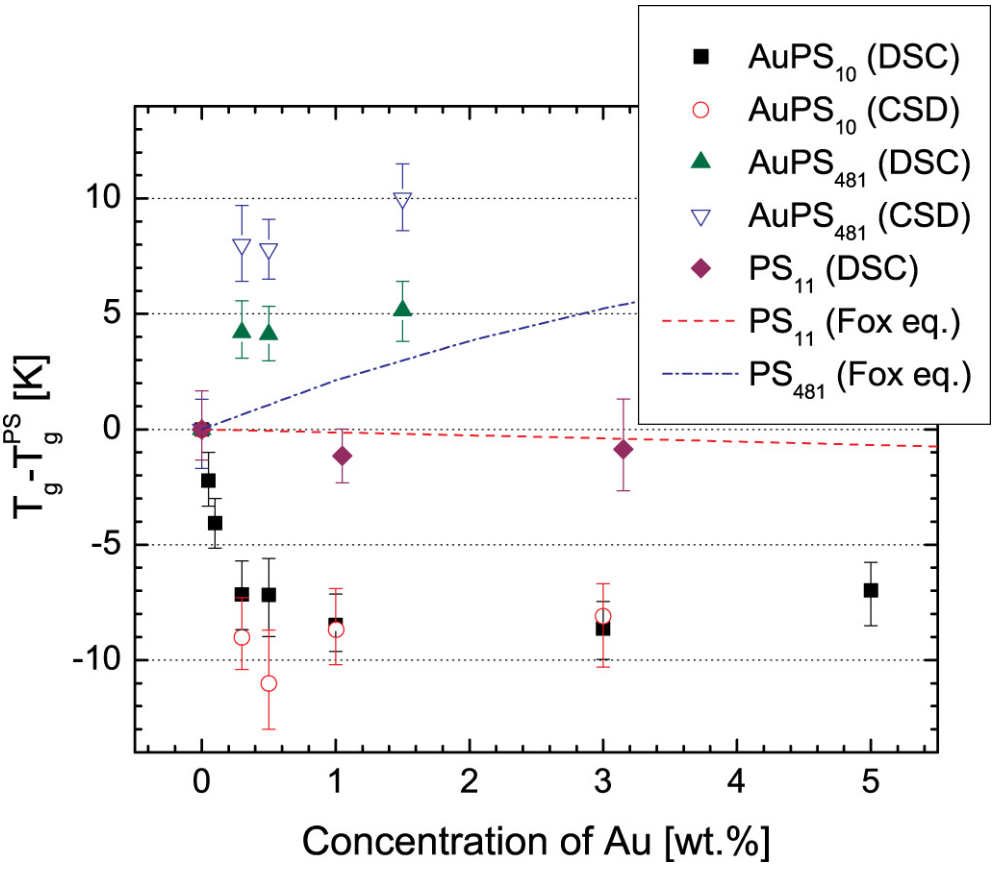

Figure 4.1 Changes in the glass transition temperatures of PS nanocomposites are shown as a function of PS-grafted gold nanoparticle weight fraction. These data were obtained using DSC and CSD techniques. The lines drawn through the data were computed using the Fox equation [17]. The error bars represent the uncertainty, associated with repeating measurements on the same sample or on samples prepared using the same preparation procedure.

The former may be readily eliminated as a viable explanation for the following reason. Oligomeric species, or short chains, are known to have a plasticizing effect, lowering the T_g, on a polymer host. This reduction is known to be due to an increase of the free volume of the system [16] and is well described by the Fox relation [17]. To this end, the T_gs of mixtures of PS host chains of P = 50 with PS chains of N = 11 were measured and plotted in Figure 4.1. These results show that this plasticizing effect is very small. Hence, the large depression of T_g may not be reconciled with this conventional free volume picture.

The T_g data cannot be reconciled with chain confinement effects, due to the proximity of the nanoparticles. STEM images in Figure 4.2 reveal that, overall, the nanoparticles are nearly uniformly distributed throughout the samples, though local aggregates are evident in some regions of PS-AuPS$_{10}$ nanocomposites for which $\phi \geq 1.0$ *wt*.%. The samples with larger concentrations of nanoparticles showed more regions with larger aggregates. The consequences of the aggregation on the dynamics and the T_g are discussed later. The interparticle spacing was estimated using $l_D/D \approx (\varphi_m/\varphi)^{1/3} - 1$, where φ is the volume fraction and φ_m = 0.638 is the maximum random packing volume fraction. Since the values of l_D range from 148 nm to 50 nm, for the highest volume fraction (ϕ = 5.0 *wt*.%, $\varphi \approx 2.9 \times 10^{-3}$), and $R_g \sim 2$ nm ($R_g \approx 0.028 \times \sqrt{M}$ [*nm*]) [18], then $l_D >> 2R_g$, suggesting that effects associated with interparticle spacing should be eliminated as the explanation.

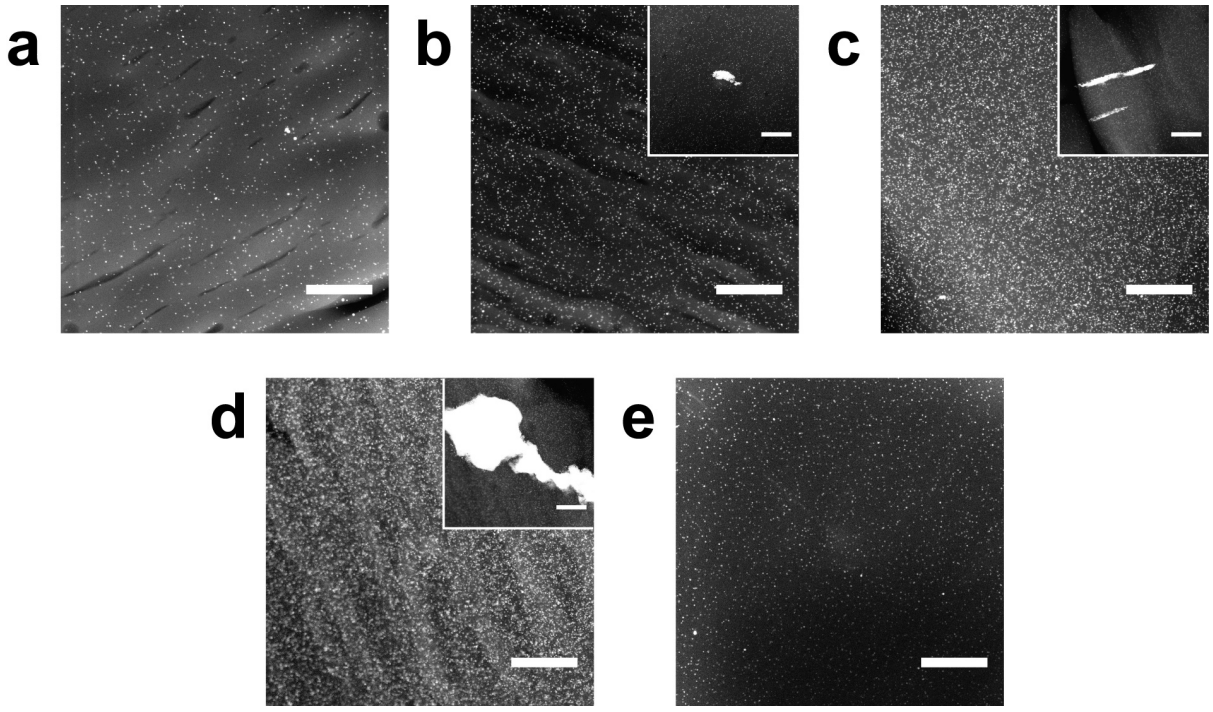

Figure 4.2 STEM images of nanoparticle distributions in ~ 250 nm thick films, microtomed from bulk PNC samples, are shown here: **a**, 0.3 *wt*.% $AuPS_{10}$/PS; **b**, 1.0 *wt*.% $AuPS_{10}$/PS; **c**, 3.0 *wt*.% $AuPS_{10}$/PS; **d**, 5.0 *wt*.% $AuPS_{10}$/PS and **e**, 1.5 *wt*.% $AuPS_{481}$/PS nanocomposites. A scale bar located at the lower right corner of each image is 300nm. Particles at, and below, the surface of the films appear in the images. The inset in each figure shows aggregates, observed at random locations in samples containing 1.0 *wt*.%, or more, nanoparticles.

The decrease of T_g in these systems should be accompanied by reductions in the chain relaxation dynamics. DS measurements (Figure 4.3) reveal that the relaxation dynamics of the PS host chains are reduced, significantly, compared to those of pure PS. The host chain dynamics of nanocomposites containing $\phi \sim$ 0.3 - 0.5 *wt*.% are nearly three orders of magnitude faster than those of pure PS; but decrease in magnitude for larger ϕ, in a manner qualitatively consistent with the changes in T_g.

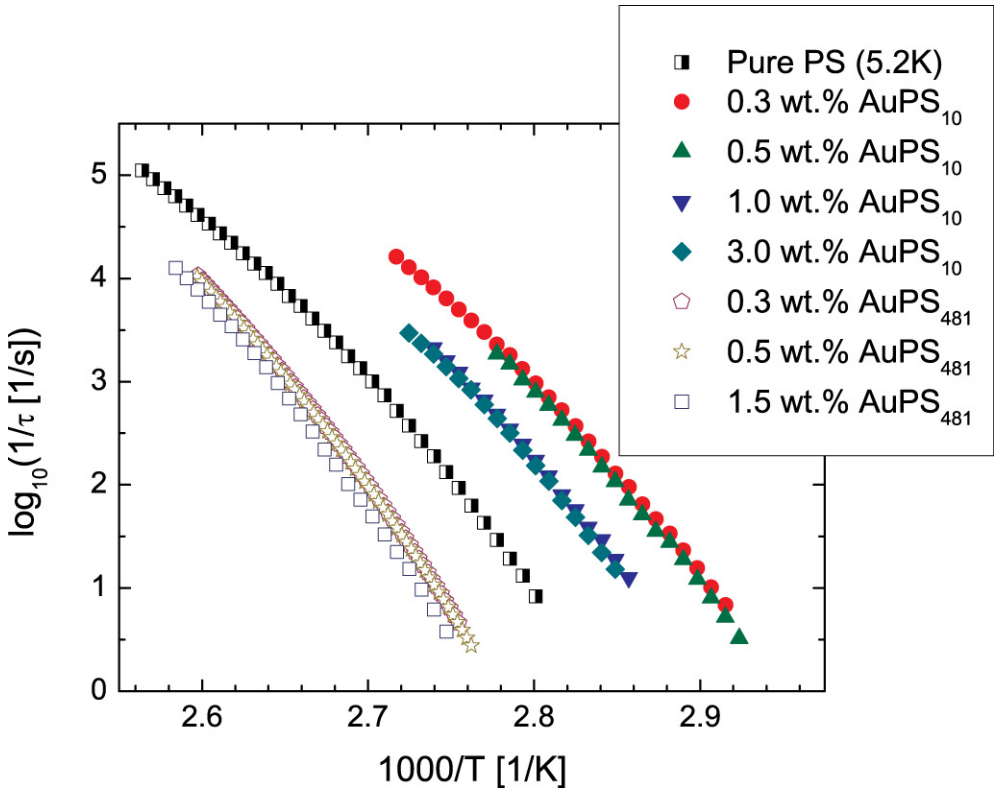

Figure 4.3 Chain dynamics in the nanocomposites. The characteristic relaxation time dynamics, taken from the peak of the dielectric spectra for different nanocomposites, are shown here.

Such large reductions in T_g and τ (or equivalently η) are unexpected. Conventional ideas, based on colloidal systems, suggest that the viscosity of the system should increase with volume fraction: $\eta/\eta_s = 1 + 2.5\varphi + 6.2\varphi^2$, where η_s is the pure solvent viscosity [19]. Secondly, as mentioned earlier, the decrease in τ is far in excess of that anticipated from the decrease of η reported for the PS/PS-nanoparticle PNCs [5, 6]. MD simulations [8] of PNCs predict that the viscosity should decrease, by factor of ~ 2, in systems where polymer chain/nanoparticle interactions are repulsive. The dependence of τ on ϕ, we observe, moreover, is also in contrast to predictions of a weak dependence of η on ϕ.

It is noteworthy that while the PS/$AuPS_{10}$ mixtures exhibited reductions in T_g and enhancements in τ, the other PNC, PS/$AuPS_{481}$, exhibited the opposite behavior; specifically, T_g increased (Figure 4.1) and the relaxation dynamics slowed down (Figure 4.3), accordingly. One potential explanation for this increase in the T_g might be due to the fact that the grafted N = 481 chains possess a higher bulk T_g than that of the host chains (P = 50) [17]. However, the increase in T_g of homopolymer mixtures, estimated by the Fox equation [17], was smaller than the T_g of the PNCs, as shown in Figure 4.1, suggesting that the increase cannot be reconciled within the framework of a conventional free volume analysis.

In systems in which T_g and τ undergo significant change, particularly due to plasticization, the temperature dependence of τ, generally reflected in the "fragility," would reflect appropriate changes. Dynamic fragility is defined as the change in τ with temperature at a reference temperature, T_{ref}, and characterized by a fragility index,

$m = d\log_{10}(\tau)/d(T_{ref}/T)\big|_{T=T_{ref}}$. In polymer systems to which low molecular weight, oligomeric, chains are added, the glass transition would decrease, accompanied by an enhancement of the dynamics; the temperature dependence of the dynamics would exhibit more "fragile" behavior, larger *m*, suggested to be due to an enhancement of the free volume in the system. To this end, we plot τ versus T_{ref}/T in Figure 4.4; the fragility indices are identified in Table 4.1. It is apparent from Figure 4.4a and the data in Table 4.1 that PS mixtures with $AuPS_{10}$ nanoparticle weight fractions of up to $\phi \sim 1.0$ *wt*.% exhibit similar temperature dependencies (comparable fragilities), though the 3.0 *wt*.% sample appears to have a larger fragility index, comparable to that of pure PS. In this 3.0 *wt*.% sample, the aggregation of the nanoparticles is significant compared to the lower weight fraction PNC samples, so the observation is not unexpected. The behavior of the other samples may be associated with an antiplasticization effect, believed to be due to a loss in the free volume, not an increase [20, 21]. The PS/$AuPS_{481}$ nanocomposites, which possess larger T_gs, exhibit virtually identical fragilities regardless of ϕ, and within experimental error, are virtually the same as that of the pure PS host. Our central point is that the significant reductions in T_g and of the magnitudes of the overall dynamics are not accompanied by commensurate changes in the temperature dependencies (fragilities) of the dynamics.

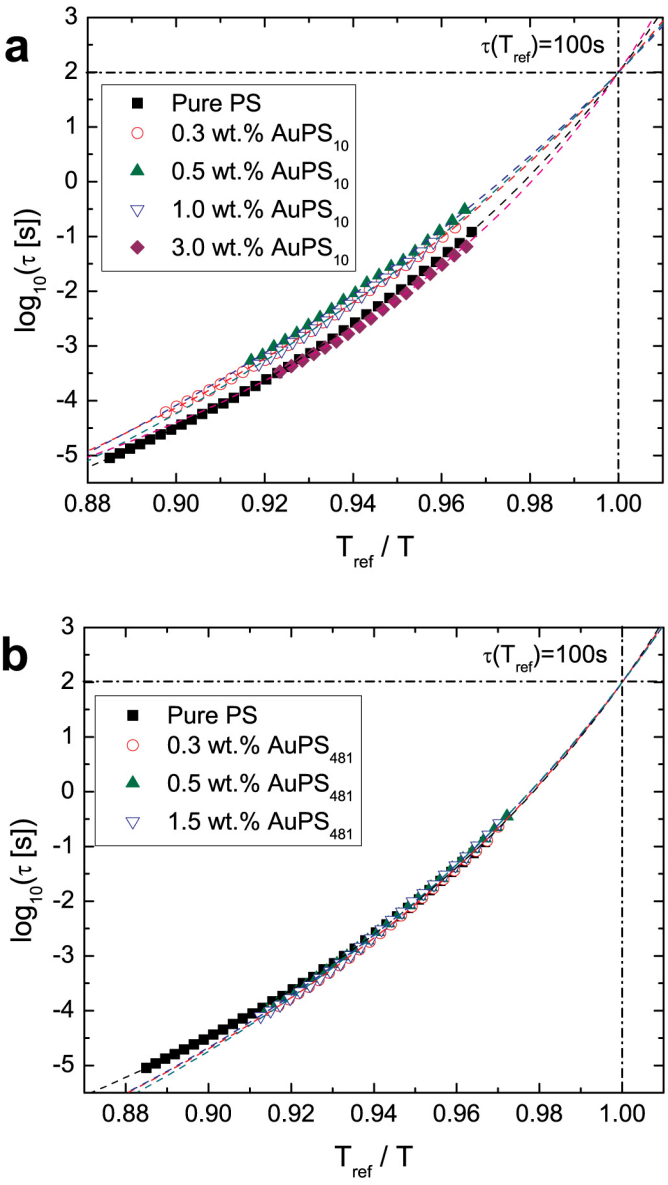

Figure 4.4 Fragility plots for the mixtures of PS-grafted gold nanoparticles and PS. **a**, PS-AuPS$_{10}$, and **b**, PS-AuPS$_{481}$ nanocomposites. The fragility was determined by the slope of the Vogel-Fulcher-Tammann (VFT) fit ($\tau = \tau_0 \exp(B/(T - T_v))$, where τ_0 is the relaxation time at infinite temperature, B is a constant being related to the activation energy and T_v is the Vogel temperature) at $T = T_{ref}$. Here, T_{ref} was defined as the temperature at which the segmental relaxation time equals 100 s.

Table 4.1 Fragility indices (*m*) for nanocomposites of polystyrene-grafted gold nanoparticles and a polystyrene host

Pure PS	$AuPS_{10}$ & PS				$AuPS_{481}$ & PS		
0 *wt*.%	0.3 *wt*.%	0.5 *wt*.%	1 *wt*.%	3 *wt*.%	0.3 *wt*.%	0.5 *wt*.%	1.5 *wt*.%
106.07	89.30	81.58	85.43	118.42	103.04	99.88	98.81

Beginning with a discussion of molecular structure, we provide some insight into the unusual, and contrasting, behavior in the dynamics and glass transition, of these two nanocomposite systems, PS/$AuPS_{10}$ and PS/$AuPS_{481}$. Since the host polymer chains and the ligands of nanoparticles are chemically identical (the Flory-Huggins interaction parameter, $\chi = 0$), entropic interactions are expected to dominate the dynamics, the glass transition and phase behavior of the systems. When chains of degree of polymerization N are grafted onto a flat surface, the interactions between the grafted chains and a melt of chains, of degree of polymerization P, are influenced strongly by the surface grafting density, σ [22]. At low grafting densities, $\sigma\sqrt{N} << (N/P)^2$, the grafted layer is strongly interpenetrated by the host melt P-chains. With increasing σ, the melt chains begin to be excluded from the grafted layer and an interfacial structure begins to be developed between the grafted layer and the free host chains [23]; such a transition occurs at $\sigma\sqrt{N} = (P/N)^{-2}$. In other words, a "dry brush" develops when $\sigma\sqrt{N} > (N/P)^2$. The implication is that a layer of free chains will dewet this grafted layer, autophobic dewetting, because the formation of this interface occurs at a cost of additional free energy. Clearly, manipulation of N, P or σ can lead to whether a "wet" or "dry" brush condition. It should be noted that even the dry brush experiences some degree of

interpenetration by the host chains; this is due to a balance between the translational entropy of the host melt *P*-chains and the elastic energy penalty associated with deformation of the grafted *N*-chains to accommodate the *P*-chains [24]. This penalty diminishes with increasing *N*.

The melt/brush layer interaction is now discussed. We performed experiments involving bi-layers, where a layer of PS chains of $P = 50$ host is placed in contact with a PS layer of $N = 10$, grafted (thiol-terminated PS with grafting density ~ 0.4) onto gold surfaces. The melt layer dewets the PS brush layer, consistent with the behavior of a "dry" brush. However, the *P*-chains are stable on a grafted layer of $N = 481$, consistent with the notion of a "wet brush" scenario. The results of these experiments highlight clear differences between the $N = 10$ and the $N = 481$ grafted chain systems. We, of course, have spherical nanoparticles to consider, and the situation is different, as the curvature of the surfaces is important. The grafted chains are not as crowded at curved interfaces. In this regard, it is important to note that the grafting density of the flat gold surfaces, described above, which is $\sigma \sim 0.4$ is smaller than that of the gold particles, which is $\sigma \sim 0.7$. It is reasonable, therefore, to consider the $AuPS_{10}$ nanoparticle layers to behave as dry brushes, which the host P-chains cannot interpenetrate.

There is an additional effect on the sample morphology, associated with grafted particles. When nanoparticles [24] or nanorods [25] come in proximity, the forces are generally attractive (minimum in the potential energy curves) when the "dry" brush layers come in contact. When the grafted particles are sufficiently far apart, the interactions are essentially zero. It is noteworthy that the attraction between the grafted nanoparticles (dry brush) is, in part, associated with the fact that when they are close, the

homopolymer chains between them are forced to experience rarer configurations, leading to a decrease in conformational entropy. This, in part, is the driving force for the attraction, which increases with increasing P. There is also an additional contribution to the attraction due to van der Waals interactions between the nanoparticles that varies as l/l_D. However, for the same grafting density, the interaction between two grafted nanoparticles is not as attractive as that between two flat surfaces. This is because the chains are less crowded when the surfaces of the particles come into contact.

We now comment on the compositional dependencies of the relaxations of PS-$AuPS_{10}$ mixtures, where dynamics becomes slower for concentrations greater than 1.0 *wt.*%. To understand this, we consider the morphology. As shown in Figure 4.2 the nanoparticles are well distributed throughout the polymer hosts. For $\phi \geq 1.0$ *wt.*% of $AuPS_{10}$ nanoparticles, however, micron-scale aggregates of nanoparticles form in some regions (see insets of Figures 4.2b ~ 4.2d) of the PS host. In addition, the number density of the aggregates and the size of the aggregates increase as the concentration of nanoparticles increases; this is not unexpected based on the discussion above. We note that we see no evidence of nanoparticle coarsening in our experiments; pure gold particles are highly mobile and detachment of the ligands would engender coarsening of the nanoparticles [26]. The absence of coarsening is confirmed from STEM analyses of samples before and after experimental analysis (not shown here). The formation of aggregates would account for a suppression of the changes in T_g and τ because aggregation reduces the effective interfacial area between the melt and nanoparticles. It follows that for the $AuPS_{10}$ nanocomposites, the T_g and dynamics are controlled by two competing processes: well dispersed particles contribute to a T_g reduction and fast

dynamics whereas aggregation of the particles has the effect of not creating new interfacial area and therefore suppresses a further reduction in T_g and the further acceleration of dynamics.

It is evident from the foregoing that both T_g and τ can be "tailored" through changes in N, P and σ. The particle size D also plays an important role in this process than one might initially surmise. Bansal et al. [27] showed that the T_g of a PNC material decreased under conditions where the grafted silica nanoparticles/host chains were non-wetting. However, this reported decrease is much smaller than that exhibited by our system. This is due to the fact that the average core diameter of our particles is 3 times smaller (3 times larger overall interfacial area for the same volume fraction). Clearly, particle size effects are very important even in this regime.

With regard to the dynamics, the dielectric spectrum exhibited a single maximum and showed no change in shape with temperature, consistent with the notion that the host chains, on average, experience the same dynamic environment. Simulations reveal that a melt of chains on a "dry" brush layer undergoes slip (non-wetting) [23]. Hence, we anticipate that when chains come in contact with the short, "dry," brush layer of the $AuPS_{10}$ nanoparticle, they experience a local reduction in friction coefficient, ζ, leading to an increase in their overall relaxation rates. MD simulations reveal that the chain center of mass diffusion is increased in nanocomposites where the particle/chain interactions are repulsive [8],[28]. Note that the center of mass diffusion D ($D \propto \zeta^{-1}$) and viscosity ($\eta \propto \zeta$) have the same temperature dependence in polystyrene homopolymer melts [29]. With regard to the other nanocomposite with the $AuPS_{481}$ nanoparticles, the slowing-down of the dynamics is associated with the brush/melt interactions, i.e.:

interpenetration of the brush layer by the host chains. An additional consideration is that the dynamics of tethered chains decrease exponentially with chain length compared to linear chains.

With this information, we are tempted to interpret the changes in the T_g, qualitatively, in terms of a dynamic percolation model [30]. The notion is that due to density fluctuations, the material might be considered to be composed of transient regions of "fast" and "slow" dynamics. The "slow" dynamics are considered to occur on time scales comparable to time scales associated with the glass transition. As the temperature decreases, the fraction of "slow" domains increases; the glass transition is denoted by the percolation of the "slow" domains. It is clear from the foregoing that the dynamics are faster due to the presence of the particles, onto which the short-chains are grafted (dry brush). In this regard, the presence of the nanoparticles increases the fraction of "fast" domains in the system. Hence, the glass transition decreases. When we graft much longer chains to the particles, the dynamics are slower due to increased interactions (interpenetration) with the host chains. One might think, qualitatively, in terms of an increase in the fraction of "slow" domains, hence an increase in T_g.

4.4 Conclusion

We now make concluding remarks regarding our observations of the dynamics and the glass transition of melts of unentangled PS chains containing compatible nanoparticles ($AuPS_{10}$ and $AuPS_{481}$). It is clear that the T_g and the time-scales of the dynamics of the systems can be "tailored" to increase, or decrease, in an unprecedented manner, through control of D, N, ϕ and σ in these systems; this has never been shown

before. Neither chain confinement effects nor the conventional free volume formalism can fully reconcile the behavior of our system. Instead, the T_g changes may be reconciled in terms of a more recent dynamic percolation model [3, 10, 30, 31]. In addition, the significant reduction of the relaxation time of the chains in the $AuPS_{10}$ nanocomposites is associated with the interactions between the host chains and the nanoparticles ("soft sphere"). Over a characteristic time scale, longest relaxation time, each chain experiences the same average dynamic environment. This is borne out by the fact that the breadth of the distribution on the dielectric spectrum remains constant throughout the temperature range. The enhanced dynamics is associated with the notion that chains undergo transient interactions with the nanoparticles: in the vicinity of a nanoparticle, a chain would experience a reduction in local friction, leading to faster relaxation rate dynamics. Since the chain spends most of its time in the host environment, and not at the nanoparticle surface, the temperature dependence of the relaxations should not be affected appreciably. Note that if the local friction of the chain is increased in the vicinity of the particle, assuming the nanoparticle/chain interaction is attractive and transient, then the dynamics would decrease (recall $\tau \propto \zeta$), and T_g would increase, as seen in the poly(methyl methacrylate)/C_{60} nanocomposite system [3, 4]. In the $AuPS_{481}$ nanocomposite, the dynamics are observed to decrease and T_g increases. The tethered chains are interpenetrated by the host chains as the host chains diffuse; the relaxation times of tethered chains are exponentially long compared to the host chains. These factors contribute, in part, to a slowing down of the dynamics of the $AuPS_{481}$ system, compared to the low molecular weight PS host.

We have presented an experimental study revealing how the relaxation dynamics

and glass transition of a polymer host can be tailored to undergo unusually large enhancements, or reductions, in magnitude with the addition of small concentrations of gold nanoparticles onto which polymer chains are grafted, through careful control of molecular parameters of the system. Mechanisms have been proposed to understand the T_g and relaxation behavior of these systems; it is our hope that these findings will motivate new simulations and theory to quantitatively account for such observations.

4.5 References

1. Tsagaropoulos, G. and A. Eisenburg, *Direct observation of two glass transitions in silica-filled polymers. Implications to the morphology of random ionomers.* Macromolecules, 1995. **28**(1): p. 396-8.

2. Starr, F.W., T.B. Schroder, and S.C. Glotzer, *Molecular dynamics simulation of a polymer melt with a nanoscopic particle.* Macromolecules, 2002. **35**(11): p. 4481-4492.

3. Kropka, J.M., et al., *Origin of dynamical properties in PMMA-C_{60} nanocomposites.* Macromolecules, 2007. **40**(15): p. 5424-5432.

4. Kropka, J.M., V. Garcia Sakai, and P.F. Green, *Local polymer dynamics in polymer-C_{60} mixtures.* Nano Letters, 2008. **8**(4): p. 1061-1065.

5. Mackay, M.E., et al., *Nanoscale effects leading to non-Einstein-like decrease in viscosity.* Nature Materials, 2003. **2**(11): p. 762-766.

6. Tuteja, A., et al., *Effect of ideal, organic nanoparticles on the flow properties of linear polymers: Non-Einstein-like behavior.* Macromolecules, 2005. **38**(19): p. 8000-8011.

7. Bansal, A., et al., *Quantitative equivalence between polymer nanocomposites and thin polymer films.* Nature Materials, 2005. **4**(9): p. 693-698.

8. Smith, G.D., et al., *A molecular dynamics simulation study of the viscoelastic properties of polymer nanocomposites.* Journal of Chemical Physics, 2002. **117**(20): p. 9478-9489.

9. Hooper, J.B. and K.S. Schweizer, *Contact aggregation, bridging, and steric stabilization in dense polymer-particle mixtures.* Macromolecules, 2005. **38**(21): p. 8858-8869.

10. Pryamitsyn, V. and V. Ganesan, *Origins of linear viscoelastic behavior of polymer-nanoparticle composites.* Macromolecules, 2006. **39**(2): p. 844-856.

11. Brust, M., et al., *Synthesis of thiol-derivatized gold nanoparticles in a two-phase liquid-liquid system.* Journal of the Chemical Society, Chemical Communications, 1994(7): p. 801-2.

12. Brust, M., et al., *Synthesis and reactions of functionalized gold nanoparticles.* Journal of the Chemical Society, Chemical Communications, 1995(16): p. 1655-6.

13. Fukao, K. and Y. Miyamoto, *Glass transition temperature and dynamics of alpha-process in thin polymer films.* Europhysics Letters, 1999. **46**(5): p. 649-654.

14. Bauer, C., et al., *Capacitive scanning dilatometry and frequency-dependent thermal expansion of polymer films.* Physical Review E: Statistical Physics, Plasmas, Fluids, and Related Interdisciplinary Topics, 2000. **61**(2): p. 1755-1764.

15. Srivastava, S. and J.K. Basu, *Experimental evidence for a new parameter to control the glass transition of confined polymers.* Physical Review Letters, 2007. **98**(16): p. 165701/1-165701/4.

16. Ferry, J.D., *Viscoelastic properties of polymers. 3rd Ed*. 1980: Wiley, New York. 641 pp.

17. Fox, T.G., *Influence of diluent and of copolymer composition on the glass temperature of a polymer system.* Bull. Am. Phys. Soc., 1956. **1**: p. 123.

18. DeMaggio, G.B., et al., *Interface and surface effects on the glass transition in thin polystyrene films.* Physical Review Letters, 1997. **78**(8): p. 1524-1528.

19. Batchelor, G.K., *Effect of brownian-motion on bulk stress in a suspension of spherical-particles.* Journal of Fluid Mechanics, 1977. **83**(NOV): p. 97-117.

20. Riggleman, R.A., J.F. Douglas, and J.J. de Pablo, *Tuning polymer melt fragility with antiplasticizer additives.* Journal of Chemical Physics, 2007. **126**(23): p. 234903/1-234903/10.

21. Vrentas, J.S., J.L. Duda, and H.C. Ling, *Antiplasticization and volumetric behavior in glassy polymers.* Macromolecules, 1988. **21**(5): p. 1470-5.

22. Ferreira, P.G., A. Ajdari, and L. Leibler, *Scaling law for entropic effects at interfaces between grafted layers and polymer melts.* Macromolecules, 1998. **31**(12): p. 3994-4003.

23. Pastorino, C., et al., *Static and dynamic properties of the interface between a polymer brush and a melt of identical chains.* Journal of Chemical Physics, 2006. **124**(6): p. 064902/1-064902/11.

24. Xu, J., et al., *Morphology and interactions of polymer brush-coated spheres in a polymer matrix.* Journal of Polymer Science, Part B: Polymer Physics, 2006. **44**(19): p. 2811-2820.

25. Frischknecht, A.L., *Forces between nanorods with end-adsorbed chains in a homopolymer melt.* Journal of Chemical Physics, 2008. **128**(22): p. 224902/1-224902/11.

26. Meli, L. and P.F. Green, *Aggregation and coarsening of ligand-stabilized gold nanoparticles in poly(methyl methacrylate) thin films.* ACS Nano, 2008. **2**(6): p. 1305-1312.

27. Bansal, A., et al., *Controlling the thermomechanical properties of polymer nanocomposites by tailoring the polymer-particle interface.* Journal of Polymer Science, Part B: Polymer Physics, 2006. **44**(20): p. 2944-2950.

28. Desai, T., P. Keblinski, and S.K. Kumar, *Molecular dynamics simulations of polymer transport in nanocomposites.* Journal of Chemical Physics, 2005. **122**(13): p. 134910/1-134910/8.

29. Green, P.F., *Kinetics, transport, and structure in hard and soft materials*. 2005: CRC Press, Taylor and Francis, New York. 353 pp.

30. Long, D. and F. Lequeux, *Heterogeneous dynamics at the glass transition in van der Waals liquids, in the bulk and in thin films.* European Physical Journal E: Soft Matter, 2001. **4**(3): p. 371-387.

31. Kropka, J.M., V. Pryamitsyn, and V. Ganesan, *Relation between glass transition temperatures in polymer nanocomposites and polymer thin films.* Physical Review Letters, 2008. **101**(7): p. 075702-4.

CHAPTER 5

THE INFLUENCE OF NANOPARTICLE DISPERSION ON PROPERTY CHANGES IN THIN FILM AND BULK POLYMER NANOCOMPOSITES

The connection between interactions, nanostructures and properties of complex polymer nanocomposite (PNC) systems has been examined systematically by altering sample dimensions, nanoparticle sizes as well as enthalpic particle-host chain interactions. It has been shown that the properties of PNCs are strongly influenced by the nanoparticle distribution. More specifically, we observed slight or no property changes in thin films (thicker than the critical confinement thickness, ~ 22nm for poly(vinyl acetate)) due to the lower miscibility of nanoparticles caused by the interfacial segregation. On the other hand, the dispersion of nanoparticles or their aggregates in the bulk led to the bigger changes. Our results provide some insight into the role of the collective interactions on structure formation in PNC systems, and suggest the importance of the nanoparticle dispersion in controlling the properties.

5.1 Introduction

Polymer hosts containing fillers of nanoscale dimensions, nanofillers, exhibit nanofiller properties that are significantly different from the polymer host, even at low concentrations. These properties are due to collective intermolecular interactions, and are sensitive to the nanostructural features of the material. This is a technologically important class of materials and there remain a number of open questions related to the connection between structure, properties and performance. Most of the research on these systems has focused primarily on the structure and properties of the bulk. In this manuscript we are particularly interested in understanding connections between the bulk and thin film behavior of the glass transition and dynamics of these systems.

The presence of the nanoparticles in a polymer host under certain conditions is known to have an important influence on both the glass transition temperature (T_g) and the chain relaxations. The T_g has been shown to increase or decrease, based on the nature of the polymer/nanoparticle interactions [1-7]. Some polymer nanocomposite (PNC) systems exhibit more than one T_g [7]. If the particle/chain interactions are particularly strong then chains would form a region around a nanoparticle or cluster of nanoparticles, where the properties in that region, the interphase, differ from regions located further away from the nanoparticles. Measurements of dynamic mechanical analysis (DMA) or differential scanning calorimetry (DSC) would reveal two separate T_gs [7]. In cases where the polymer/nanoparticle interactions are attractive yet weak, only a single T_g may be observed [4, 5]. In a recent paper (Chapter 4) [6], we showed that in a PNC containing gold nanoparticles onto which polystyrene (PS) chains of degree of polymerization N, were grafted at particularly high grafting densities, the T_g was very

sensitive to the nature of the brush/host chain interactions. When the host chains were completely excluded from the brush layer, the T_g showed significant decreases with nanoparticle concentration. Otherwise the T_g would increase when there was significant interpenetration of free chains into the brush layer. Qualitatively, commensurate changes in the center of mass relaxation dynamics were observed in these systems.

In bulk PNCs, nanoparticle miscibility is determined by the competition between enthalpic effects associated with particle/particle and particle/chain interactions as well as various entropic effects. Dispersion of the nanoparticles within the host is favored by the entropy of mixing: $F_{mix} \sim (\varphi / D^3) \ln \varphi$, where φ is the particle volume fraction and D is the diameter of the nanoparticles[8, 9]. Mixing would be opposed by the elastic energy of the host chains which increases as $F_{stretching} \sim (R_{NP}{}^2 / Pb^2)$, with increasing nanoparticle radius, R_{NP}; P and b denote the degree of polymerization of host chains and the monomer size, respectively [10]. An additional entropic feature is that host chains tend to migrate away from between particles in proximity in order to gain entropy [11], further contributing to aggregation of the nanoparticles [12]. The particle-particle interactions can become attractive, due to the van der Waals forces, which opposes dispersion. If the nanoparticles are grafted with homopolymer chains then the nanoparticles would have a tendency to aggregate if a finite interfacial tension exists between the brush layer and the host chains [11]. This effect would be significant for under "dry brush" conditions, where interpenetration of the brush layer by the host chains is minimal. The finite interfacial tension between the brush and the host chains leads to a long-range attraction between nanoparticles; this attraction decreases with decreasing P/N. The other so-called "wet" brush situation is associated with interpenetration of the brush

layer by the host chains. This condition favors dispersion of the nanoparticles.

When nanoparticles are incorporated into polymer thin films, the particles may exhibit a tendency to segregate to interfaces, due to a number of effects. The free chains gain conformational entropy when they are displaced from the interfaces [13]. This is a function of the relative polymer/nanoparticle size and monomer/particle size. The relative surface energies of the nanoparticles and chains may have an important effect on surface segregation [14]. There may exist attractive van der Waals forces between the nanoparticles and the substrate [15]. If the nanoparticles are grafted with polymer chains, then entropic constraint due to the penetrability of host chains into grafted brush layers becomes an important consideration. If the particles aggregate, they exhibit a tendency to migrate near interfaces in order to minimize the particle/host chain interfacial area. Overall, these factors contribute to preferential segregation of the nanoparticles to interfaces, which influences the composition and structure of the PNC.

Important questions, related to the connection between structure, dynamics and, the T_g of PNCs, remain unanswered. In pure melts, the magnitude of the diffusion coefficient depends on the temperature above the glass transition of the melt, as described by the Williams-Landel-Ferry (WLF), or equivalently the Vogel-Fulcher-Tamman (VFT) equation. The relaxation rates are determined by the local monomer friction factor, ζ. In PNCs, the T_g and ζ may be influenced by the heterogeneous structure. In thin films, where the interfaces play an important role toward determining the nanoparticle distribution, the connection between the bulk and thin film dynamics and T_g is also unclear.

In this study, we investigate the relation between structure and dynamics in bulk

and thin film in polyvinyl acetate (PVAc) based PNCs that contain three different types of nanoparticles. The nanoparticles have varying degrees of compatibility with the host, from immiscible to compatible. We examine the role of interfaces on the structure and dynamics of thin film PNCs. One of the important findings is that the interfaces in thin films can exhibit dominant role toward determination of the nanoparticle distribution to the point that changes in average chain relaxation dynamics are suppressed.

5.2 Experimental Section

Three different types of bulk and thin film PVAc based nanocomposite samples were prepared for analysis using DSC and broadband dielectric spectroscopic (DS) examination: (1) PVAc with gold nanoparticles, functionalized with thiol-terminated PS; (2) PVAc/fullerene (C_{60}); (3) PVAc/polyethylene glycol-polyhedral oligomeric silsesquioxane cages (PEG-POSS). The morphologies of these samples were determined using scanning transmission electron microscopy (STEM), dynamic secondary ion mass spectrometry (DSIMS) and optical microscopy (OM).

Important characteristics of the materials are now described. The number average molecular weight of the PVC, obtained from Polymer Source Inc., was M_n = 145,000 g/mol (M_w/M_n = 1.5). The PEG-POSS was obtained Hybrid Plastics Inc.; the PEG ligands, one grafted to each of the 8 ~ 12 corners of the POSS cages, possessed a molecular weight of ~ 644 g/mol (N ~ 15 monomers). The C_{60}, of 99.5 % purity, was obtained from Sigma-Aldrich Co. The Gold nanoparticles, of average diameter 4.8 nm, functionalized with thiol-terminated PS (M_n = 1,000 g/mol, M_w/M_n = 1.4), grafting density σ ~ 2.0 chains/nm^2, were synthesized using procedures described in earlier

publications [16, 17]. Hereafter these nanoparticles will be identified as Au_5PS_{10}. All samples were prepared first by dissolving mixtures of varying compositions in toluene, followed by mixing at 1000 rpm using the orbital shaker.

Thin films of these blends were prepared and confined between two aluminum (Al) electrodes following sample preparation procedures described elsewhere [18]. Specifically, Al electrodes (~ 0.5 mm in width and ~ 100 nm in height) were evaporated on the glass substrates, which had been thoroughly cleaned using glass detergent and acetone in the ultrasonic cleaner. After cleaning the Al-coated glass substrates using toluene, thin films were spin-coated on them. A range of average film thicknesses, h_{avg}, from 42 nm to 142 nm, were prepared and measured by Scanning Probe Microscope (SPM; Veeco Instruments Inc.). The samples were then vacuum-dried at room temperature for a day and subsequently annealed at 360 K (well above the T_g of PVAc) for an additional day. The annealing temperature was slightly lowered to 353 K for gold nanoparticles to eliminate the possibility of PS ligand detachment from the particle surface.

Counter electrodes were prepared by evaporating a layer of Al onto the surface of each film. Since water is polar molecule, which can influence the relaxations of polymer, samples were annealed once more in a nitrogen atmosphere at 360 K (or 353 K) for 12 hours to eliminate possibly absorbed water during the sample transfer. Note that samples for other experiments (discussed below) were annealed at the same temperature and time conditions as above. After in-situ annealing, DS measurements were performed, using a Novocontrol Technologies GmbH instrument, in the frequency range from 0.1 Hz to 3 MHz at the temperatures between 300 K and 360 K.

In addition to the DS measurements, DSIMS measurements were performed on specially prepared samples in order to determine the concentration profile of nanoparticles as a function of depth within the films. The presence of the interface would influence the spatial distribution of the species added to the PVAc. While it is not possible to determine the spatial distribution of C_{60} with the PVAc host, due to the lack of contrast with PVAs, the concentration profiles of the Au_5PS_{10} and the PEG-POSS can be readily be determined using DSIMS. It is not possible to determine the profiles of these species within the Al/nanocomposite/Al sandwiched layer due to either charging or roughening problem on the upper Al one, so special samples had to be made. Specifically, films of thicknesses of approximately 145 nm samples, containing 5 *wt*.% Au_5PS_{10} nanoparticles or PEG-POSS were prepared on silicon (Si) substrates onto which 100 nm Al layers had been deposited (i.e. sample/Al/Si structures) for DSIMS measurements. These experiments provided information about the effect of Al substrates on the spatial distribution of the added species (Au_5PS_{10} or PEG-POSS).

In DSIMS experiments, it is necessary to place a sacrificial layer on the sample surface in order to reliably control the etch rate and to determine the upper interface; this enables accurate determination of depth profiles. Therefore, after the samples were prepared, a film of thickness ~ 75 nm, composed of a blend films of 40:60 deuterated PS:hydrogenated PS, was floated on top of the samples from a bath of water. These samples were then vacuum-dried overnight. Physical Electronics 6650 Quadrupole instrument (performed by Tom Mates at University of California at Santa Barbara) was used to monitor negative secondary ions of hydrogen (H), deuterium (D), carbon (C), oxygen (O), Al, Si and Au. The sputtering time axis was converted into the depth scale

based on the film thickness, measured by the spectroscopic ellipsometry (SE; J.A. Woollam Co., Inc.).

The samples were also analyzed using STEM to determine the lateral distribution of the Au_5PS_{10}. These measurements were performed on thin films of thickness ~ 145 nm, containing 2 *wt*.% gold nanoparticles. These films were spin-coated on Al-deposited silicon nitride TEM grids and then vacuum-annealed. We note that the thickness of Al layers was reduced to ~ 20 nm in order to improve the transparency. Their images were generated in the STEM mode by the JEOL 2010F Analytical Electron Microscope equipped with a high angle annular dark field (HAADF) detector.

As mentioned earlier, bulk samples were also prepared. They were prepared by blending solutions of PVAc (112,000 g/mol, M_w/M_n = 2.2) and nanoparticles using toluene as a solvent and subsequently dried in air for at least three days prior to annealing. Fully annealed PNCs were divided into two or three pieces for OM, DSC and DS. PNCs for OM were sandwiched between carefully-cleaned glass slides at temperatures below 373 K, and then photographed using a Nikon Optiphot Microscope. For T_g measurements, PNC samples, sealed in Al cells, were repeatedly heated up at 10 K/min, annealed for 10 min, and cooled down at 50 K/min between 243 K and 373 K using a TA instruments Q200 DSC. Their T_gs were then determined by the half-height midpoint of the transition at the third heating. Lastly, PNCs with up to 5 *wt*.% of Au_5PS_{10} nanoparticles were compression-molded between two brass electrodes at 360 K for DS measurements. These samples, having an average thickness of ~ 0.17 mm, were measured under the experimental conditions described for thin films.

5.3 Results and Discussion

DS measurements were performed on bulk and thin film nanocomposites. Based on the temperature and frequency ranges over which our experiments were conducted, only a single relaxation process was observed. This process was assigned to the cooperative segmental motion of the polymer chains directly connected to dynamic α relaxation. It is well known that PVAc also exhibits a secondary relaxation (β relaxation) at low temperatures (below T_g) which is believed to originate from the polar side group (—$OCOCH_3$) [19]. However, only the longest relaxation processes are of interest in this study.

We first direct our attention to the data in Figure 5.1a, which describes the relaxations occurring in the PVAc/Au_5PS_{10} nanocomposite thin films of average thicknesses 135 nm. These data reveal that the nanoparticles have no effect on the relaxation dynamics of the PVAc chains. Additional measurements were performed on bulk PVAc/Au_5PS_{10} samples of identical composition and, in contrast, differences between the relaxation rates were observed at different compositions, Figure 5.1b. The relaxation rates increase with the addition of the nanoparticles and gradually decrease beyond 0.5 *wt*.% of particles, though the overall changes are small. An assessment of the glass transition temperatures, using DSC (Figure 5.2a), revealed a small decrease of the T_g at low concentration, followed by a comparable increase with more nanoparticles. This is qualitatively consistent with the DS data.

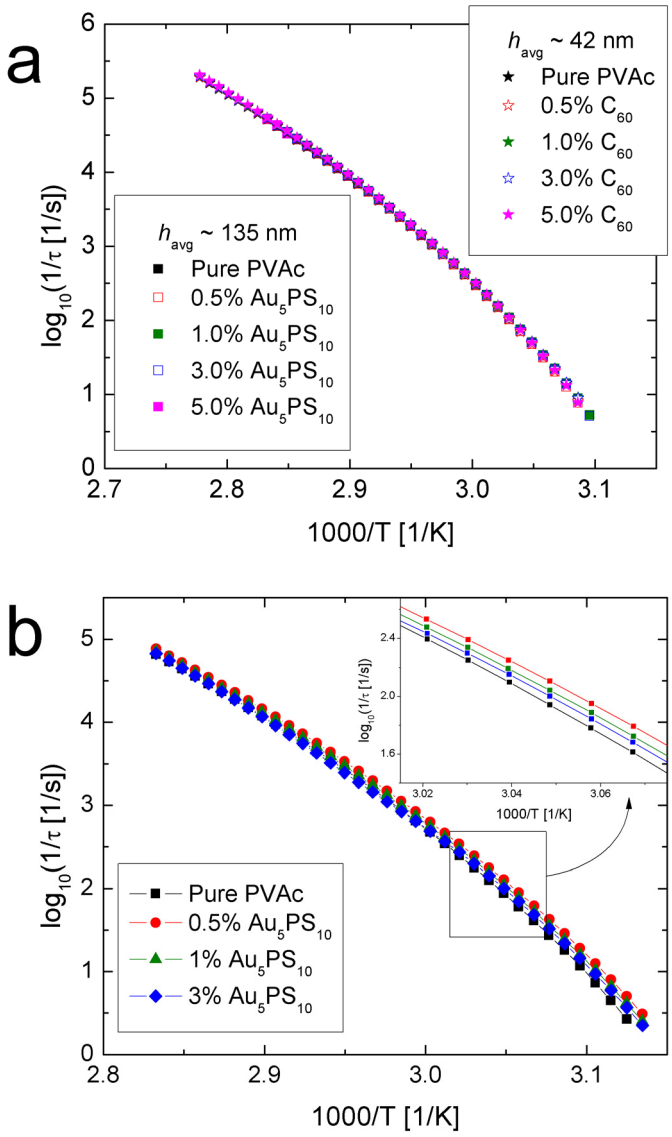

Figure 5.1 Activation plots (relaxation rate vs inverse temperature) for **a**, thin film and **b**, bulk PVAc composites with immiscible nanoparticles (Au_5PS_{10} and C_{60}). Practically, no shift was observed in dynamics of thin film PNC samples, whereas changes in dynamic were induced in bulk PNCs due to the dispersion of aggregates.

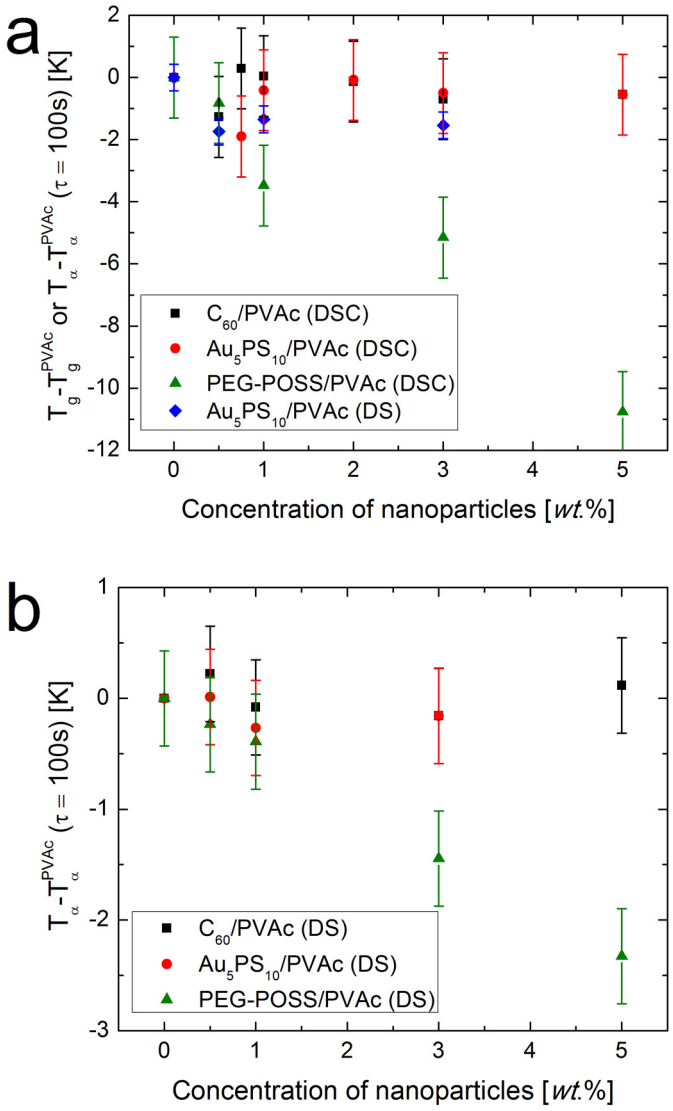

Figure 5.2 Changes in T_gs or T_αs (τ = 100 s), measured by DSC and DS, are shown here for **a**, bulk and **b**, thin film PVAc PNCs. Errors for DSC and DS experiments, calculated by applying the Student's t-distribution for small number of data points, are ± 1.30 K and ± 0.43 K with confidence of 95%, respectively.

The foregoing indicates that the effect of the nanoparticles on the dynamics is apparent in the bulk samples, whereas they are not in thin films. These small differences between the dynamics of the pure system and the PNCs are surprising in light of the results of our prior study [6] of the polystyrene based nanocomposites, containing the same Au_5PS_{10} nanoparticles. In the PS/Au_5PS_{10} system the relaxation dynamics increased by an order of magnitude with approximately 1 *wt*.% nanoparticles; the glass transition decreased in a manner nearly commensurate with the changes in dynamics. The brush layer density and chain length were such that the host chains did not interpenetrate the brush layers (dry brush condition).

Parenthetically, the host chain-brush layer interaction is determined by three parameters: P, N, and σ, the grafting density of the brush layer [20]. When the brush layer is sparsely grafted with sufficiently long chains the host chains readily interpenetrate (wet brush). However, by increasing σ or P/N, the host chains become partially extruded from the brush layer for entropic reasons. The implication is that these interfacial conditions can lead to attractive or repulsive entropic interactions between nanoparticles. We also know that dewetting of a thin homopolymer layer from an underling brush occurs under dry brush conditions. Such a layer is otherwise stable under wet brush conditions [2, 6]. It follows that host chains in the vicinity of the nanoparticles experience a lower "friction" in the vicinity of the dry brush layer leading to a shorter relaxation time. If the brush/host interactions are such that the host chains interpenetrate the brush layer then the dynamics of the host chains would slow down. In fact, simulations show that in cases where the nanoparticle/host chain interactions are attractive the dynamics slow down, while the dynamics increase when the host

chain/nanoparticles are repulsive [21, 22].

In the case of the PVAc/Au_5PS_{10} system, the host chains are incompatible with the nanoparticles, as such the interactions are weak/repulsive, which should in principle lead to an enhancement of the host chain dynamics. These differences are only apparent in the bulk samples and not observed in the thin film PVAc/Au_5PS_{10} system. Moreover, the difference in rates between the pure polymer and the PNCs is quite significant in the PS/Au_5PS_{10} compared to the PVAc/Au_5PS_{10} samples.

Further insight into the behavior of the PVAc/Au_5PS_{10} PNC might be gained by examining the morphology. We begin by noting that that the Au_5PS_{10} nanoparticles are well dispersed within the bulk PS/Au_5PS_{10} samples, whereas they are not in the PVAc/ Au_5PS_{10}. Information obtained from OM, STEM and DSIMS measurements indicate that the nanoparticles form large aggregates in the PVAc hosts. The OM analysis reveals the existence of large aggregates of nanoparticles in the bulk sample (Figure 5.3a). Additionally, the STEM measurements also indicate the presence of aggregates within the films (Figure 5.3b). The DSIMS experiments indicate significant segregation of the nanoparticles at the Al interface (Figure 5.4). The indication here is that a significant amount of the nanoparticles resides at the Al interfaces in the sample on which the DS measurements were performed. Clearly, Au_5PS_{10} aggregates of a wide distribution of sizes exist within the films. In light of the morphological structure of this sample, it is not entirely surprising that no effect of the Au_5PS_{10} nanoparticles on the dynamics of thin film PVAc was observed. The aggregation of nanoparticles also accounts for the suppression of the T_g change, observed in bulk PVAc/Au_5PS_{10} sample because it reduces the effective interfacial area between the host chains and nanoparticles [5, 6].

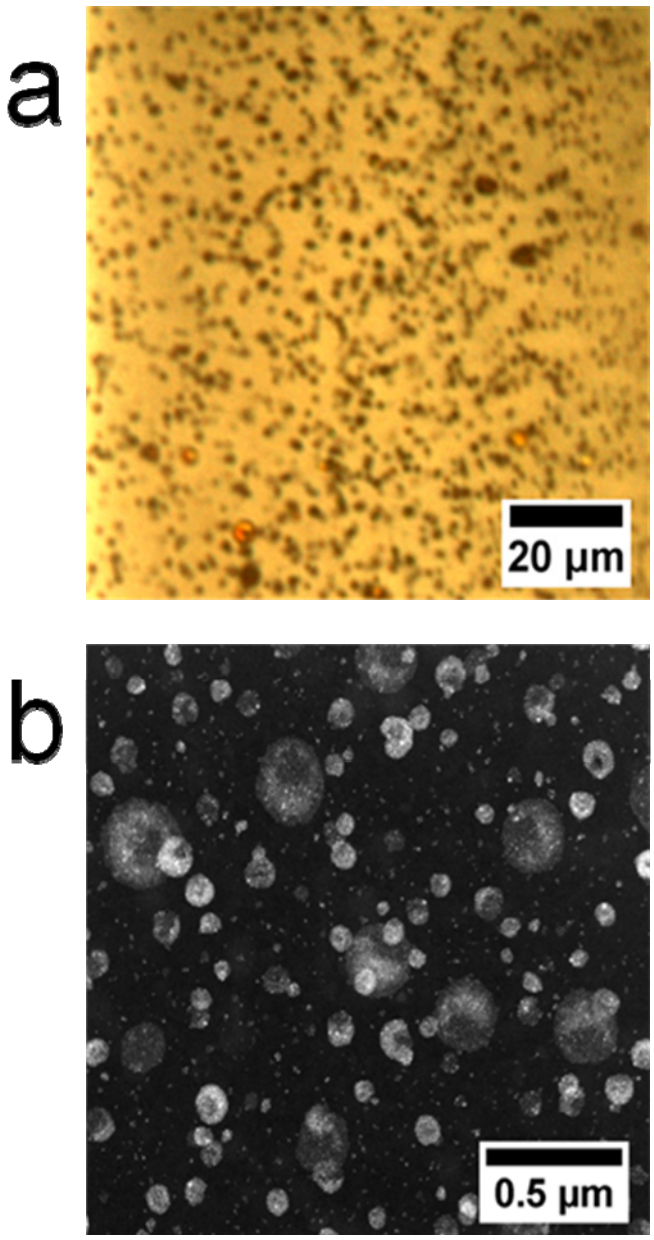

Figure 5.3 Morphology of PVAc PNCs, characterized by means of **a**, OM for a bulk sample with 1 *wt*.% Au_5PS_{10} nanoparticles and of **b**, STEM for 2 *wt*.% Au_5PS_{10}/PVAc of thickness ~ 145 nm. Evidence for the aggregation of nanoparticles was obtained from both techniques.

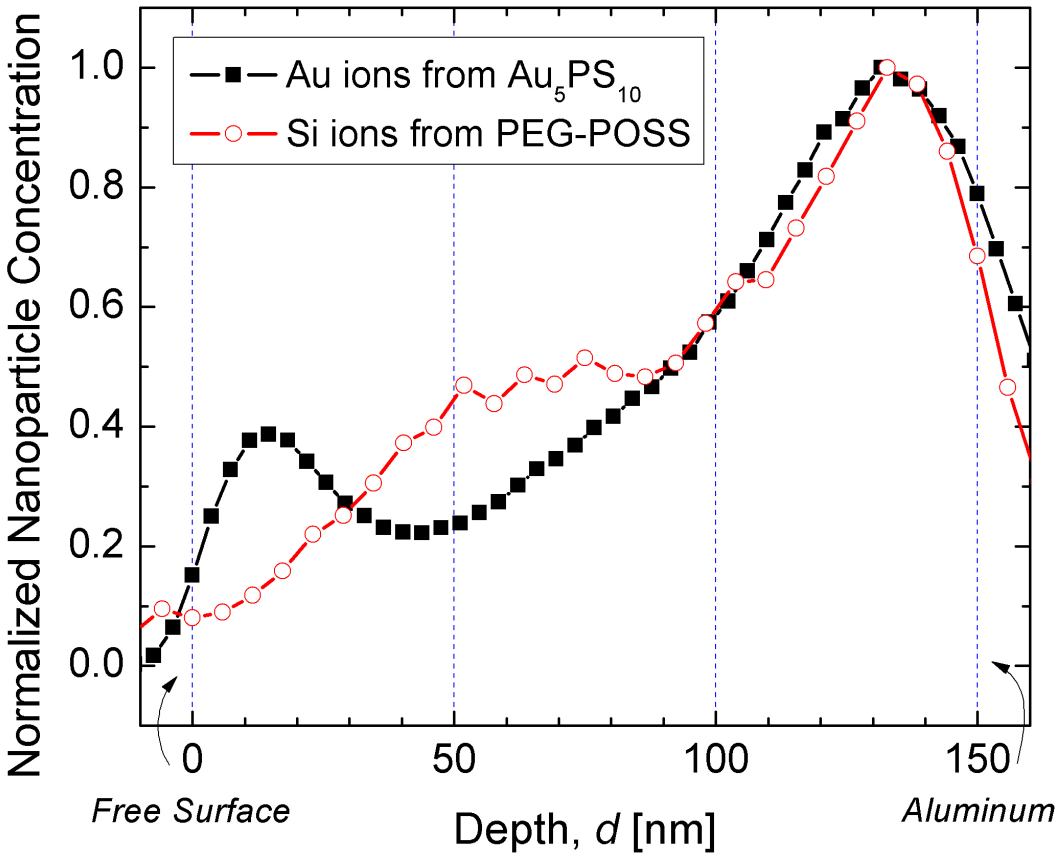

Figure 5.4 Depth profiles of Si ions (implying PEG-POSS) and Au ions (implying Au_5PS_{10}) for ~ 145 nm PVAc nanocomposite thin films with 5 *wt*.% of PEG-POSS and Au_5PS_{10} nanoparticles. For the convenience of comparison, the profile of each sample was normalized by the intensity of the peak near the Al substrate.

PVAc/C_{60} nanocomposite films of average thickness 42 nm were examined using DS and similar observations were made; the relaxation dynamics of the PVAc molecules were not affected by the C_{60} (Figure 5.1a). An examination of the morphology of these films, using OM (Figure 5.5a), also reveals the existence of large aggregates of C_{60}, which is consistent with the immiscibility of the system. A tendency toward aggregation is further enhanced in the C_{60} system compared to the Au_5PS_{10} system, due to the London-van der Waals forces. This attractive interaction is inversely proportional to the six power of the distance separating particles and to the masses of the particles.

The effect of nanoparticles with which the host chains have a preferential attraction on the host chain dynamics was also investigated. PEG-POSS molecules served this purpose; PEG molecules ($N \sim 15$) are attached to each corner of the POSS cube, of size ~ 0.5 nm. PEG chains possess a negative Flory-Huggins interaction parameter value for their blends with PVAc chains at high PVAc contents ($\phi_{PVAc} \geq 40$ *wt*.%), implying that this blend would be thermodynamically stable (or miscible) [23]. The nanoparticles are reasonably well dispersed, as indicated by the SIMS (Figure 5.4) and OM studies (Figure 5.5b). The PEG-POSS nanoparticles show a tendency to preferentially migrate toward the Al interface, though a much higher concentration of molecules resides in the interior of the film, compared to the Au_5PS_{10} nanoparticles. In this regard, the PEG-POSS nanoparticles are better dispersed in PVAc.

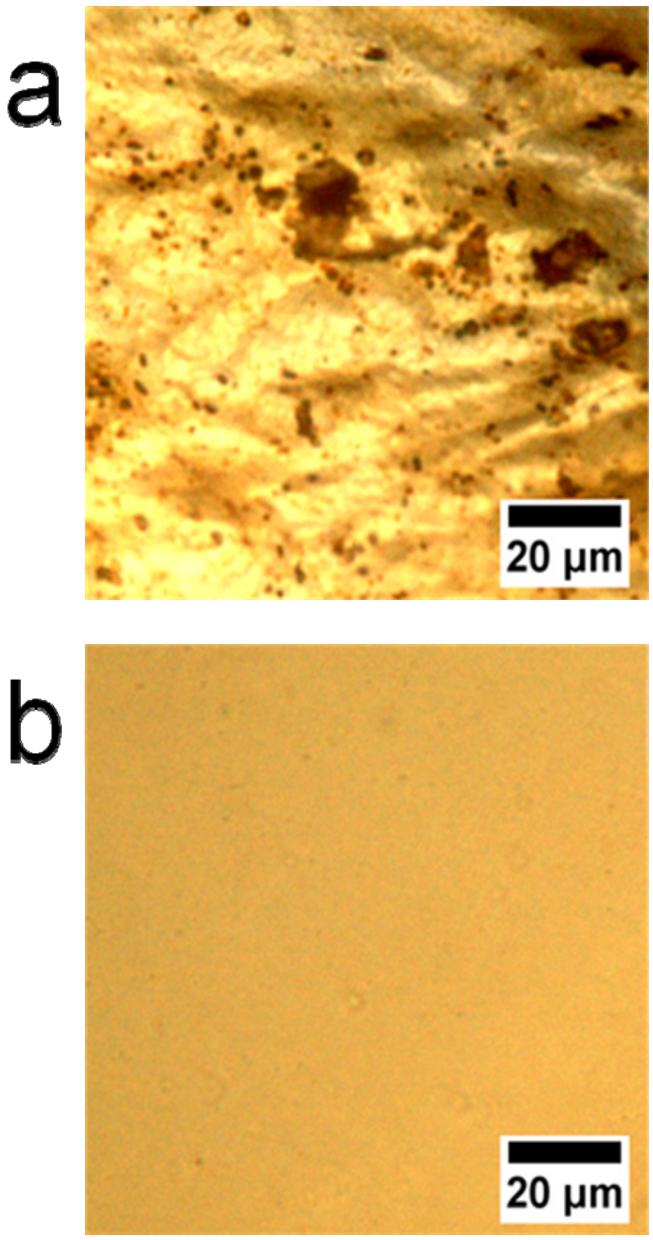

Figure 5.5 Optical micrographs of PVAc PNC bulk samples with **a**, 1 *wt*.% of C_{60} and **b**, PEG-POSS nanoparticles. It is clearly shown that miscible PEG-POSS particles are well dispersed, while the other immiscible particles form micron-sized aggregates.

When polymer films are confined in external walls, the dynamics of chains in contact with the walls are strongly influenced; they may become slower or faster depending on the interfacial interactions. Pure PVAc films with thickness more than ~ 22 nm show no appreciable changes in dynamics [24]. So it is not surprising that since the interior of the film is composed of pure PVAc, as is the case for the C_{60} and Au_5PS_{10} nanoparticles, that the dynamics of this system exhibits no change in dynamics. On the other hand the dynamics increase with increasing PEG-POSS as shown in Figure 5.6. A measurement of the bulk T_gs of this system (Figure 5.2a) reveals that the T_g decreases significantly with increasing PEG-POSS concentration. The change is likely associated with the fact that PEG possesses a much lower T_g than PVAc and due to the miscibility the average T_g of the blend decreases. The dynamics necessarily increase because the effective T-T_g increases with increasing POSS-PEG concentration.

Estimates of the T_g changes for the thin films could be made based on the dynamics. To this end, the T_gs were estimated by fitting the DS activation plots (Figures 5.1 and 5.6) with the VFT equation: $\tau = \tau_0 \exp(B/(T - T_v))$, where τ_0 is the relaxation time at infinite temperature, B is a constant being related to the activation energy of the relaxation process, and T_v is the Vogel temperature at which the segments would be frozen if they were at equilibrium. This is possible due to the fact that T_α (the peak temperature of α relaxation at a given frequency) at which the average relaxation time reaches 100 s is comparable to T_gs measured by other techniques [25]. As expected, the T_g changes, exhibited by the PVAc/PEG-POSS nanoparticles, were smaller than those observed in the bulk (Figure 5.2b). The T_g data for the other thin film PNCs are not inconsistent with the data on the dynamics; they were independent of composition, within

experimental error.

It is clear from the foregoing that if the nanoparticles are not miscible with the host chains, they show a strong tendency to segregate to the interfaces, for reasons described above. In the bulk, however, the effective concentration of nanoparticles is higher because of the lower driving force toward phase separation. Under these conditions, the nanoparticles are more miscible in bulk than in thin films and therefore have an effectively larger impact on the dynamics of the host chains in the bulk.

5.4 Conclusion

It has been shown that the nanoparticles have a stronger influence on the relaxation dynamics of host chains in bulk systems than in thin films due to a higher degree of compatibility with the bulk. In thin films, the nanoparticles exhibit a tendency to segregate toward interfaces, as discussed earlier, leading to lower miscibility. Furthermore, the T_g was observed to decrease and the dynamics increase in two PNCs for different reasons. In the case of the PVAc/PEG-POSS, the decrease in T_g was due to a thermodynamic compatibility with the PEG-POSS molecules that possess lower T_g than the host. Necessarily the host chain dynamics increase in this compatible system. In the other case, PVAc/Au_5PS_{10}, the increase in the dynamics was due to a "repulsive" host chain brush interaction. The extent of the change is strongly dependent on the extent of dispersion of the nanoparticles in the host.

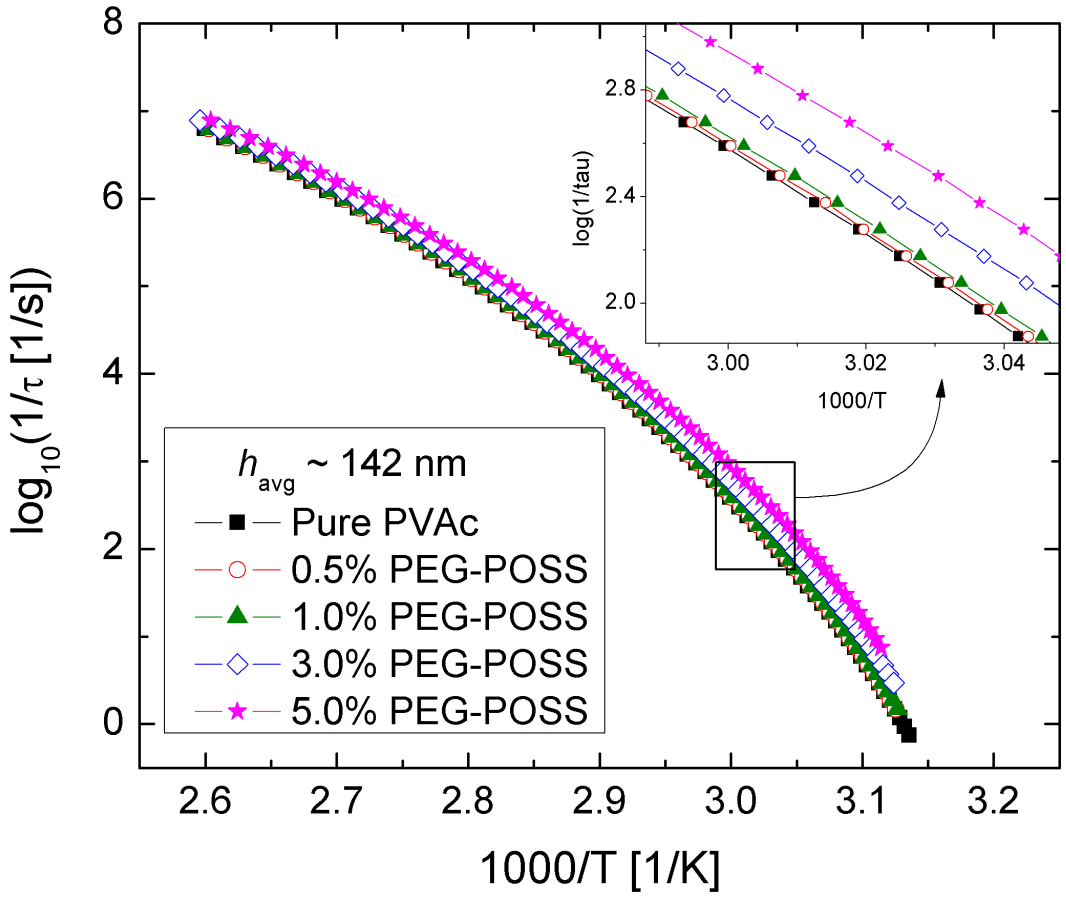

Figure 5.6 Activation plot for thin film PNCs of PVAc and PEG-POSS. The dynamics of these samples became gradually faster with the addition of miscible PEG-POSS nanoparticles.

5.5 Reference

1. Ash, B.J., R.W. Siegel, and L.S. Schadler, *Glass-transition temperature behavior of alumina/PMMA nanocomposites.* Journal of Polymer Science, Part B: Polymer Physics, 2004. **42**(23): p. 4371-4383.

2. Bansal, A., et al., *Controlling the thermomechanical properties of polymer nanocomposites by tailoring the polymer-particle interface.* Journal of Polymer Science, Part B: Polymer Physics, 2006. **44**(20): p. 2944-2950.

3. Bansal, A., et al., *Quantitative equivalence between polymer nanocomposites and thin polymer films.* Nature Materials, 2005. **4**(9): p. 693-698.

4. Kropka, J.M., V. Garcia Sakai, and P.F. Green, *Local polymer dynamics in polymer-C_{60} mixtures.* Nano Letters, 2008. **8**(4): p. 1061-1065.

5. Kropka, J.M., et al., *Origin of dynamical properties in PMMA-C_{60} nanocomposites.* Macromolecules, 2007. **40**(15): p. 5424-5432.

6. Oh, H. and P.F. Green, *Polymer chain dynamics and glass transition in athermal polymer/nanoparticle mixtures.* Nature Materials, 2009. **8**(2): p. 139-143.

7. Tsagaropoulos, G. and A. Eisenburg, *Direct observation of two glass transitions in silica-filled polymers. Implications to the morphology of random ionomers.* Macromolecules, 1995. **28**(1): p. 396-8.

8. Lee, J.Y., G.A. Buxton, and A.C. Balazs, *Using nanoparticles to create self-healing composites.* Journal of Chemical Physics, 2004. **121**(11): p. 5531-5540.

9. Lee, J.Y., Z.Y. Shou, and A.C. Balazs, *Predicting the morphologies of confined copolymer/nanoparticle mixtures.* Macromolecules, 2003. **36**(20): p. 7730-7739.

10. Ginzburg, V.V., *Influence of nanoparticles on miscibility of polymer blends. A simple theory.* Macromolecules, 2005. **38**(6): p. 2362-2367.

11. Xu, J., et al., *Morphology and interactions of polymer brush-coated spheres in a polymer matrix.* Journal of Polymer Science, Part B: Polymer Physics, 2006. **44**(19): p. 2811-2820.

12. Hooper, J.B. and K.S. Schweizer, *Contact aggregation, bridging, and steric stabilization in dense polymer-particle mixtures.* Macromolecules, 2005. **38**(21): p. 8858-8869.

13. McGarrity, E.S., A.L. Frischknecht, and M.E. Mackay, *Phase behavior of polymer/nanoparticle blends near a substrate.* Journal of Chemical Physics, 2008. **128**(15).

14. Chen, X.C. and P.F. Green, *Control of morphology and its effects on the optical*

properties of polymer nanocomposites. Langmuir, 2010. **26**(5): p. 3659-3665.

15. Meli, L., A. Arceo, and P.F. Green, *Control of the entropic interactions and phase behavior of athermal nanoparticle/homopolymer thin film mixtures.* Soft Matter, 2009. **5**(3): p. 533-537.

16. Brust, M., et al., *Synthesis and reactions of functionalized gold nanoparticles.* Journal of the Chemical Society, Chemical Communications, 1995(16): p. 1655-6.

17. Brust, M., et al., *Synthesis of thiol-derivatized gold nanoparticles in a two-phase liquid-liquid system.* Journal of the Chemical Society, Chemical Communications, 1994(7): p. 801-2.

18. Serghei, A. and F. Kremer, *Unexpected preparative effects on the properties of thin polymer films*, in *Characterization of polymer surfaces and thin films*, K. Grundke, M. Stamm, and H.J. Adler, Editors. 2006, Springer-Verlag Berlin: Berlin. p. 33-40.

19. McCrum, N.G., B.E. Read, and G. Williams, *Anelastic and dïelectric effects in polymeric solids*. 1967, London: Wiley. xv, 617 p.

20. Ferreira, P.G., A. Ajdari, and L. Leibler, *Scaling law for entropic effects at interfaces between grafted layers and polymer melts.* Macromolecules, 1998. **31**(12): p. 3994-4003.

21. Smith, G.D., et al., *A molecular dynamics simulation study of the viscoelastic properties of polymer nanocomposites.* Journal of Chemical Physics, 2002. **117**(20): p. 9478-9489.

22. Starr, F.W., T.B. Schroder, and S.C. Glotzer, *Molecular dynamics simulation of a polymer melt with a nanoscopic particle.* Macromolecules, 2002. **35**(11): p. 4481-4492.

23. Kalfoglou, N.K., D.D. Sotiropoulou, and A.G. Margaritis, *Thermal and morphology characterization of blends of poly(ethylene oxide) with poly(vinyl acetate).* European Polymer Journal, 1988. **24**(4): p. 389-394.

24. Serghei, A., M. Tress, and F. Kremer, *Confinement effects on the relaxation time distribution of the dynamic glass transition in ultrathin polymer films.* Macromolecules, 2006. **39**(26): p. 9385-9387.

25. Roland, C.M. and R. Casalini, *Temperature dependence of local segmental motion in polystyrene and its variation with molecular weight.* Journal of Chemical Physics, 2003. **119**(3): p. 1838-1842.

CHAPTER 6

THE DYNAMIC RESPONSE OF POLY(VINYL METHYL ETHER) IN POLY(VINYL METHYL ETHER) AND DEUTERATED POLYSTYRENE BLEND THIN FILMS

The miscible polymer blends with large difference in the glass transition temperatures, T_gs, are known to have broad dielectric relaxation peaks, the intensity of which changes rapidly with the temperatures, especially for the blends with high contents of high T_g polymers. When miscible poly(vinyl methyl ether)/deuterated polystyrene (PVME/dPS) blends are confined in thin film geometry, the segmental dynamics of PVME chains speeds up with an increase of the molecular weight of dPS as opposed to the conventional concept for the bulk blends. It is also shown that the dynamics become faster as the thickness decreases. These observations are due to the micro-phase separation at the substrate leading to a reduction in the effective concentration of PVME chains constrained in rigid dPS chains as well as an increase in fast PVME regions near the substrate. We show that the dynamic behavior of α' relaxation process is also associated with this effective concentration reduction. In addition, we suggest the proper analytical method for the miscible blend system.

6.1 Introduction

Polymer blending is as old as the polymer industry but is still a very attractive way to produce materials with the desired macroscopic properties due to its efficiency and practicality. Thus, up to the present, considerable effort has been invested toward understanding the dynamics of miscible polymer blends by means of different techniques such as nuclear magnetic resonance (NMR), quasielastic neutron scattering (QENS), rheology, dielectric spectroscopy (DS) and thermally stimulated depolarization current (TSDC) [1-15]. These experiments have reported local heterogeneities in weakly interacting athermal miscible polymer blends, though blends are macroscopically mixed and the segmental relaxation time distribution remains unimodal (but anomalously broad). There are two main theoretical approaches, suggested for dynamic heterogeneity: (1) "thermal concentration fluctuations" (interchain contribution) and (2) "self-concentration effect" or "chain connectivity" (intrachain contribution).

The thermal concentration fluctuation models [9, 16] describe that the concentration fluctuation leads to a distribution of α relaxation processes throughout blends which explains the broadening of the relaxation spectra of miscible blends. On the other hand, the self-concentration models [17, 18] explain the dynamic heterogeneity by assuming that the local environment around a segment of polymer A is necessarily rich in polymer A compared to the average macroscopic concentration due to the chain connectivity. More recently, simulation-based studies [19, 20] revealed that both concentration fluctuations and self-concentration effects are essential for a quantitative understanding of all aspects of miscible blend dynamics. Thus, a plausible understanding on the dynamics in miscible polymer blends is phenomenologically and theoretically well

established but is limited only to bulk systems.

There has been much interest in studying the properties of polymers with finite thicknesses in the nanometer range and numerous studies have shown that the properties of thin films including dynamics, glass transition temperature (T_g), photoconductivity, moisture sorption, morphology, phase separation temperature and diffusion coefficient, are very different from those of bulk systems [21-29]. Furthermore, when films are confined to dimensions, comparable or smaller than the characteristic length scales of chains, a change in properties become intensified due to the enthalpic and entropic contributions. For example, the T_g of pure polystyrene (PS) supported on a silicon (Si) substrate with native oxide decreases with decreasing thickness because the free surface, which has faster dynamics and lower T_g than any other place in the sample, dominates the T_g behavior. On the other hand, 20 % of polystyrene-b-poly(methyl methacrylate) (PS-b-PMMA) chains in PS thin films on a Si substrate induces the opposite trend, i.e., an increase in T_g with decreasing thickness due to the attractive interactions between the native Si oxide layer and PS-b-PMMA chains, segregated to the substrate [25].

In this work, DS experiments are performed to research the dynamics of miscible blend thin films of poly(vinyl methyl ether) (PVME) and deuterated PS (dPS) by altering the molecular weight (MW) of dPS as well as the film thickness. We focus selectively on the dynamics of PVME components in the blends since PS chains have very weak dipole moments and hence only PVME chains are dielectrically active. It is shown that confining polymer blends in thin films induces the micro-phase separation due to interfacial interactions and redistributes chain relaxation times accordingly. This redistribution results in the speeding-up of dynamics as the film thickness decreases

and/or the MW of dPS increases. In addition, we suggest a proper method to analyze the dynamics of the miscible blend system.

6.2 Experimental Section

The PVME with number average molecular weight, M_n, of 24.4 kg/mol and polydispersity index (PDI) of 1.08 was obtained from Polymer Source Inc. and refrigerated with a desiccant until it was used. To prepare blend solutions for bulk and thin film samples, PVME was dissolved in toluene with different molecular weights of dPS (Polymer Source Inc.) in the weight ratio of 25/75 PVME/dPS. dPS in the M_n range of 3.8 to 525 kg/mol was used and will be hereafter abbreviated on the basis of molecular weights as follows; dPS3.8 (M_n: 3.8 kg/mol, PDI: 1.05), dPS4 (M_n: 4 kg/mol, PDI: 1.5), dPS10.9 (M_n: 10.9 kg/mol, PDI: 1.05), dPS132 (M_n: 132 kg/mol, PDI: 1.06), dPS190 (M_n: 190 kg/mol, PDI: 1.15) and dPS525 (M_n: 525 kg/mol, PDI: 1.09). Prepared solutions were well mixed at 1000 rpm using the orbital shaker (MS 3 digital, IKA).

For differential scanning calorimetry (DSC) measurements, blend solutions were completely dried and annealed at 340 K which is below a lower critical solution temperature (LCST) [29-31] for 48 hours. Bulk blend samples were heated at 10 K/min and cooled at 50 K/min alternatively between 233 K and 433 K using a TA instruments Q200 DSC. The T_gs of the bulk samples were then determined by the half-height midpoint of the transition at the second heating. Single T_gs of 291 K, 292 K, 314 K, 319 K, 321 K and 323 K with average accuracy of ± 2 K were observed over broad glass transitions for blend samples with dPS3.8 to dPS525, respectively.

Thin films of PVME/dPS blends were prepared and confined between two

aluminum (Al) electrodes using the following sample preparation procedure which can be found elsewhere [32]. Al electrodes with 0.5-0.8 mm in width and ~ 100 nm in thickness were evaporated on glass substrates (1 cm × 1 cm × 1 mm) which were thoroughly cleaned using glass detergent and acetone in the ultrasonic cleaner. After cleaning the Al-coated glass substrates using toluene, thin films with thicknesses of 102 ± 8 nm were spin-coated on these substrates. Additionally, 297 nm and 770 nm thick films were prepared only for PVME/dPS4 blends. A scanning probe microscope (SPM; Veeco Instruments Inc.) was used to measure the film thicknesses. Samples were then vacuum-dried overnight at room temperature and subsequently annealed at $T_{annealing}$ = 340 K for 48 hours (bulk $T_{g,blend} < T_{annealing} << LCST$ [29-31]). To make counter electrodes, Al layers were deposited on top of the thin films. Since polar water molecules can influence the relaxations of polymer [32], samples were annealed once more in a nitrogen atmosphere at 340 K for 10 hours to remove the possibility of water absorption during the sample transfer. After in-situ N_2 annealing, dielectric measurements were performed using DS (Novocontrol Technologies GmbH) in a frequency range of 0.1 Hz to 3 MHz at temperatures between 250 K and 325 K. Here, we briefly mention that only segmental relaxation of PVME was active in this experimental window. A thin film of ~ 145 nm poly(vinyl acetate) (PVAc; Polymer Source Inc.) with M_n of 145 kg/mol (PDI = 1.5) was also prepared in the same way to PVME/dPS DS samples except for the fact that the former was annealed at different conditions (vacuum for 24 hours and N_2 for 10 hours at 353K).

Samples for dynamic secondary ion mass spectroscopy (DSIMS) were prepared as follows. PVME/dPS blend thin films of ~ 105 nm thickness were spin-cast on the Al-

deposited Si substrates and annealed at 340 K for 48 hours. ~ 50 nm films of hydrogenated polystyrene (hPS; Pressure Chemical Co., M_n = 143.4 kg/mol, PDI = 1.06) were floated onto warm de-ionized water which is a non-solvent for PVME above 308 K [33]. These hPS films were then placed promptly on the top of the blend thin films as a sacrificial layer. DSIMS experiments were performed on a Physical Electronics 6650 Quadrupole instrument at the University of California at Santa Barbara. A CS^+ primary ion beam (6 keV and 50 nA) was used to sputter the samples with a 350 μm × 450 μm raster area, and negative secondary ions of hydrogen (H), deuterium (D), carbon (C), oxygen (O), Al and Si were monitored from the center 15% of the crater area. The film thickness, measured by the spectroscopic ellipsometry (SE; J.A. Woollam Co., Inc.), was used to convert the sputtering time axis into the depth scale.

6.3 Results and Discussion

We begin by discussing the difference between miscible polymer blends and homopolymers in an aspect of molecular dynamics analysis. Figures 6.1a and 6.1b represent the activation plots, showing the relationship between relaxation rate and inverse temperature, for PVME in PVME/dPS (25/75) blends obtained from the temperature dependence of the peak frequencies (frequency sweep) as well as from the frequency dependence of the peak temperatures (temperature sweep). Likewise, the activation plot for pure PVAc is illustrated in Figure 6.1c.

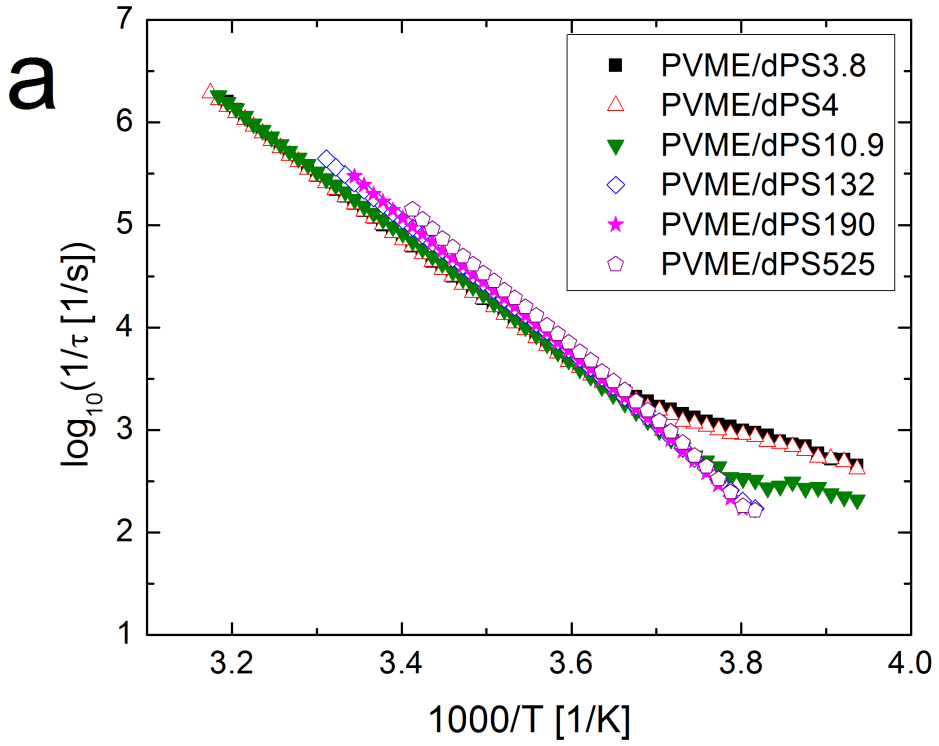
a
PVME/dPS3.8
PVME/dPS4
PVME/dPS10.9
PVME/dPS132
PVME/dPS190
PVME/dPS525
log10(1/τ [1/s])
1000/T [1/K]
1
2
3
4
5
6
7
3.2
3.4
3.6
3.8
4.0

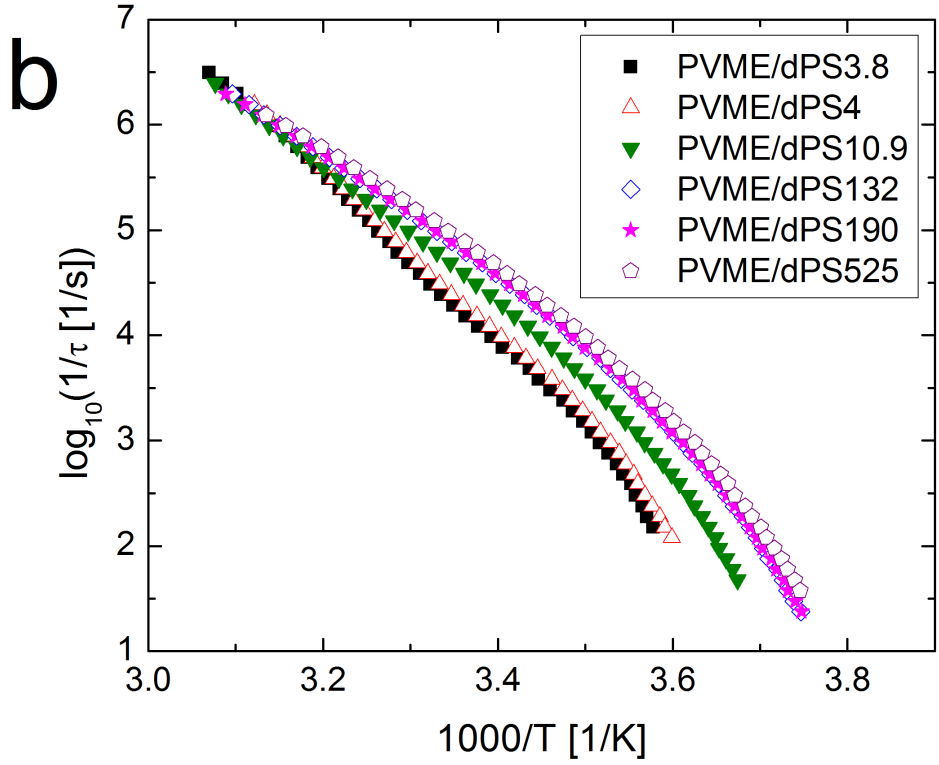
b
PVME/dPS3.8
PVME/dPS4
PVME/dPS10.9
PVME/dPS132
PVME/dPS190
PVME/dPS525
log10(1/τ [1/s])
1000/T [1/K]
1
2
3
4
5
6
7
3.0
3.2
3.4
3.6
3.8

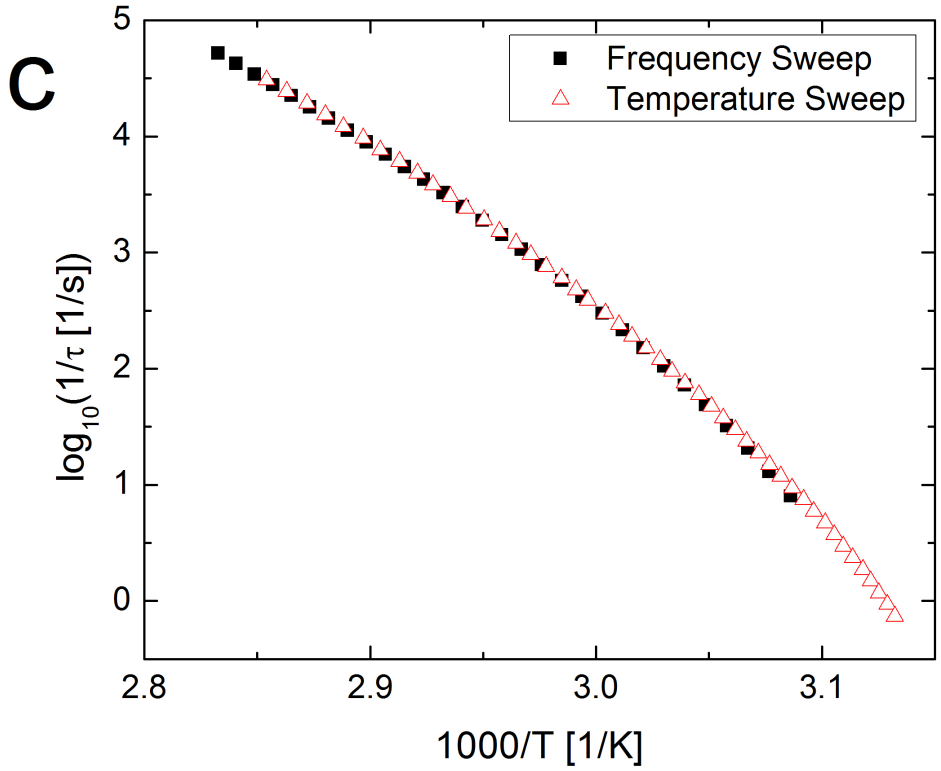

Figure 6.1 Activation plots (relaxation rate vs inverse temperature) for 25/75 PVME/dPS blend thin films obtained from **a**, frequency sweep and **b**, temperature sweep. The molecular weight of dPS varies from 3.8 kg/mol to 525 kg/mol. **c**, A pure PVAc thin film shows perfect overlap between activation plots from frequency sweep and temperature sweep.

First it is evident from the data in Figure 6.1a, where relaxation times from frequency sweep are plotted, that the relaxation times of PVME segmental (α) relaxation process deviate from high temperature behavior upon temperature reduction and become faster. This kind of behavior has been observed for the miscible polymer blends with large differences in the T_gs, and with higher concentration of high T_g polymers due to the constraints of the low T_g polymer segmental motion by the rigid high T_g one [6, 12, 13,

15]. Therefore, at low enough temperatures ($T < T_{g,blend}$) the cooperative motion of PVME chains is restricted in rigid dPS chains and possible motions are only faster local relaxation processes which follow Arrhenius-like behavior ($\tau(T) = \tau_0 \exp(B/T)$) [6, 12, 13, 15]. Here, τ_0 denotes the relaxation time at infinite temperature and B is a constant being related to the activation energy of the relaxation process. Hereafter, this Arrhenius-like relaxation process will be called α′ relaxation. It is noteworthy that we were not able to determine α′ relaxation process for blends with the first three high MW dPS (dPS132, dPS190 and dPS525) due to the fact that the intensity of the corresponding dielectric loss, ε″, peaks decreases with an increase in the MW of dPS. The details will be dealt with later in this paper. Figure 6.1b shows the activation plot from the temperature sweep where we find a striking discrepancy of about one order of magnitude in relaxation rates from the plot in Figure 6.1a. Moreover, no α′ relaxation process has been found in any blends. This discrepancy is unexpected, although activation plots from both the frequency sweep and the temperature sweep consistently show that α relaxation of PVME in PVME/dPS blends slows down with smaller MW dPS. It is generally known that dynamics analyses, carried out in both frequency sweep and temperature sweep, produce equivalent results [34]. This is clearly shown in Figure 6.1c for the activation plots of pure PVAc.

To understand what cause the unforeseen divergence, isothermal ε″ spectra of PVME in PVME/dPS4 blends as well as those of PVAc for the sake of comparison are plotted in Figures 6.2a and 6.2b.

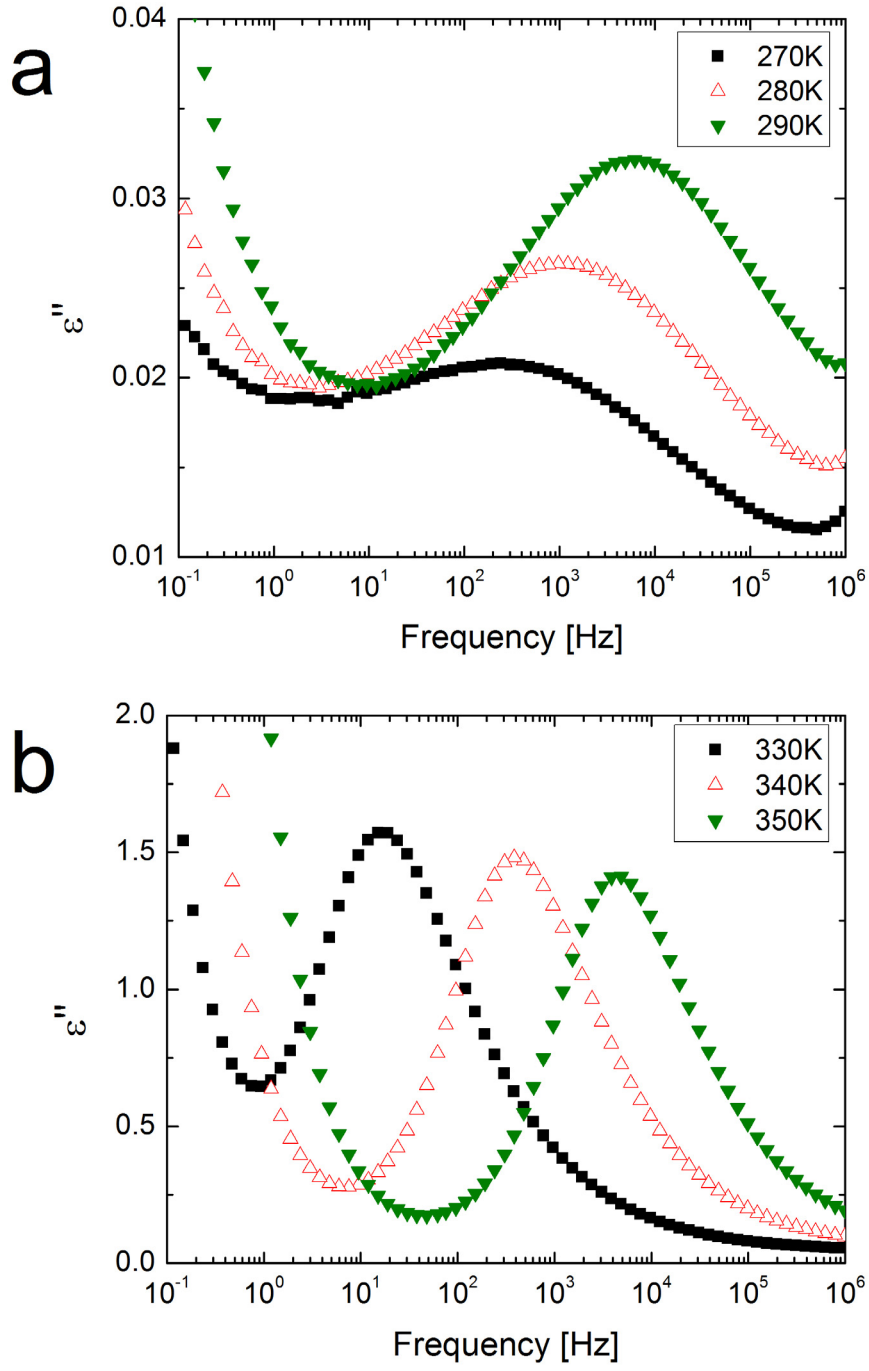

Figure 6.2 Frequency dependence of dielectric loss ε″ at different temperatures for **a**, PVME/dPS4 blend and **b**, pure PVAc thin films.

Two factors are noticeable: intensity change and breadth of the relaxation peaks. Normally, the intensity of main relaxation peak for amorphous polymers slightly decreases with increasing temperature [35]. The peak intensity of PVAc decreases by ~ 10 % with a temperature increase of 20 K as expected, while that of PVME changes nearly 3.5 times faster for the same temperature increase. The aforementioned restriction of PVME chain cooperative rearrangements in rigid dPS is responsible for this rapid temperature decrease. This means that the dipole reorientations are more restricted at lower temperatures and the dielectric response becomes weak with decreasing temperature, accordingly [15]. The other obvious difference is that the breadth of PVME relaxation peaks is much broader than that of PVAc peaks. In fact, it has been reported that the shape of the main relaxation peak for PVME in PVME/hPS blends is strongly affected by blending and that the full width at half maximum (FWHM) increases with an increase of hPS contents [5, 15]. As mentioned in Chapter 6.1, the heterogeneous local environment in blends (micro-phase separation) accounts for this broadening [8-10, 16-20]. Due to these two characteristics of blends, i.e. a sharp change of broad relaxation peaks, a marked deviation from the actual dynamics takes place when dielectric spectra are analyzed at constant temperatures or frequencies. This is obvious as it appears in Figures 6.3a and 6.3b where the three-dimensional (3D) curve and the contour map of ε'' are plotted as a function of both frequency and temperature. Strictly speaking, the relaxation times have to be derived from the maxima of the dielectric loss peaks in the frequency and temperature plane. However, for systems with homopolymers, analysis of data either from the frequency sweep or from the temperature sweep has been generally accepted because the discrepancy in activation plots is negligibly small (See Figure 6.1c).

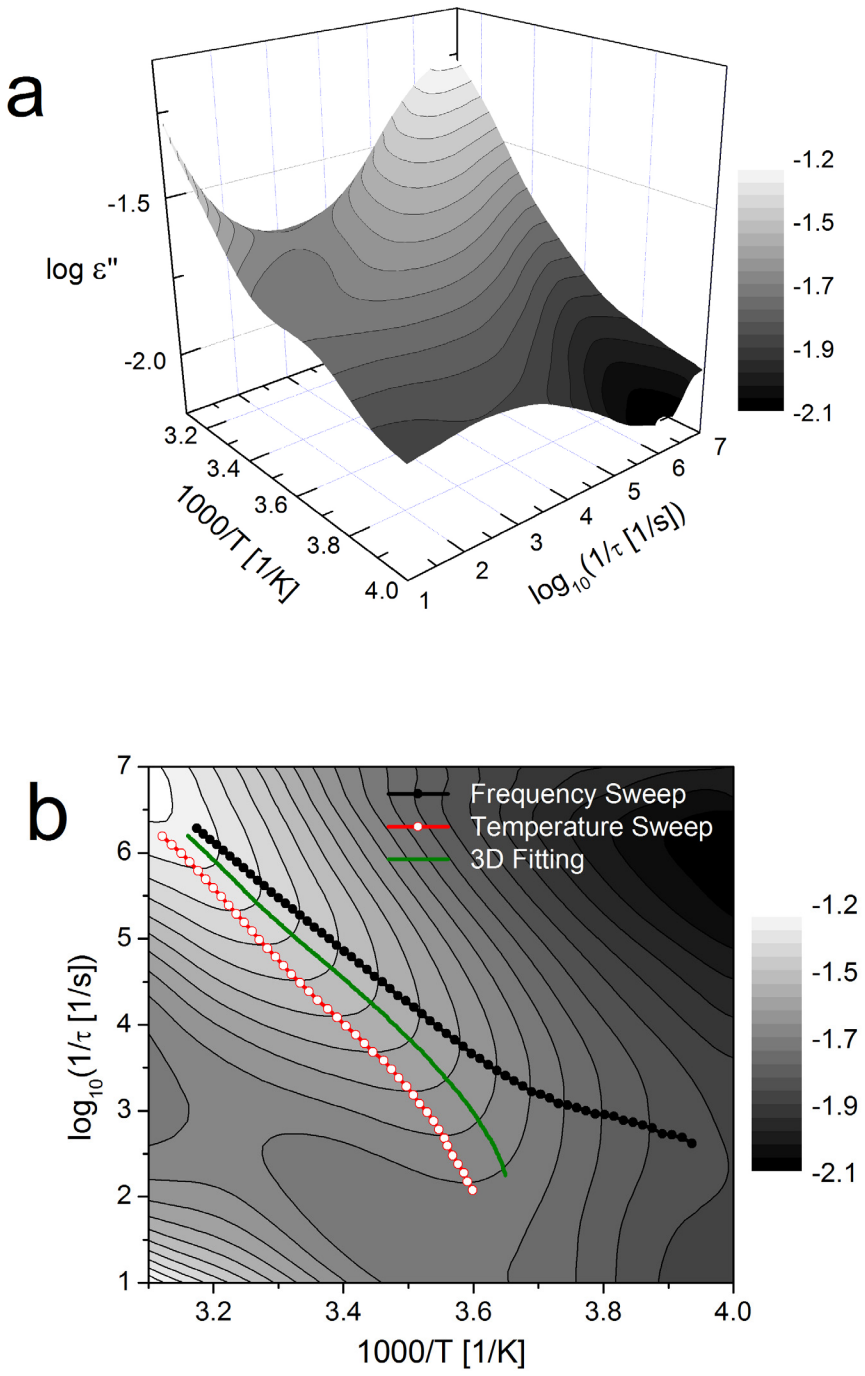

Figure 6.3 **a**, 3D and **b**, Contour map of ε″ for a PVME/dPS4 blend thin film as a function of frequency and temperature. Relaxation rates derived from three different analytical methods are plotted on the contour map.

On the other hand, more attention needs to be paid to the analysis of blend relaxation peaks. As shown in Figure 6.3b, a steep decrease of broad relaxation peaks generates blunt and wide contour lines. Therefore, relaxation times, taken from frequency sweeps (points of tangency to contour lines at constant temperatures) and temperature sweeps (points of tangency to contour lines at constant frequencies), are indeed placed at shoulders of relaxation peaks in the 3D plot, while actual relaxation times fall in between those values. Note that the α′ relaxation, obtained from a frequency sweep at low temperatures, is still acceptable due to the fact that its direction is almost parallel to the temperature axis, and so no significant difference from actual dynamics occurs.

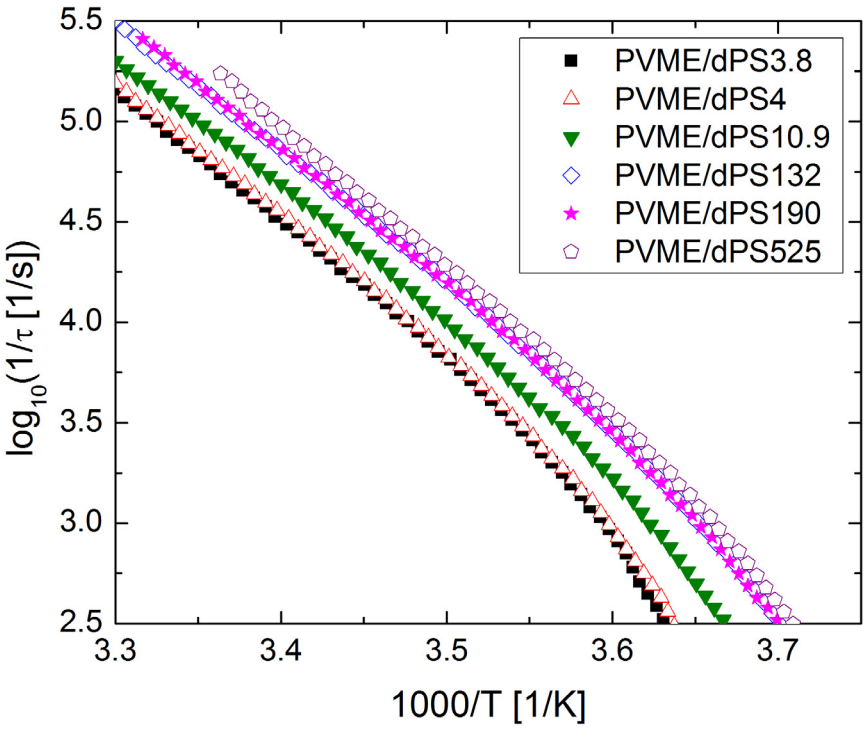

Figure 6.4 Actual activation plots, calculated from the fitting of ε″ 3D surfaces, for PVME blend thin films with different molecular weight of dPS, as indicated.

Figure 6.4 represents actual activation plots of α relaxation in PVME/dPS blends with different MWs of dPS, calculated based on 3D dynamics. As observed in Figures 6.1a and 6.1b, dynamics of PVME in these blends still become faster with an increase in MW of dPS. It is well accepted that the segmental dynamics of one component in weakly interacting miscible blends with high T_g polymers are slower than those with low T_g ones [4, 11]. In this respect, bulk blends of PVME and dPS having higher MWs (hence, higher T_gs and stiffer physical properties) should show slower PVME dynamics than blends with lower MW dPS. Therefore, it is quite extraordinary that the exactly opposite behavior is observed in our system (Figure 6.4).

Recall that the dynamics of thin film blends with thicknesses of ~ 102 nm are examined in this study. Although significant changes in thin film properties occur below thicknesses of 40-60 nm due to the influence of the confinement effect and of the interfacial interactions between polymer films and external interfaces [21-27, 29], it has been also reported that the interfacial interaction still affects the film properties up to 150-250 nm [25, 28]. DSIMS was employed to explore the possibilities that the interfacial interaction might cause the morphological change and even the peculiar dynamic behavior in our system. We note that, unlike the actual DS samples, DSIMS samples on Al-coated substrates were not covered with another Al electrodes since we observed that the depth profiles from Al-sandwiched films show the rising slope of the lines, a discontinuity at the Al-to-polymer interface and poor depth resolution due to either charging or roughening problem on the top Al layer. However, the morphology near the top Al electrode in Al-sandwiched DS samples can be easily expected by that near the bottom electrode due to their symmetric structure. In Figures 6.5a and 6.5b,

signals of H ions from PVME and D ions from dPS are plotted as a function of the depth, *d*, from the upper interface between a hPS sacrificial layer and a PVME/dPS blend film. It is clearly observable in these figures that the intensity of H ions in the interior of the blended thin films strongly increases around all the interfaces, while that of D ions decreases, regardless of the MW of dPS. The signal intensity increase at the upper interface is partly due to the tail of the H ion intensity peak from the hPS sacrificial layer. Since DSIMS samples were annealed without a sacrificial layer, the segregation of PVME chains to the free surface due to their lower surface tension [29, 31] is also responsible for this intensity increase. In this study, our interest lies primarily in the Al-to-polymer interface (the lower interface in DSIMS samples) where the intensity of H ions increases differently depending on the MW of dPS. It has been reported in studies of PVME/dPS blend thin films that dPS chains enriches a hydrophilic substrate, whereas a hydrophobic substrate is significantly wet by PVME chains [29, 31]. Hence, it makes sense that PVME chains preferentially segregate to the substrate due to the hydrophobic native oxide layer, Al_2O_3, which grows instantly onto bare Al substrates [36]. It is important to note that, within the resolution limit of DSIMS (~ 10 nm), PVME chains in the middle (i.e. sufficiently far from the interfaces) are highly miscible even with dPS525 chains since samples were processed well below the LCST of PVME/dPS blends which is much higher than that of blends with hPS due to a stronger intermolecular attraction [29-31]. Therefore, we can rule out the possibility of the macro-phase separation in the interior of the film that would induce an increase in fast PVME-rich domains and, consequently, a change in dynamics.

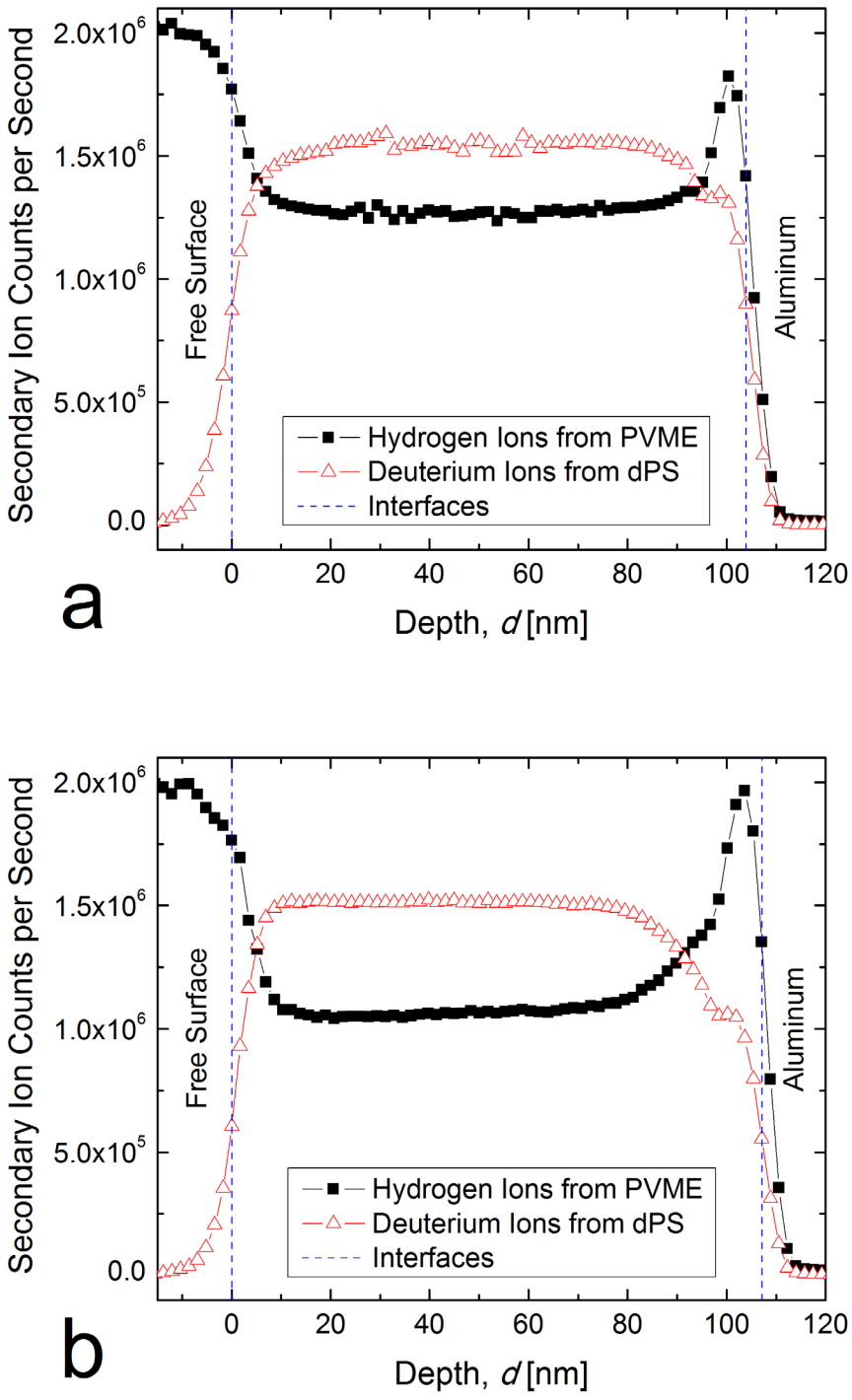

Figure 6.5 Depth profiles of hydrogen ions (implying PVME) and deuterium ions (implying dPS) for **a**, PVME/dPS3.8 and **b**, PVME/dPS525 blend thin films.

We now address the MW-dependent phase separation near Al substrates in the light of entropic effects at the interfaces between chemically similar polymer melts and grafted chains on flat surfaces. It has been suggested that when chains of degree of polymerization, N, grafted onto a flat surface, are interacting with host chains of degree of polymerization, P, the interfacial condition is strongly affected by N, P and the grafting density of a brush layer, σ [37]. For a low σ, free host chains easily penetrate and swell the grafted brush layer. These penetrated chains begins to be expelled from the brush layer when $\sigma\sqrt{N} = (P/N)^{-1/2}$ if $P/N < 1$ and $\sigma\sqrt{N} = 1$ if $P/N > 1$. With increasing σ or P/N until $\sigma\sqrt{N} > (P/N)^{-2}$, a surface tension between host chains and a brush layer becomes positive. In other words, host chains dewet the grafted brush layer (a dry brush condition). This scaling theory [37] has been successfully used to explain the interfacial conditions of athermal systems on a flat and a curved surface [38, 39]. Since a Flory-Huggins interaction parameter, χ, for the PVME/dPS blends in our experimental temperature range is weakly negative, implying weak attractive interactions between PVME and dPS chains [40], the brush layer in our system might require slightly higher σ or P/N to drive out host chains than that in athermal systems. Nevertheless, it still cannot be questioned that, qualitatively, the brush layer will become drier with higher P at a given σ or N. Put differently, higher MW host chains are less compatible with the brush layer. Figure 6.5 shows that PVME and dPS525 chains start phase-separating at $d \sim 80$ nm, while this occurs right near the Al substrate in the PVME/dPS3.8 system. As a PVME-enriched layer of ~ 20 nm has been reported for PVME blends with high MW PS [41], it is not surprising to observe such a wide layer in our PVME/dPS525 thin film. As a result, higher and lower concentrations of H ions are observed near the substrate and in

the inner part for the PVME/dPS525 blend film, respectively. This is reasonable, based on aforementioned criteria, because lower miscibility of PVME and dPS525 chains near the substrate induces the stronger segregation of PVME chains to the substrate.

MW effects on the surface enrichment of PVME could be simply explained from a surface tension point of view as well. Since the surface tension of homopolymer chains increases with an increase in MW, higher MW dPS induces a stronger driving force for the PVME segregation at the surface. It has been reported that this driving force results in an increase in the average surface composition of PVME [42]. Therefore, it is reasonable that more PVME chains enrich the surface of PVME/dPS525 than that of PVME/dPS3.8 (See Figure 6.5).

Peculiar dynamic behavior, shown in Figure 6.4, can be interpreted in terms of changes in relaxation time distribution caused by the micro-phase separation near the substrate. In PVME/dPS3.8 blend thin films, most of the PVME chains are affected by rigid dPS chains. So, their segmental dynamics are much slower than pure PVME chains. By increasing the MW of dPS chains, however, the PVME chains near the substrate gradually tend to release dPS chains and form dPS-free regions where their motions are less restricted. As a fraction of fast domains (near the substrate) increases and that of slow domains (in the interior) decreases, the distribution of dynamics moves toward faster relaxation rates. Consequently, PVME chains in blends with higher MW dPS, on average, have faster dynamics than those in lower MW dPS blends. There are a few questions remaining unanswered regarding the α' relaxation process. As mentioned early in this paper, ε'' peaks for this process diminished in intensity with increasing MW of dPS and were barely discernible in blends with dPS132, dPS190 or dPS525 (See Figure 6.1a).

This is due to the fact that blends with higher MW dPS possess lower effective concentration $\varphi_{PVME,interior}$ of PVME chains in the interior where dynamics of PVME chains are limited by the rigid matrix of the dPS chains. As a consequence, for these three blends with high MW dPS, the dielectric strength of ε″ peaks related to the α′ relaxation process decreases and peaks are not recognizable anymore because of the conductivity peak shown at low frequencies in Figure 6.2a.

We are also interested in the transition temperature, T_{tr}, from α relaxation to α′ relaxation. As stated above, this transition takes place due to the constraint of PVME segmental motions by the frozen dPS chain matrix under the conditions of $\varphi_{PVME}/\varphi_{PS} < 1$ and $T < T_{g,blend}$. For bulk blends, it can be easily expected that T_{tr} increases with $T_{g,blend}$ since the matrix of higher $T_{g,blend}$ samples would start to freeze at higher temperatures. However, in our system this occurs at the lower temperature with slower α′ relaxation for the blend with higher MW dPS (Figure 6.1a). It is necessary to understand the distribution of the heterogeneity throughout the thin films in order to explain this phenomenon. Each domain in the interior has a PVME concentration around $\varphi_{PVME,interior}$ which is less than 25 *wt*.%. As approaching toward the substrate, the φ_{PVME} of domains increases rapidly in the intermediate region between the interior and the PVME-rich layer. Finally, PVME chains start to surround the dPS chains and form a brush layer near the substrate. Therefore, as the temperature decreases, α′ relaxation is first activated by domains in the interior which have the highest local $T_{g,blend}$. By lowering the temperature, more frozen domains gradually contribute to an increase in the intensity of α′ relaxation process. At last, the α–α′ transition occurs when α′ relaxation process from higher local $T_{g,blend}$ domains dominates the whole dynamics over α relaxation process from low local

$T_{g,blend}$ domains. As shown in Figure 6.5, due to the stronger segregation of PVME chains, blend thin films with higher MW dPS possess the broader intermediate region where domains mostly have higher φ_{PVME}, and therefore lower $T_{g,blend}$ compared to those in the interior. As a result, the lower T_{tr} is observed for the higher MW dPS sample because there are more domains requiring lower temperature to activate the α' relaxation process.

A last concern regarding α' relaxation process is that it slows down with an increase in the MW of dPS, even though blend thin films with higher MW dPS contain a larger portion of domains with lower local $T_{g,blend}$ inducing faster segmental dynamics. This might be due to the confinement effects. It has been reported that when the concentration of PS in the bulk PVME/PS mixtures increases, samples show faster α' relaxation processes, believed to be associated with the confinement effects [13]. In the same manner, a decrease of φ_{PVME} in the intermediate region leads to a speeding-up of α' relaxation processes when the MW of dPS chains decreases.

Before concluding, we would like to touch briefly on the thickness dependence of PVME segmental dynamics in PVME/dPS blend films. Figure 6.6 shows the temperature dependence of the normalized dielectric loss at a frequency of 3.9 kHz for PVME/dPS4 films with three different thicknesses. Apparently, the peak temperature increases with an increase in the film thickness and shows a tendency to converge for thick films above 297 nm which might be considered as a bulk. This means that the α relaxation of the PVME chains becomes slower in thicker films and approaches to the bulk value. Now this behavior is not surprising at all. As already explained, when this blend film is thin enough, the segregation of PVME chains to the substrate leads to an increase in speed of the dynamics. For thicker films, however, PVME chains mostly contribute to the

increase of slow domains in the interior due to the limited number of PVME chains that could saturate the substrate. As the thickness increases further, $\varphi_{PVME,interior}$ would get close to the bulk concentration and also the dynamics of the fast domain near the substrate would be negligible due to the vast majority of PVME chains trapped in the rigid PS matrix. As a result, the segmental dynamics of PVME chains slows down with an increase in the film thickness until it reaches the bulk dynamics.

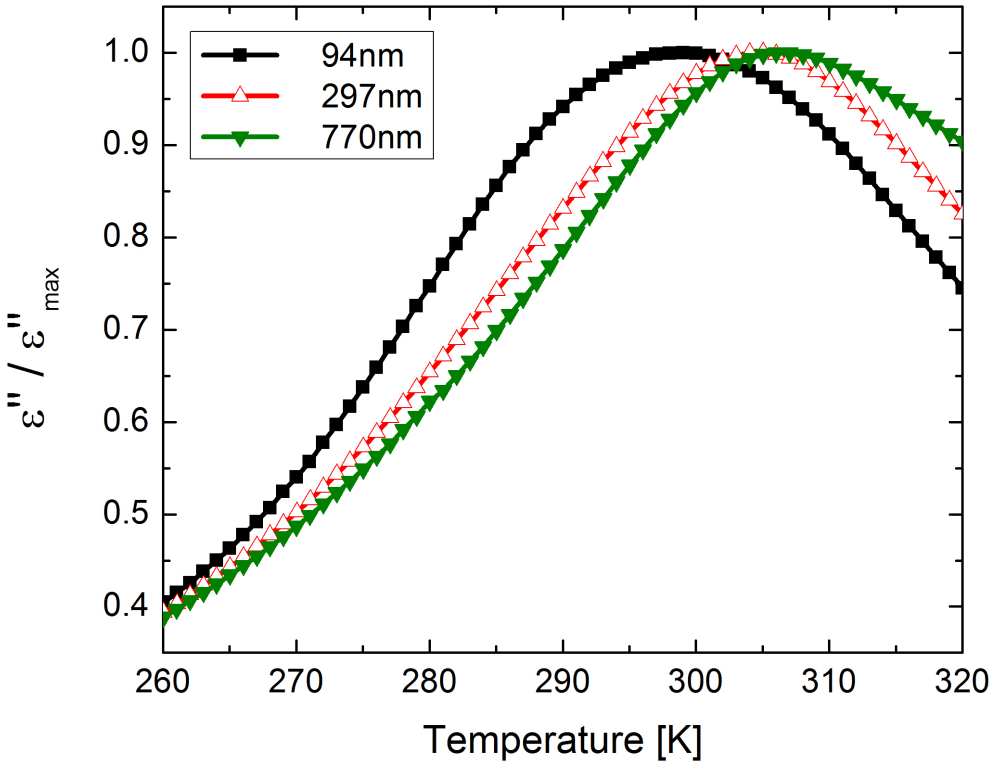

Figure 6.6 Temperature dependence of the normalized dielectric loss with respect to the maximum value of each peak, $\varepsilon''/\varepsilon''_{max}$, at a constant frequency of 3.9 kHz for PVME/dPS4 blend films with thicknesses of 94 nm, 297 nm and 770 nm.

6.4 Conclusion

In this study, we have examined the dynamics of PVME chains within thin film blends of PVME and dPS. The typical way of analyzing the characteristic relaxation times is to take the data at the maximum of the relaxation peaks from either a frequency sweep or a temperature sweep. This simple analysis works great for systems with homopolymers. However, a large discrepancy between the relaxation times from the frequency and from the temperature sweep was observed in our system, which consisted of miscible polymer blends with large difference in T_gs. To our knowledge, this has not been reported before. We found that this discrepancy is due to a rapid intensity change of broadened relaxation peaks, caused by the micro-phase separation in PVME/dPS blends and the restriction of PVME chain motions in rigid dPS chains. A fitting of relaxation peaks in the frequency and temperature plane shows that actual relaxation times exist between values from frequency sweep and temperature sweep. We observed from actual dynamics of α processes that an increase in the MW of dPS resulted in faster α processes of PVME chains, quite contrary to the conventional concept for miscible bulk blends. In our system, the interfacial interactions between polymer films and the substrates caused the micro-phase separation, leading to the redistribution of concentrations of PVME chains throughout films. This redistribution was highly influenced by the PVME brush layer condition, i.e. the degree of the dPS chain penetration into the brush layer (or miscibility). Due to a tendency for PVME chains to drive higher MW dPS chains out of the brush layer, the effective PVME chain concentration near the substrate (fast region) increased, while that in the interior (slow region) decreased. Hence, the blends with higher MW dPS showed faster dynamics. This change in the effective concentration of

PVME chains also accounts for the MW dependence behavior of α' processes. Lastly, we showed that the dynamics of thicker films is slower. This is because additional PVME chains introduced by increasing the thickness are mostly used to expand the slow domains in the interior due to the limited space near the substrate and consequently fast PVME-rich region becomes insignificant.

6.5 References

1. Kwei, T.K., T. Nishi, and R.F. Roberts, *Study of compatible polymer mixtures.* Macromolecules, 1974. **7**(5): p. 667-674.

2. Schmidtrohr, K., J. Clauss, and H.W. Spiess, *Correlation of structure, mobility, and morphological information in heterogeneous polymer materials by 2-dimensional wideline-separation NMR-spectroscopy.* Macromolecules, 1992. **25**(12): p. 3273-3277.

3. Lemenestrel, C., et al., *C-13 NMR investigation of local dynamics in compatible polymer blends.* Macromolecules, 1992. **25**(12): p. 3020-3026.

4. Lutz, T.R., Y.Y. He, and M.D. Ediger, *Segmental dynamics of dilute polystyrene chains in miscible blends and solutions.* Macromolecules, 2005. **38**(23): p. 9826-9835.

5. Cendoya, I., et al., *Effect of blending on the PVME dynamics. A dielectric, NMR, and QENS investigation.* Macromolecules, 1999. **32**(12): p. 4065-4078.

6. Genix, A.C., et al., *Neutron scattering investigation of a diluted blend of poly(ethylene oxide) in polyethersulfone.* The Journal of Chemical Physics, 2008. **128**(18): p. 184901-11.

7. Pathak, J.A., et al., *Dynamics in miscible blends of polystyrene and poly(vinyl methyl ether).* Macromolecules, 1999. **32**(8): p. 2553-2561.

8. Rellick, G.S. and J. Runt, *A dielectric study of poly(ethylene-co-vinyl acetate) polyvinyl-chloride) blends .2. Loss curve broadening and correlation parameters.* Journal of Polymer Science Part B-Polymer Physics, 1986. **24**(2): p. 313-324.

9. Zetsche, A. and E.W. Fischer, *Dielectric studies of the alpha-relaxation in miscible polymer blends and its relation to concentration fluctuations.* Acta Polymerica, 1994. **45**(3): p. 168-175.

10. Katana, G., et al., *Influence of concentration fluctuations on the dielectric alpha-relaxation in homogeneous polymer mixtures.* Macromolecules, 1995. **28**(8): p. 2714-2722.

11. Mansour, A.A., S.A. Madbouly, and G.W.H. Hohne, *Dielectric investigation of molecular dynamics of blends .3. Effect of molecular weight in TMPC/PS blends.* Polymer International, 1996. **41**(4): p. 395-406.

12. Sy, J.W. and J. Mijovic, *Reorientational dynamics of poly(vinylidene fluoride)/poly(methyl methacrylate) blends by broad-band dielectric relaxation spectroscopy.* Macromolecules, 2000. **33**(3): p. 933-946.

13. Lorthioir, C., A. Alegria, and J. Colmenero, *Out of equilibrium dynamics of poly(vinyl methyl ether) segments in miscible polystyrene-poly(vinyl methyl ether) blends.* Physical Review E, 2003. **68**(3): p. 031805.

14. Takeno, H., M. Kobayashi, and T. Aikawa, *Localized cooperative molecular motion in miscible polymer mixtures with large difference in glass-transition temperatures.* Macromolecules, 2006. **39**(6): p. 2183-2190.

15. Schwartz, G.A., J. Colmenero, and A. Alegria, *Single component dynamics in miscible poly(vinyl methyl ether)/polystyrene blends under hydrostatic pressure.* Macromolecules, 2007. **40**(9): p. 3246-3255.

16. Kumar, S.K., et al., *Concentration fluctuation induced dynamic heterogeneities in polymer blends.* Journal of Chemical Physics, 1996. **105**(9): p. 3777-3788.

17. Chung, G.C., J.A. Kornfield, and S.D. Smith, *Compositional dependence of segmental dynamics in a miscible polymer blend.* Macromolecules, 1994. **27**(20): p. 5729-5741.

18. Lodge, T.P. and T.C.B. McLeish, *Self-concentrations and effective glass transition temperatures in polymer blends.* Macromolecules, 2000. **33**(14): p. 5278-5284.

19. Salaniwal, S., et al., *Computer simulations of local concentration variations in miscible polymer blends.* Macromolecules, 2002. **35**(24): p. 9211-9218.

20. Shenogin, S., et al., *Dynamics of miscible polymer blends: Predicting the dielectric response.* Macromolecules, 2007. **40**(16): p. 5767-5775.

21. Fukao, K., et al., *Relaxation dynamics in thin supported polymer films.* Journal of Non-Crystalline Solids, 2002. **307**: p. 517-523.

22. DeMaggio, G.B., et al., *Interface and surface effects on the glass transition in thin polystyrene films.* Physical Review Letters, 1997. **78**(8): p. 1524-1528.

23. Tsui, O.K.C., T.P. Russell, and C.J. Hawker, *Effect of interfacial interactions on the glass transition of polymer thin films.* Macromolecules, 2001. **34**(16): p. 5535-

5539.

24. Ellison, C.J. and J.M. Torkelson, *The distribution of glass-transition temperatures in nanoscopically confined glass formers.* Nature Materials, 2003. **2**(10): p. 695-700.

25. Oh, H. and P.F. Green, *Role of diblock copolymers toward controlling the glass transition of thin polymer films.* Macromolecules, 2008. **41**(7): p. 2561-2566.

26. Zhang, X.J., S.A. Jenekhe, and J. Perlstein, *Nanoscale size effects on photoconductivity of semiconducting polymer thin films.* Chemistry of Materials, 1996. **8**(8): p. 1571-1574.

27. Huang, H.L., Y.G. Xu, and H.Y. Low, *Effects of film thickness on moisture sorption, glass transition temperature and morphology of poly(chloro-p-xylylene) film.* Polymer, 2005. **46**(16): p. 5949-5955.

28. Frank, B., et al., *Polymer mobility in thin films.* Macromolecules, 1996. **29**(20): p. 6531-6534.

29. Tanaka, K., et al., *Ultrathinning-induced surface phase-separation of polystyrene poly(vinyl methyl ether) blend film.* Macromolecules, 1995. **28**(4): p. 934-938.

30. Yang, H., et al., *Deuteration effects on the miscibility and phase-separation kinetics of polymer blends.* Macromolecules, 1986. **19**(6): p. 1667-1674.

31. Karim, A., et al., *Phase-separation-induced surface patterns in thin polymer blend films.* Macromolecules, 1998. **31**(3): p. 857-862.

32. Serghei, A. and F. Kremer, *Unexpected preparative effects on the properties of thin polymer films*, in *Characterization of polymer surfaces and thin films*, K. Grundke, M. Stamm, and H.J. Adler, Editors. 2006, Springer-Verlag Berlin: Berlin. p. 33-40.

33. Maeda, H., *Interaction of water with poly(vinyl methyl ether) in aqueous-solution.* Journal of Polymer Science Part B-Polymer Physics, 1994. **32**(1): p. 91-97.

34. Serghei, A. and F. Kremer, *Confinement-induced relaxation process in thin films of cis-polyisoprene.* Physical Review Letters, 2003. **91**(16): p. 165702.

35. Schlosser, E. and A. Schonhals, *Recent development in dielectric-relaxation spectroscopy of polymers.* Colloid and Polymer Science, 1989. **267**(11): p. 963-969.

36. Tseng, S.Y., et al., *Glycan arrays on aluminum-coated glass slides.* Chemistry-an Asian Journal, 2008. **3**(8-9): p. 1395-1405.

37. Ferreira, P.G., A. Ajdari, and L. Leibler, *Scaling law for entropic effects at*

interfaces between grafted layers and polymer melts. Macromolecules, 1998. **31**(12): p. 3994-4003.

38. Jopp, J. and R. Yerushalmi-Rozen, *Autophobic behavior of polymers at the melt-elastomer interface.* Macromolecules, 1999. **32**(21): p. 7269-7275.

39. Oh, H. and P.F. Green, *Polymer chain dynamics and glass transition in athermal polymer/nanoparticle mixtures.* Nature Materials, 2009. **8**(2): p. 139-143.

40. Shibayama, M., et al., *Study of miscibility and critical phenomena of deuterated polystyrene and hydrogenated poly(vinyl methyl ether) by small-angle neutron-scattering.* Macromolecules, 1985. **18**(11): p. 2179-2187.

41. Thomas, K.R., et al., *Wetting induced instabilities in miscible polymer blends.* Soft Matter, 2010. **6**(15): p. 3517-3523.

42. Bhatia, Q.S., D.H. Pan, and J.T. Koberstein, *Preferential surface-adsorption in miscible blends of polystyrene and poly(vinyl methyl ether).* Macromolecules, 1988. **21**(7): p. 2166-2175.

CHAPTER 7

CONCLUSION

Considerable efforts have been invested toward developing functional nanostructured polymeric materials, and understanding their properties for applications include coatings, displays, photovoltaic devices, aerospace components and automobile parts. The interest in these systems is based on their unique and exceptional properties that often exceed those of conventional materials; it is generally difficult to predict their properties by conventional mean field theoretical approaches. Despite the extensive scientific research on nanostructured polymer composites, many questions regarding physical mechanisms behind the property changes still remain unanswered, and in some cases controversial. Therefore, the work presented in this dissertation has been focused primarily on understanding the connection between complex interactions, nanostructures and properties of polymeric nanocomposites. Additionally, attempts were made at developing rules to understand how to tailor their properties. To achieve these objectives, we examined the properties of the nanocomposites, with designed nanostructures by blending bulk and/or thin film homopolymers with three different kinds of nanoscale additives: diblock copolymers (micelles), nanoparticles and other homopolymers.

In Chapter 3 it was shown how the nanostructured materials that were developed due to the addition of polystyrene-b-poly(methyl methacrylate) (PS-b-PMMA) diblock copolymers to PS host influenced the glass transition temperature (T_g) of PS thin films,

supported on silicon (Si) substrates (with native oxide layers). It was observed that with the addition of only 3 *wt*.% of PS-b-PMMA chains the T_g increased by 10 K throughout the entire thickness range. With a continued increase in copolymer content the trend was reversed. The increase in the T_g for ~ 20 nm thin films with 20 *wt*.% copolymers was approximately 35 K. This significant change is associated with the strong segregation of PS-b-PMMA chains toward the Si substrate. Within the notion of dynamic percolation theory, the fraction of the slow domains in the system increased, leading to the increase of T_g. We found that this preferential segregation also resulted in suppression of micelle formation, compared to the bulk. The critical micelle composition is orders of magnitude smaller in the bulk. The other finding is that the T_gs of blend thin films were not influenced by the presence of micelles; the micelles can be considered as soft core/shell nanoparticles. This will be briefly revisited below.

In Chapter 4 we explored the structure and dynamics of athermal bulk polymer nanocomposites (PNCs) of PS and gold nanoparticles onto which PS chains were grafted ($AuPS_x$; x denotes the degree of polymerization of grafted PS chains). It was shown that despite the fact that short ligand (N = 10) grafted nanoparticles ($AuPS_{10}$) aggregated within the PS hosts at relatively high concentrations, significant reductions of the T_g and the relaxation times of the polymer chains were observed. The aggregation is because unfavorable entropic interactions between grafted ligands under these "dry brush" conditions where penetration of host chains into the grafted ligand brush is prohibited. Consequently, host chains in contact with the brush layers experience less local friction at the nanoparticle surface. Therefore the T_g and the relaxation time of the PS host chains decrease. On the other hand, for the case of longer ligand (N = 481) attached

nanoparticles ($AuPS_{481}$) a "wet brush" condition is achieved; interpenetration of the host chains occurs. Due to the extremely slow dynamics of these long tethered chains compared to the host chains, the dynamics of the host chains slow down (longer relaxation times). Eventually, these PNCs have the slower dynamics and the higher T_g than pure PS.

In Chapter 5, we extended our interest to both bulk and thin film PNCs where we considered the influence of enthalpic interactions. The main finding of this study is that the properties of PNCs are strongly affected by the nanoparticle distribution. In other words, the segregation and/or aggregation of nanoparticles, induced by the interfacial interactions or the thermodynamics compatibility, lower the nanoparticle effects on properties. Hence, bulk compatible PNCs generally exhibit more significant changes in properties than thin film PNCs and PNCs in which the host/brush interactions are incompatible.

The observation that the micelles did not influence the bulk T_g can now be reconciled. Recall that micelles in PS/PS-b-PMMA blend thin films didn't affect the changes in the T_gs. Based on Chapter 4, due to the extremely high P/N of ~ 12.8, micelles were supposed to form the dry brush which induced their segregation toward the interfaces as shown in Figure 3.4. Therefore, It is not surprising that micelles in this system had no effects on the T_g behavior as described in Chapter 5.

Finally, the dynamics of miscible polymer/polymer blend thin films were examined in Chapter 6. These blends are known to possess microscopic compositional heterogeneities, but macroscopically miscible. These systems, due to the local compositional heterogeneties, exhibit to thermodynamically complex behavior, in their

rheological and dielectric responses. The dynamics of these become more complex when they are confined in the external "walls" due to the interfacial interactions. We observed that the dynamics of poly(vinyl methyl ether)/deuterated polystyrene (PVME/dPS) blend thin films between aluminum (Al) substrates became faster with an increase in the molecular weight of dPS. In addition, the PVME showed slower dynamics as the film thickness increased from ~ 100 nm to ~ 800 nm. It was shown in Chapter 6 that these two unexpected results were related with the strong phase segregation of the PVME chains to the Al substrates, which increased with increasing on the molecular weight of dPS.

My research thus far has revealed how the complex interactions in polymer composites influence the nanostructure formation, which influences their properties. It has been also shown that the properties of the nanostructured polymer composites could be tailored through control of various molecular interactions. It is my hope that a fundamental understanding of these findings will provide new insights into the structure-properties-processing relations and help effectively produce nanostructured polymer composites with the desired properties for the industrial applications.

APPENDICES

These appendices cover step-by-step experimental procedures for the frequently used techniques in this dissertation. In the first part, we show the preparation of the capped thin film samples for dielectric studies, based on the Dr. Anatoli Serghei's Ph.D. dissertation. These samples are extremely sensitive to dusts and contaminant which could cause a high conductivity or even a short circuit. Therefore, they need to be carefully prepared in a clean environment. Second, the synthesis procedures for polymer-grafted gold nanoparticles are described in detail. This work is based on a standard two-phase arrested precipitation method by Dr. Mathias Brust.

Appendix A Preparation of Capped Thin Films for Dielectric Studies

- Preparation of Glass Substrates

Note: All the procedures are performed in the laminar flow hood.

1. Clean the work-table with acetone and toluene.
2. Wash the ultrasonic cleaner with water multiple times and fill it with water.
3. Set the temperature of the ultrasonic cleaner at 60 °C.
4. Rinse glass dishes (or beakers) with deionized (DI) water 5 times.
5. Sonicate the glass holder and the mask in the DI water-filled dishes for ~ 1 hour.
6. Rinse tweezers with acetone and dry them with N_2.
7. Wipe the ruler using ethanol.
8. Gently wipe the glass slides using acetone.
9. Cleave them to make ~ 21 1 cm x 1 cm glass substrates.
10. Put them in the glass holder and refill the dish with fresh DI water.
11. Place the glass holder in the dish and sonicate glass substrates.
12. Inject 0.5 % ~ 2 % of glass detergent (e.g. ~ 3 ml for a 2/3-filled 90 cm × 50 cm glass dish) and wait for ~ 20 minutes.
13. Set the temperature of the ultrasonic cleaner at room temperature.
14. Wash another glass dish with DI water 5 times and fill it with DI water.
15. Transfer the glass holder into the glass dish with fresh DI water.
16. Wash 1st glass dish with DI water 5 times and refill the fresh DI water.
17. Put the glass holder back into the 1st glass dish.
18. Repeat step 14 ~ 17 until all detergent bubbles disappear.
19. Wash one glass dish with acetone 5 times and fill it with acetone.
20. Take out the glass holder and dry it with N_2.
21. Sonicate glass substrates in the acetone-filled dish for several minutes.
22. Wash the petri-dish with acetone 5 times, dry it with N_2.
23. Take out the mask and rinse it with acetone.
24. Dry it with N_2 and place it in the petri-dish.
25. Take out and rinse the glass substrates with acetone one by one.
26. Immediately dry substrates with N_2 and place only clean ones in the mask.
27. Cover the petri-dish with the lid.

- Evaporation of 1st Electrode

1. Load the mask with substrates quickly in the chamber.
2. Vacuum out the chamber down to 10^{-8} mbar.
3. Evaporate aluminum (Al) at the rate of ~ 10 nm/s or max. rate and deposit 70 ~ 100 nm of Al.
4. Cool down and vent the chamber.
5. Keep the mask in the petri-dish and carry them into the laminar flow hood.
6. Wash and fill the small glass beaker with toluene.
7. Sonicate one glass substrate in the toluene-filled beaker for ~ 1 minute.
8. Dry it with N_2.

9. Repeat step 7 ~ 8 for all other glass substrates.
10. Keep only very clean glasses in the labeled sample box.

- Spin-coating Procedure

1. Clean the spin-coater with acetone and toluene.
2. Place the glass substrate on the spin-coater and rotate it.
3. Inject 2 ~ 3 ml toluene directly on the sample and let it dry for ~ 1 minute.
4. Stop the rotation, cover the glass substrate with a sample solution and rotate it.
5. Repeat step 2 ~ 4 for all other solutions.
6. Keep them in the sample box till annealing procedure.
7. Place samples in the cleaned oven.
8. Vacuum-dry and anneal the samples under the proper annealing conditions.
9. Cool down the chamber slowly under the vacuum.
10. Rinse the glass petri-dish and the mask with acetone.
11. Dry them with N_2 and place the mask in the petri-dish.
12. Place the samples in the mask.
13. Cover the petri-dish with the lid.

- Evaporation of 2nd Electrode

1. Follow the step 1 ~ 5 of 'Evaporation of 1st Electrode'.
2. Put the samples in the labeled sample box.

- Sample Loading (Step 6 can be skipped if the ε' of the polymer at the low temperature and high frequency is already known.)

1. Clean the top and bottom brass electrodes with acetone and toluene.
2. Select the best condenser which doesn't have any particles and defects.
3. Measure the dimension of that condenser using optical microscope.
4. Isolate that condenser by scratching the electrodes with a razor.
5. Scratch the lower electrode near the condenser with a plastic tool.
6. Measure the film thickness using Atomic Force Microscopy.
7. Measure the resistivity of the condenser with the voltage meter to check if it has short circuit.
8. Measure the resistivity of each electrode (should be ~ 2 Ω or less).
9. Clamp the sample with the bottom brass electrodes.
10. Make sure that it has a short circuit between the bottom electrode and Al electrode.
11. Connect the top electrode to another Al electrode.
12. Make sure that it has a short circuit between the top electrode and Al electrode.
13. Make sure that it has an open circuit between the top electrode and bottom electrode.

Appendix B Synthesis of Polymer Functionalized Gold Nanoparticles

- 1 kg/mol polystyrene-grafted gold nanoparticles of 5 nm in diameter ($AuPS_{10}$)

1. Dissolve 0.305 g chloroauric acid ($HAuCl_4$) [0.9 mmol] in 30 ml DI water.
2. Dissolve 2.187 g tetraoctylammonium bromide (TOAB: phase transfer catalyst and stabilizing agent) [4 mmol] in 80 ml toluene.
3. Mix and stir $HAuCl_4$ and TOAB solutions for ~ 30 min, then discard the clear aqueous phase.
4. Dissolve 0.378 g sodium borohydride ($NaBH_4$: reducing agent) [10 mmol] in 25 ml DI water.
5. Add $NaBH_4$ solution into the organic phase from step 3, and then stir vigorously for 24 hours.
6. Dissolve 0.225 g thiol-terminated polystyrene (PS-SH) with M_n of 1 kg/mol [0.225 mmol] in 5 ml toluene [molar ratio of PS-SH : $HAuCl_4$ = 1 : 4].
7. Slowly add PS-SH solution into nanoparticle solution from step 5, and then stir vigorously for 24 hours.
8. Completely discard the aqueous phase.
9. Remove abnormally big nanoparticle aggregates or unreacted nanoparticles by centrifuging the nanoparticle solution from step 8 with a minimal amount of methanol.
10. Collect the solution from step 9 and clean unbound PS-SH ligands by mixing it with methanol.
11. Repeat the cleaning step at least 10 times.

- 50 kg/mol polystyrene-grafted gold nanoparticles of 5 nm in diameter ($AuPS_{481}$)

1. Follow the $AuPS_{10}$ synthesis procedure.
2. At step 6, use the molar ratio of 1 : 19 for PS-SH (M_n of 50 kg/mol) solution.
3. The amount of material can be reduced proportionally if necessary.